TREATMENT OF SELENOCYANATE (SeCN⁻) CONTAMINATED AQUEOUS STREAMS USING Fe-BASED SYSTEMS

BY

Sameh Abdelfattah Araby Ahmed

A Thesis Presented to the
DEANSHIP OF GRADUATE STUDIES

KING FAHD UNIVERSITY OF PETROLEUM & MINERALS

DHAHRAN, SAUDI ARABIA

In Partial Fulfillment of the
Requirements for the Degree of

MASTER OF SCIENCE

In

CIVIL ENGINEERING

May 2017

KING FAHD UNIVERSITY OF PETROLEUM & MINERALS

DHAHRAN- 31261, SAUDI ARABIA

DEANSHIP OF GRADUATE STUDIES

This thesis, written by **Sameh Abdelfattah Araby Ahmed** under the direction of his thesis

advisor and approved by his thesis committee, has been presented and accepted by the

Dean of Graduate Studies, in partial fulfillment of the requirements for the degree of

MASTER OF SCIENCE IN CIVIL ENGINEERING.

Dr. Salah U. Al-Dulaijan

Department Chairman

Dr. Salam A. Zummo
Dean of Graduate Studies

17/5/17

Date

Dr. M. S. Vohra
(Advisor)

Dr. M. S. Al-Suwaiyan
(Member)

Dr. Alaadin Bukhari
(Member)

TREATMENT OF SELENOCYANATE (SeCN⁻) CONTAMINATED AQUEOUS STREAMS USING Fe-BASED SYSTEMS

Sameh Abdelfattah Araby Ahmed

CIVIL AND ENVIRONMENTAL ENGINEERING DEPARTMENT

May 2017

KING FAHD UNIVERSITY OF PETROLEUM & MINERALS

DHAHRAN- 31261, SAUDI ARABIA

DEANSHIP OF GRADUATE STUDIES

This thesis, written by **Sameh Abdelfattah Araby Ahmed** under the direction of his thesis advisor and approved by his thesis committee, has been presented and accepted by the Dean of Graduate Studies, in partial fulfillment of the requirements for the degree of **MASTER OF SCIENCE IN CIVIL ENGINEERING.**

_____

Dr. M. S. Vohra
(Advisor)

_____

Dr. Salah U. Al-Dulaijan

Department Chairman

_____

Dr. M. S. Al-Suwaiyan
(Member)

_____

Dr. Salam A. Zummo
Dean of Graduate Studies

_____

Dr. Alaadin Bukhari
(Member)

_____

Date

Dedication

To my beloved wife Reen, dear parents, my brothers & sisters

& all my friends for their endless love & support

ACKNOWLEDGMENTS

TABLE OF CONTENTS

LIST OF TABLES

LIST OF FIGURES

LIST OF ABBREVIATIONS

Se(0) : Elemental Selenium

$SeCN^-$: Selenocyanate

SeO_3^{2-} : Selenite

SeO_4^{2-} : Selenate

AOPs : advanced oxidation processes

FP : Fenton process

PF : Photo-Fenton process

Fe(II) : Ferrous ion

Fe(III) : Ferric ion

SiO_2 : Silica

2LFh : Two-Line Ferrihydrite

UV : Ultraviolet

H_2O_2 : Hydrogen peroxide

TiO_2 : Titanium dioxide

ABSTRACT

Full Name : Sameh Abdelfattah Araby Ahmed

Thesis Title : Treatment of Selenocyanate (SeCN⁻) Contaminated
Aqueous Streams Using Fe-Based Systems

Major Field : Civil Engineering

Date of Degree : May 2017

The presence of selenocyanate species in some specific industrial wastewaters pose risk to human and animal health. Considering this, the present work investigated the removal of aqueous phase selenocyanate using different iron-based systems including Fenton/Photo-Fenton (PF) process, 2 Line Ferrihydrite (2LFh), and $Fe(III)/SiO_2$ binary oxide system. The results showed that Fenton process was efficient with about 90% selenocyanate removal achieved at 360 min at pH 4. However, the use of photo-Fenton process showed comparatively reduced selenocyanate removal. The surface characterization of 2LFh and $Fe(III)/SiO_2$ solids was also completed with XRD and ATR-FTIR techniques. The XRD findings indicated both 2LFh and $Fe(III)/SiO_2$ to be amorphous, and ATR-FTIR results showed several Fe and O-based surface groups. Furthermore, selenocyanate adsorption onto 2LFh and $Fe(III)/SiO_2$ was also explored. The adsorption capacity of 2LFh and $Fe(III)/SiO_2$ for selenocyanate were about 3 and 2.65 mg/g, respectively. In addition, it was noted that the results of selenocyanate adsorption onto 2LFh better fitted to the Langmuir model isotherm, whereas those for $Fe(III)/SiO_2$ better fitted to the Freundlich model isotherm. The q_e/C_e results for respective Fe-adsorbents also supported the above mentioned results, i.e., a plateau was noted for 2LFh system, whereas the $Fe(III)/SiO_2$

showed an increasing qe/Ce trend. This work was further extended to examine the selenocyanate removal using TiO_2-based system photocatalysis followed by the adsorption of released Se-species by 2LFh or $Fe(III)/SiO_2$ system. In this regard, PCD process using TiO_2 initiated the selenocyanate complex degradation with selenite and selenate species formed over 360-min reaction time. The results from the mixed TiO_2 photocatalysis and 2LFh adsorption showed that the combination of the two systems though efficient, but was affected by process variables including pH. Complete selenium removal was achieved at pH 5, whereas the removal decreased significantly with an increase in pH to 9. This was attributed to lower degradation of selenocyanate at higher pH during photocatalysis. Furthermore, the response surface methodology (RSM)-based models also showed that the RSM approach can be used to predict aqueous phase selenocyanate removal under a varying set of operational conditions. A similar trend was also observed for TiO_2 and $Fe(III)/SiO_2$ system. In general, the present work showed successful removal of selenocyanate species from aqueous phase under varying set of process conditions using several Fe-based systems.

ملخص الرسالة

الاسم الكامل: سامح عبدالفتاح عربي احمد

عنوان الرسالة: معالجة مياة الصرف من مركب السيلينوينات باستخدام مركبات الحديد المختلفة

التخصص: الهندسة المدنية

تاريخ الدرجة العلمية: مايو 2017

إن وجود مركبات السيلينوسيانات ($SeCN^-$) في مياة الصرف الناتجة من عمليات تكرير البترول وصناعات التعدين تشكل خطرا كبيرا علي حياة الانسان والحيوان. اخذا هذا بعين الاعتبار, فإن هذا البحث يعمد الي معالجة مياة الصرف من هذه المركبات بستخدام مركبات الحدد المختلفة مثل عملية Fenton/Photo-Fenton و مركبات الحديد 2LFh و $Fe(III)/SiO_2$. نتايئج البحث اظهرت ان استخدام عملية Fenton تؤثر تأثيرا كبيرا علي عملية المعالجة حيث تم معالجه مياة الصرف بنسة 90% , في حين ان استخدام عملية Photo-Fenton اظهرت عدم فعاليتها. من ناحية اخري, تم حضير كلا من مركب 2LFh و $Fe(III)/SiO_2$ وتم استخدام تقنيات XRD و FTIR لتعين بعض خواص هذه المواد. اتضح من نتائج هذه الاختبارت انهما مواد غير منتظمة ترتيب الذرات amorphous وان هناك بعض مجموعات OH عند اسطح العينات. في هذا البحث ايضا تم استخدام مركبات 2LFh و $Fe(III)/SiO_2$ لمعالجة مياة الصرف من مركبات $SeCN^-$ عن طريق امتزازها علي اسطح مركبات الحديد المذكورة. وعلي هذا فإن النتائج اظهرت قابلية مركبات الحديد السابق ذكرها لمركبات $SeCN^-$ ولكن قابليتها ضعيفة جدا, حيث يصل اقصي سعة امتزاز لكلا من 2LFh و $Fe(III)/SiO_2$ الي 3 و 2.65 مجم/جم علي التوالي. وتم نمذجة عملية الامتزاز طبقا لنموزج Langmuir وكذلك Second order kinetics في حالة استخدام 2LFh. هذا وقد تم ايضا استخدام عملية Photocatalysis معتمدة اولا علي استخدام TiO_2 لكسر الرابطة في مركب $SeCN^-$ وتحويلها الي عنصر السيلينيوم ومن ثم اكسدتها الي SeO_3^{2-} ثم الي SeO_4^{2-}. جمبا الي جمب تم استخدام مركبات الحديد 2LFh او $Fe(III)/SiO_2$ مع TiO_2 في عملية Photocatalysis لمعالجة مصادر السليلنوم المتكونة في مياة الصرف عن طريق ايضا امتزاز ها علي اسطح مركبات الحديد المذكورة. هذه التقنية ساعده كثيرا للتخلص من مركبات $SeCN^-$ بشكل كبير.

CHAPTER 1

INTRODUCTION

Selenium is considered as an intrinsic micronutrient for human and other living organisms' growth. In contrast, at high concentrations, selenium species show toxic behavior both for human and other life forms. Skin diseases, defects in gastrointestinal system, central nervous system damage, etc., are attributed to presence of high selenium concentrations [1]. Due to its high toxicity, the World Health Organization (WHO) guideline of 10 µg L^{-1} for selenium in drinking water has been adopted in many countries. Furthermore, other countries have taken into consideration the regulation limits of U. S. EPA of 50 ppb for drinking water whereas the Se discharge limit is 5 ppb [2]. Selenium is widely distributed in soils and natural waters resources through variety of species that are linked by many biogeochemical transformation reactions [3]. In natural environment, selenium usually occurs in one of four oxidation forms including Se(VI), Se(IV), Se(0) and Se(-II). Oxyanions selenite (SeO_3^{2-}) and selenate (SeO_4^{2-}) are usually found in oxidized systems, while Se(0) and Se(-II) appear in anaerobic zones and unweathered mineral formations. A special attention has been given to selenium removal from water bodies because of its toxicity. Some refinery and mining wastewater generated from processing oil or minerals from seleniferous formations such as marine shales, contains high levels of selenocyanate ($SeCN^-$), which poses a great risk to humans and the environment. As such, several remediation methods have been investigated to remove or decrease selenium species from polluted water. Previous studies proved that several selenium based species could be removed by adsorption techniques such as (activated carbons, carbon nano–tubes),

coagulation by ferric sulfate, nano–filtration, reverse osmosis, and advanced oxidation processes (AOPs) [4–10].

Classical Fenton-process has shown promising results in organic and inorganic contaminants removal from wastewater. Fenton process has several advantages, including minimum waste by-products, low operational temperature, use of a non-toxic chemical like H_2O_2, and convenient concentration of Fe(II). Classical Fenton-process has lot of applications in removal of contaminants from industrial wastewater, including drug (NSAID) ibuprofen (IBP), synthetic azo dyes, CI Basic Yellow 51, pesticides, leachates, nalidixic acid (NXA), and the removal of tartrazine [11–18].

Other iron based systems have also been used for the remediation of selenium contaminated streams[19,20]. The efficiency of Fe(III)/SiO_2 binary oxides system to decontaminate both selenite and selenate from synthetic wastewater has also been assessed. In another study, the use of ferrihydrite to adsorb selenate from the aqueous phase was noted to be useful [21]. The above given brief details along with more as given in the literature review section (Chapter 2) provide motivation to investigate the removal of selenocyanate from the synthetic wastewater using Fe based systems. For example, use of Fenton reaction for selenium removal has not been studied to the best of our knowledge. Also, there is no work on the treatment of selenocyanate using 2LFh. Hence, this work intends to investigate the efficiency of some Fe-based systems including, the classical Fenton-process (FP), Fe oxy-hydroxides (2LFh), and Fe(III)/SiO_2 binary oxide systems to remove selenocyanate from synthetic wastewater. The role Fe-species in these systems varies from an oxidizing agent (in case of FP) to simply an adsorbent (in case of 2LFh, etc.). The present work also intends to come up with system that can incorporate existing technologies such as TiO_2-based

2

photocatalysis to destroy the selenocyanate complex, followed by uptake of produced selenium species (selenite and selenate) by Fe-based adsorbents such as 2LFh and Fe(III)/SiO$_2$ binary oxide system. The application of iron combined system for the treatment of selenocyanate contaminated streams has not been reported, to the best of our knowledge. The results reported in chapter 5 are very encouraging, and we hope that outcomes will be beneficial for the remediation of respective wastewater streams.

CHAPTER 2

LITERATURE REVIEW

2.1 Selenium occurrence

Selenium, in low concentrations, is deemed as an intrinsic micronutrient for human health. However, it has been limited with an approximate range between (0 to <40 μg/day), and toxic range (>400 μg/day) [22]. Hence, it is critical to assess and determine the amount of selenium released into natural environment from sources like industrial wastes, agricultural effluents, and flue gas desulfurization processes [23]. Furthermore, effluents from oil refineries also contribute to selenium in surface water [24]. Selenium can present in both organic and inorganic forms, however, most extensive species are selenite (SeO_3^{2-}) and selenate (SeO_4^{2-}) [25], whereas selenocyanate is also noted in specific streams such as those from crude oil refining. Petroleum refinery process water containing approximately 6-7 mg/L selenocyanate with pH 9.6 [26]. Also, other studies reported that wastewater contain about 5 mg/L as selenocyanate species at pH 7.8 [27,28]. The U.S. Environmental Protection Agency (EPA) has set 50 ppb selenium as acceptable in water bodies [29].

2.2 Selenium Chemistry

Selenium (Se) is a naturally occurring trace element noted in four conventional oxidation states (+VI, +IV, 0, and −II). In particular, both selenite (SeO_3^{2-}) and selenate (SeO_4^{2-}) most common selenium species [30–32]. Figure 1 depicts the pourbaix diagram of selenium in water [33]. Selenium species like selenate can be presented in aqueous solutions in forms of biselenate ($HSeO_4^-$) or selenate (SeO_4^{2-}) with pKa of 1.8 [30]. It has low capacity of precipitation and adsorption as well as it is very soluble. Selenite also exists

in aqueous solutions as weak acid in forms of selenious acid (H_2SeO_3), biselenite ($HSeO^{3-}$), with pKa of 2.70 ± 0.06 (H_2SeO_3/ $HSeO_3^-$) and 8.54 ± 0.04 ($HSeO_3^-$/SeO_3^{2-}) [30].
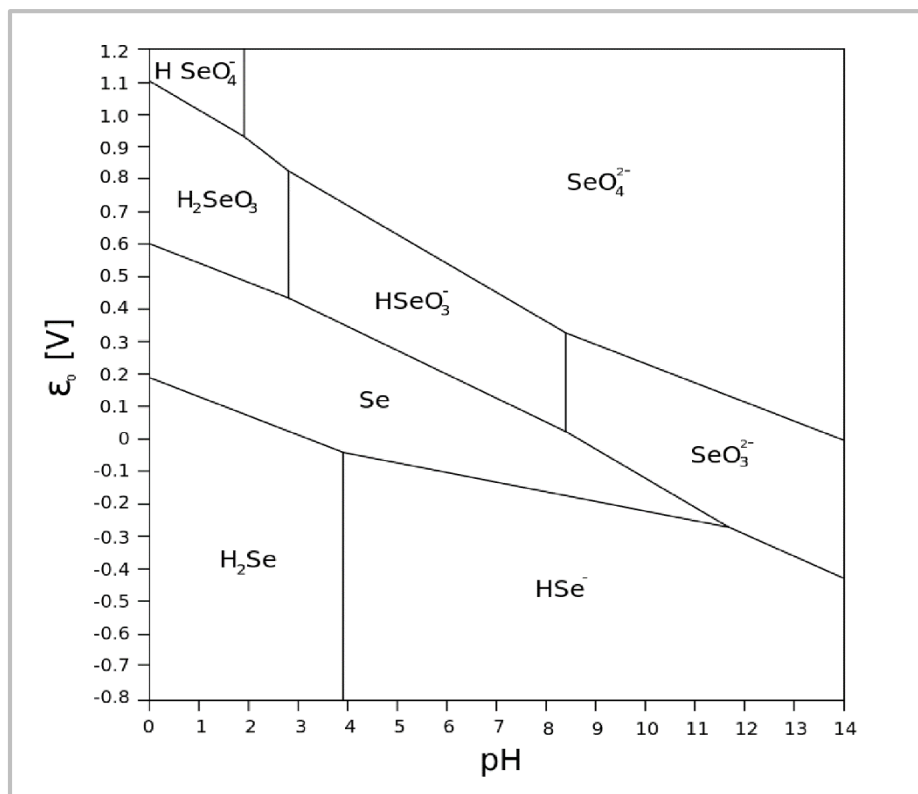
Figure 1 pE–pH diagram for the Se–O–H system at 298 K [28].

2.3 Health Effects

Selenium is an important trace nutrient for human beings and animals. In humans, selenium helps in the healthy functioning of several bio organisms such as the thyroid gland, and hence, lack of selenium can lead to potential diseases. However, research shows that a high concentration of selenium in natural environment may cause many problems [34,35]. According to National Institutes of Health, selenious may develop in concentrations greater than 400 micrograms per day, and the symptoms may include gastrointestinal disorders, hair loss, sloughing of nails, fatigue, irritability and neurological damage.

The toxicity of selenium is not only related to its chemical similarity to sulfur and to its ability to be substituted during the assembly of proteins, but also to the oxidative stress [36]. Selenium species, particularly the inorganic ones, react with thiols and generate oxygen free radicals that account to selenium toxicity to cells [37]. Typically, inorganic selenium species are 40 times more toxic than organic ones, with selenite species being more toxic than selenate [38,39]. Recommended dietary allowance dose is 55 μg/d (according to U.S. Food and Nutrition Board of the Institute of Medicine) and tolerable upper intake level for adults is 400 μg/d in the USA and 300 μg/d in Europe[38–40].

2.4 Principles of Advanced Oxidation Processes (AOPs)

AOPs are oxidative processes, which have been used for pollution control. Typically, they show positive results for contaminants removal from wastewater via the generation of highly oxidative species such as hydroxyl radicals (•OH) that have the capability to oxidize the wastewater pollutants. AOPs include homogeneous or heterogeneous system with irradiated or dark conditions [66–68]. Recently, a great attention has also been paid to

photocatalysis and photo-Fenton (Fe(II)/H₂O₂/UV) advance oxidation processes since they show high capability to oxidize several contaminants in aqueous solutions.

2.4.1 Photo-Fenton Process (PF)

PF process is one of AOPs that uses Fe(II) species serving and H₂O₂ as an oxidant in the presence of the UV radiation to enhance the oxidation process. It is considered an efficient technique to remediate wastewater [46,47]. The PF process includes classical Fenton reaction and PF process as given bellow [48,49],

1. During the classical Fenton reaction, hydroxyl radicals are produced by reaction between H_2O_2 and iron species (Fe(II)) at low pH conditions (acidic solutions), as following,

$$Fe^{2+} + H_2O_2 \rightarrow Fe^{3+} + HO^- + HO^\bullet \qquad (1)$$
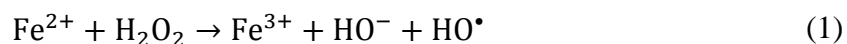
2. Sequentially, Fe(II) is reproduced according to equations (2 and (3,

$$Fe^{3+} + H_2O_2 \leftrightarrow Fe-OOH^{2+} + H^+ \qquad (2)$$

$$Fe-OOH^{2+} \rightarrow Fe^{2+} + HO_2^\bullet \qquad (3)$$
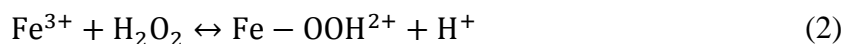
3. Photo-sensitized reaction for PF process are also given below,

$$Fe(OH)^{2+} + h\nu \rightarrow Fe^{2+} + HO^\bullet \qquad (4)$$

$$Fe^{2+} + H_2O_2 \rightarrow Fe(OH)^{2+} + HO^\bullet \qquad (5)$$

Hence, the regenerative PF reaction is supported to be more efficient and economical.

2.5   Selenium removal from water phase

Many methods with different concepts are used to remediate selenium species in water/wastewater. The most common ways are biological treatments, adsorption, precipitation, oxidation, and reduction.

2.5.1   Removal of Selenium Species Using Photocatalysis Techniques

Photocatalysis techniques have shown to be efficient for wastewater treatment. Vohra (2015) [50] investigated the destruction of selenocyanate complex using TiO_2 assisted photocatalyst. The effect of UV lamp only and the addition of TiO_2 on the removal process was examined. Using only UV lamp did not show $SeCN^-$ removal along 2-hr experiment period. However, with addition of TiO_2, the selenocyanate complex was broken down and released elemental selenium was oxidized to selenite (SeO_3^{2-}), which decreased gradually because of its adsorption onto TiO_2 surface and its conversion to selenate ion (SeO_4^{2-}).

Tan et al., (2003-a) [51] explored selenate and selenite photocatalytic reduction over UV-illuminated TiO_2. The influence of different organic hole scavengers, formic acid, acetic acid, methanol, ethanol, sucrose and salicylic acid, on the process was investigated. Only the three organic compounds, formic acid, methanol, and ethanol were efficient for photoreduction of Se ions. The most rapid was formic acid, and the slowest was ethanol. This could be attributed to their capability to generate reducing radicals. In case of formic acid, selenate (VI) and selenite (IV) efficient photoreduction was noted at pH 3.5 and 4.0 values.

Tan et al., (2003-b) [52] compared unmodified TiO_2 and nano-Ag particles modified onTiO_2 (Ag-TiO_2) as photocatalyst for photocatalytic reduction of selenate (VI) ions.

Significant selenium species reduction i.e., Se (VI) to Se^{2-}, was reported. Furthermore, nano-Ag particles introduced a simultaneous Se (VI) reduction with hydrogen selenide production at ultimate reduction at 3.5 pH value with only 0.5 % Ag loading.

Wang et al., (2004) [53] investigated reduction of selenate species using an online UV/TiO_2 photocatalysis reduction device (UV/TiO_2– CRD). Sol–gel process was chosen to formulate nano-TiO_2 covered onto a glass fiber surface. With the UV energy, significant selenate removal was accomplished. The results unveiled that removal efficiency of Se (VI) was enhanced to 53.3 % in the comparison with the old systems with KBH4 and HCl. Moreover, it was applicable for the detection of four different selenium species in synthetic aqueous solutions. Also, selenate (VI) removal using TiO_2 assisted photocatalysis and HCOOH as an electron hole scavenger has been reported by Tsunenori et al., (2011) [54]. A synthetic wastewater simulating the wastewater of wet flue gas desulfurization (FGD) was prepared and exposed to the UV irradiation. The results revealed efficient removal of selenium species, and the photocatalytic reduction resulted in the precipitation of Se(0). Nevertheless, abundant HCOOH amount was required to attain efficient removal of Se(VI) from wastewater.

Labaran and vohra, (2014) [55] assessed selenite and selenate species removal from synthetic wastewater using TiO_2 as a photocatalyst together with a hole (h^+) scavenger (EDTA). High selenium species removal was noted at pH of 4 and 6. Furthermore, use of thiocyanate as a potential hole scavenger did not show any selenate/selenite removal. In contrast, significant selenite and selenate removal was achieved when EDTA was employed as a hole scavenger.

2.5.2   Removal of Selenium Species Using Iron Base Systems

Wasewar et al., (2009) [56] used ferric chloride ($FeCl_3$) coated bagasse fly ash (BFA) in adsorption of selenium (Se^{4+}) from the aqueous solutions. The study explained an inverse relationship between the adsorption of selenium and the initial pH values. It was confirmed to maintain the pH value between 2 and 3 to have more than 90% selenite removal at 20°C. In addition, 4 g/L BFA was optimum yielding about 91% selenite removal [56].

Because of their large specific surface area, the oxide of aluminum, iron, and silica are also used for the remediation of multiple contaminants from the aqueous solution [19]. Chan et al., (2009) [20] assessed the efficiency of the mix of Al^{3+} or Fe(III) binary oxides systems and the silica noncrystalline SiO_2 to remove selenite (SeO_3^{2-}) and selenate (SeO_4^{2-}) from synthetic wastewater. They elucidated the reaction mechanism happening between the selenium species and the adsorbent surfaces at pH 5. Typically, Fe(III)/SiO_2 showed near complete selenite adsorption and around 60% selenate removal. Nonetheless, the selenite adsorption on the Al(III)/SiO_2 surface was embodied with low removal efficiency, but it showed high affinity to adsorb selenate anion even more than Fe(III)/SiO_2. However, the results revealed high selenite/selenate adsorption capacity on the surfaces of Al(III)/SiO_2 more than on Fe(III)/ SiO_2.

Das et al., (2013) [21] completed a comparison study between three iron species 2LFh, goethite, and lepidocrocite for selenate adsorption from the aqueous solutions at near to pH 7. 2LFh showed 34% selenate removal with only 0.1 g/L solid concentration. In sharp contrast, both goethite & lepidocrocite showed no considerable selenate removal. Also, 4 g/L 2LFh was enough to completely remove selenate species, whereas about 91% selenate

was adsorbed onto100 g/L of goethite or lepidocrocite. Thus, 2LFh was noted to be most effective and efficient selenate adsorbent among the mentioned iron oxy-hydroxides.

Meng et al., (2002) [27] investigated use of zero valent iron (ZVI) for selenocyanate reduction to elemental selenium, which in turn could be precipitated. The study revealed a relationship between pH values and both ZVI amount and selenocyanate concentration. At acidic pH values, the ZVI particles efficiently initiated the reduction of selenocyanate to elemental state. A 3-hr mixing time was sufficient to gain more than 97% selenocyanate removal at pH 5.5.

Zhang et al., (2005) [57] examined zero-valent iron (ZVI) to remove selenate from contaminated streams in the presence of arsenate and molybdate. The results showed arsenate disappearance along As(V) concentration range, which disappeared in 16-hr reaction time. However, the selenate species took 31 hr to be removed. However, the authors reported about 73% molybdate removal in 16-hr reaction time with 78% selenate removal, showing negative molybdate influence on selenate removal. The study suggested selenate reduction to selenite, which in turn was rapidly adsorbed onto produced Fe oxyhydroxes (FeOH).

Use of zero-valent iron nanoparticles (Nano Fe^0) was also demonstrated for the removal of selenium species (Se(VI)). Fe(0) was compared to 100 mesh Fe(0) for selenate removal at pH 8.0. The results revealed higher selenate species uptake with the iron nanoparticles at 0.10 molar ratio of (Se:Fe). Furthermore, the reaction kinetics for selenate uptake using nano-ZVI showed four times improvement (more than the traditional ZVI), which are attributed to its higher specific surface area. Langmuir adsorption isotherm showed

11

selenium species uptake capacity of 1.75 mmol/g (Se/Fe(0)). On the other hand, 50% selenate removal was obtained in 2 hr using the normal ZVI. The selenate depletion was ascribed to its reduction to selenide species (Se(-II)), which precipitates combined with some iron(0) corrosion products such as magnetite (Fe_3O_4) and Fe(III) oxyhydroxide [58].

Liang et al., (2013) [59] performed selenite removal attempt as a function of pH using ZVI system. They also discussed in details the removal mechanism. It was indicated that about 98% selenite removal was generally achieved in 2hr along pH range between 4 and 7 with only 1-g/L of solids. No significant selenite removal was noted at pH 8.0 within 24 hr. The selenite specific removal rate as investigated by Johnson et al., (1996) was determined using a pseudo-first-order kinetic model. It showed a significant decrease in specific rate constants of selenite removal from 92.87 to 6.87 (L/h.m2) with an increase in pH value from 4.0 to 7.0. In addition, the study explained the Oxidation Reduction Potential (ORP) change, which reduced from +158 to -541mV at pH 4.0 and from +413 to -212 mV at pH 7.0 during the period of the complete selenium species removal. In contrast, after achieving the complete removal, it showed an obvious increase to +90, and +124mV within 24hr. However, the ORP of the selenite removal remained constant at pH 8.0. Typically, the results confirmed the negative effect of high pH values on the selenium species depletion. Also, the ORP drop was essential to remove the selenite species from aqueous solutions using a ZVI system, the variation of ORP was considered as an indication of the reaction between selenite and ZVI. In this regard, a positive correlation between the selenite reduction rate and the generation rate of iron (II) indicated critical role of Fe(II) in Se(IV) removal by ZVI. The Fe(II) produced is the main reason for the drop in the reaction ORP playing as an electron generation source required for the selenite reduction to elemental

selenium. Iron(II) species were adsorbed onto the ZVI surfaces, and iron (III) was formed. In brief, the removal Se(IV) was initiated by its adsorption followed by its reduction to elemental selenium.

Liang et al., (2014) [60] demonstrated the role of weak magnetic field (WMF) in the enhancement of selenite depletion by ZVI. Complete selenite removal was obtained at pH 4 in 15 min using WMF, while almost no selenite removal was introduced at pH ≥ 7 in the absence of WMF. The presence of WMF caused a sharp decrease in the Oxidation Reduction Potential (ORP) of ZVI system and then allowed the Fe(II) ions to release rapidly at different pH values, so it improved significantly the selenite removal where about 97.5% Se(IV) removal was achieved in 3hr at pH 7. In the absence of WMF, the removal of low selenite concentrations using only ZVI faced the problem of formation of passive layer on the ZVI system and then took long time to be removed comparing to higher selenite concentration. On the other side, the application of WMF showed remarkable results. Typically, it promoted the electron transfer though the passive layer due to increasing the Fe(II) release reducing the selenite life time compared to their counterparts in case of no WMF.

Tang et al., (2014) [61] examined the ferrous aqueous phase and corrosion products were in the reduction process of selenate ion using ZVI. The Fe(II) showed effective selenate removal up to 100% removal in 7 hr when it was added initially. It was also reported that Fe(II) was gradually consumed by the selenium species during the removal process until it was stable while selenate continuously decreased. The characterization experiments showed that the selenate removal was a step-by-step reduction to selenite and elemental selenium with time. The ZVI system played as the major electron donor for the selenate

reduction where the ferrous species facilitated and improved the passive layer of the iron coating. Finally, the iron corrosion products were media for electron transfer and reactive interfaces for selenium adsorption and reduction.

Also, in an extension study for the previous work, the effect of both Mn^{2+} and Co^{2+} combined with the ZVI system on the selenate removal was reported [62]. The effect of ZVI alone on the selenate removal as mentioned the previous study was around 4%. However, selenate species was completely depleted in 3hr with 50 g/L ZVI and 1.0 M Co^{2+} added initially. The use of Co^{2+} only showed no improved selenate depletion. Therefore, the combined Co^{2+} and ZVI synergistic was the main reason for the noted selenate reduction to the selenite due to the promotion of ZVI oxidative dissolution. In brief, the result evaluated that the cobalt ion contributed around 69% electrons required for selenate reduction. Similarly, manganese ion (Mn^{2+}) significantly assisted in the selenate reduction but not like the cobalt ion. It provided about 30% of electrons for the reduction of selenate in two steps, reduction to selenite and elemental selenium.

Another research explained the removal of selenate species using a combination of magnetite and iron (II) with zero-valent iron [63]. This combination creates the so-called by hybridized zero-valent iron (ZVI) system (hZVI). The use of magnetite and Fe (II) prevented the surface passivation of ZVI and increased the ZVI reactivity in terms of selenate reduction. The selenate removal was introduced in 90-min reaction. However, selenate took about 450 min to be removed in case of no precondition duration. The study showed the significance of precondition of (ZVI/Fe_3O_4/Fe(II)) in augmentation of the selenium removal in the first 24 hr. Also as Tang et al., (2014) [61] previously mentioned, removal of selenate consumed Fe(II) rapidly till its complete removal showing main role

of Fe(II) in the removal mechanism, and its combination with the magnetite increased significantly the removal of selenate.

Additionally, the application of zero-valent iron and ultrasound combination has been investigated for the removal of selenite (SeO_3^{2-}) species from wastewater [64]. The using of only ultrasonic condition showed no significant selenium removal. Nevertheless, about 50% of 10 mg/L selenite was removed using the ZVI in the presence of ultrasound irradiation at acidic conditions. The slight removal was attributed to the reduction of selenite species to elemental selenium, which precipitates, by ZVI-ultrasound combination. The study attributed this to higher hydroxyl radicals, which could be generated at low pH due to Fenton reaction caused because of the ultrasound radiation. As a result, selenite ion was oxidized to selenate species, and both were eventually reduced to elemental selenium.

Similarly, the effect of iron (II) species amount on the selenate reduction using ZVI has been investigated [65]. About 50% selenate removal was achieved at pH 6 in 10 hr. However, the addition of iron(II) enhanced the selenate removal up to 100% using ZVI-Fe(II) combination. Moreover, the effect of anoxic conditions on the removal process was illustrated in this study; only about 20% selenate removal was obtained with adding 50 mg/L Fe(II). Those outcomes evidently revealed that the anoxic conditions significantly decreased the kinetics of selenium species removal.

Ling et al., (2015) [66] assessed the application of nanoscale zero-valent (nZVI) in the detoxification of selenite species from aqueous phase solutions. They revealed that 5 g/L nZVI was enough to completely removed 1.3 nM Se(IV) in 3-min reaction time. The selenium species Se(IV) was degraded by its reduction to elemental selenium due to

Se(IV)-Fe(0) reaction where the attraction of selenite species onto nZVI surface, showing nZVI affinity for selenium.

In another study for selenium species removal, selenite and selenate adsorption using the iron(III)-modified natural zeolitic tuff (Fe-CLI) from the Serbian deposit Zlatokop were reported by Jevtic et al., (2014) [67]. In the beginning, zeolitic lattice with the negative charge showed no significant adsorption for both of selenite and selenate species. Therefore, it was investigated to alter its surface charge to get more affinity for the removal of selenate. In addition, the modified iron (III) species was applied as an adsorbent for the selenium anions showing that degradation of these species declined at higher pH values, which was attributed to competitive reaction between selenium species and the hydroxyl ions to bond at the Fe-CLI surface. It also showed higher affinity for selenite than selenate while the kinetics data following the pseudo-second-order model revealed higher selenate adsorption and desorption rates.

Other iron species have also been used for the removal of selenium (IV) and (VI) from water phase systems. Wei et al., (2012) [68] examined the synthesized nano-magnetite as an adsorbent used for the aqueous phase selenite and selenate removal. About 50% removal of selenite was achieved in only 30-min contact time, followed by a decreased removal rate and then reaching to no remarkable selenium species removal after 24 hr when 5% of 100 µg/L selenite was remaining using only 0.1 g/L of nano-magnetite at pH 4.0, demonstrating the best performance in selenite removal due to its large specific surface area compared to nano-iron and natural magnetite. However, the nano-iron showed the highest affinity for the selenate removal, attributing this to its powerful ability to covert selenate anion to

selenite, which is easy to be adsorbed. Finally, the ionic strength barely affected the selenite adsorption.

2.5.3 Removal of Selenium Species Using Other Techniques

A comparison study to examine each of lanthanum oxide, activated γ-alumina, and activated α-alumina to disinfect both selenite ion Se (IV) and arsenic using adsorption mechanism was studied by Davis & Misra (1997) [69]. The adsorption model embodied an evidence that lanthanum oxide has a great capacity to remove selenite species more than activated γ-alumina.

Youwen et al., (2001) [70] evaluated the influence of Layered double hydroxides (LDHs) on the removal selenium species selenite and selenate. They assessed the adsorption mechanism on the surfaces of both Magnesium–aluminum (Mg^{2+}/Al^{3+}) and zinc–aluminum (Zn^{2+}/Al^{3+}). The chloride salts ($MgCl_2$, $AlCl_3$, and $ZnCl_2$) were chosen to prepare the adsorbents with mix of 2 to 4 for Mg/Al-(molar ratio) while the molar ratio of Zn/Al was 2. The authors reported a rapid selenite adsorption on the Mg/Al surface where 60-min contact time was enough for 0.63 cmol/L selenite to get the quasi-equilibrium. It was indicated that the adsorbent species adsorbed selenite in rate more than selenate. In addition, Mg/Al mix was more effective than Zn/Al in the removal of selenium species, which were also affected by the molar ratio of each adsorbent. Also, the adsorption of selenium increased with a decrease in the respective molar ratio.

The mechanisms of selenium species adsorption onto aluminum species have been studied by many researchers. Yamani et al., (2013) [71] examined the of selenite and selenate remediation using n-Al_2O_3 impregnated chitosan beads (AICB), which was produced from

nanocrystalline aluminum oxide. The adsorption results were also compared to the result from Nanocrystalline forms of titanium dioxide (n-TiO$_2$), n-Al$_2$O$_3$ alone, and chitosan. It is indicated that 2 mg/L initial selenium concentration from each species removed completely using n-Al$_2$O$_3$ only with 30% more than n-TiO$_2$. AICB showed high removal efficiency about 98% and 85 % for selenite and selenate respectively, with a significant selenium removal over a small pH range from 4.5 to 6.

Manceau and Gallup (1997) [26] studied the removal of selenocyanate ion (SeCN$^-$) from industrial wastewater using a set of complex reactions and also examined whether the removal results from the conversion of selenocyanate to elemental selenium. In this regard, they used sodium thiosulfate and sulfites to reduce cupric ions to cuprous ions, which promoted co-precipitation that generated Cu(S0.91Se0.09)CN(s). After filtration to remove the solid, caustic soda or sodium sulfide can be added to precipitate the excess copper. They also concluded that the efficiency of selenium removal with cupric ions could reach as high as 95%, when pH value was about 9. However, for more excess copper added, it became difficult to remove the excess copper.

The above literature review shows use of different methods for the removal of several selenium species. Also, the use of FP process for the removal of selenocyanate is not explored. It is clear that though the 2LFh has been used for selenate adsorption however its use for selenocyanate removal is not investigated. Similarly, Fe(III)/SiO$_2$ binary oxide system has also been investigated for the removal of selenate, but for selenocyanate removal is not studied. Though the TiO$_2$-based photocatalysis has been employed for selenite, selenate, and selenocyanate removal, but the respective works indicate use of a hole scavenger added at a specific time specifically to ensure complete destruction of

selenocyanate complex by hydroxyl radicals before the addition of hole scavenger to avoid its competitive oxidation. The present work also considers use of above mentioned iron-based systems i.e., under a varying set of conditions, and explore the use of both adsorption and mix of oxidation/adsorption based system to remove both the parent compound selenocyanate and Se-based reaction by products. The use of such mixed system, for the application has never been reported, to the best of our knowledge.

CHAPTER 3

RESEARCH OBJECTIVES

The fundamental aim of this research is to evaluate the efficiency of Fe-based systems along with advanced oxidation for the treatment of selenocyanate ($SeCN^-$) contaminated aqueous streams. The specific Fe-based processes for selenocyanate removal will include the classical Fenton process, Photo-Fenton process, Fe oxy-hydroxide 2LFh, and Fe(III)/SiO_2 binary oxides adsorption systems with TiO_2 photocatalysis. The specific objectives include:

1. To investigate the treatment of selenocyanate species using the classical Fenton/photo-Fenton processes.

2. To investigate selenocyanate adsorption onto 2LFh under varying conditions, (pH, solids amount).

3. To study use of 2LFh both without and with TiO_2 photocatalysis for selenocyanate and associated Se-species removal via advanced oxidation and adsorption mixed system.

4. To investigate selenocyanate adsorption onto Fe(III)/SiO_2 under varying conditions, (pH, solids amount).

5. To study use of Fe(III)/SiO_2 binary oxide system both without and with TiO_2 photocatalysis for selenocyanate and associated Se-species removal via advanced oxidation and adsorption mixed system.

CHAPTER 4

RESEARCH METHODOLOGY

4.1 Materials

A variety of materials and equipment were used in the present work. Several high purity reagent grade quality chemicals were used including potassium selenocyanate KSeCN (ALDRICH, USA), sodium selenate Na_2SeO_4 (ALDRICH, USA), sodium selenite Na_2SeO_3 (ALDRICH, USA) adisodium EDTA (FISHER, USA), hydrogen peroxide H_2O_2 (30% w/w, F. Maia), ferrous sulphate $FeSO_4.7H_2O$ (FISHER, USA), ferric chloride $FeCl_3$ (BDH, England), TiO_2 powder (P25, DEGUSSA, Germany), powder silica gel (63-200 μm, ALDRICH, USA) $NaHCO_3$ (BDH, England), Na_2CO_3 (BDH, England), liquid nitrogen, nitrogen gas, HCl (FISHER, USA), H_2SO_4 (FISHER, USA), HNO_3 (FISHER, USA), NaOH (FISHER, USA), and pH calibration standards (FISHER, USA). 0.2 μm filter papers (Whatman, Germany) were also used

4.2 Experimental setup and apparatus

A pyrex-glass batch type reactor with dimensions of 7 cm diameter and 30 cm long and a 15 W UV lamp (F15T8-BLB 15W, Sankyo Denki, Japan) with 315- 400 nm wavelength range (peak maximum at ~352) were used to run the photocatalytic experiments (Figure 2). Furthermore, a 1000-mL glass beaker, titration equipment, FreeZone 4.5 Liter Benchtop Freeze Dry System (model 7750031, LABCONCO, USA) were used for 2LFh and Fe(III)/SiO_2 solids preparation. ADX-2500 X-ray Diffraction and Perkin-Elmer 16PC FT-IR spectrometer (USA) were used for material characterization. Atomic absorption spectrometer (AAnalyst™ 700 Perkin-Elmer, USA), and advanced ion chromatograph

equipment (IC 861, METROHM, Switzerland) were used for selenium species determination.

4.3 Solution preparation

High purity distilled water (CORNING Mega Pure^{TM}) system and the aforementioned reagent grade chemicals were used for preparing all the stock solutions. Finally, the solutions were covered with aluminum foil, to avoid any photoreaction. The prepared stock solutions were 1000 mg/L of selenocyanate, selenite, and selenate. As such, the stock solutions of hydrogen peroxide and the ferrous sulphate were also made with concentrations of 10,000 and 1,000 mg/L respectively. A 10,000 mg/L stock solution of EDTA was also used.

4.4 Selenocyanate removal using Classical Fenton/Photo-Fenton experiments

4.4.1 Experimental procedure

In this section, the producer used for classical Fenton/PF experiments is explained. Firstly, 1100 mL selenocyanate solution with desired concentration was prepared. Then, a 100-mL blank sample was taken from the solution to examine the initial selenium concentration. After that, the remaining 1,000 mL was transferred to the empty reactor (Figure 2). To make sure that there is no external light in the experiments, an aluminum foil was used to cover the glass reactor during the experiments. The pH of the mixed solution was adjusted to the desired value using HCl or NaOH solutions. Subsequently, 300 mg/L H_2O_2 and desired Fe(II) amounts were directly added to the solution in the reactor while the solution was mixed using a magnetic stirrer set up. A filtered sample was directly taken after adding the amount of Fe(II) and H_2O_2, at zero time. In case of PF experiments, a glass sleeve was

used to place the UV lamp (Sankyo Denki, Japan) at the center of the reactor that separates

the UV lamp from the solution as illustrated in Figure 2. Thereafter, samples were taken

after adding Fe(II) and H_2O_2, at varying time. As mentioned before, the Fenton experiments

had the same procedure as photo-Fenton process but without the UV lamp. The procedure

is also summarized in in Table 1.
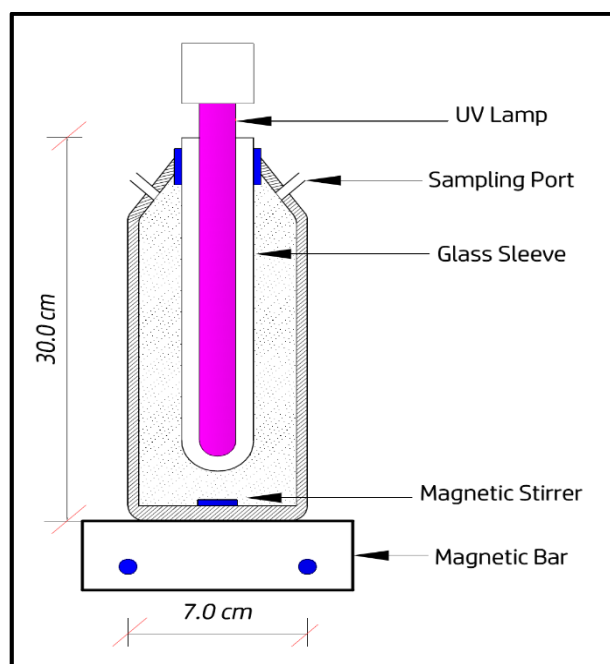
Figure 2 The layout of experimental reactor used for Fenton and Photo-Fenton expriment

Table 1 list of expeiments completed using classical Fenton/Photo-Fenton processes for selenocyanate removal

Variable	System	Experimental Conditions	Variation
Effect of pH	Selenocyanate + Fe(II)	20 mg/L selenocyanate 50 mg/L(Fe(II))	pH4
			pH 10
	Selenocyanate + UV Light + Fe(II)	20 mg/L selenocyanate 50 mg/L Fe(II)	pH 4
			pH 10
	[Fenton process] Selenocyanate + Fe(II) + H_2O_2	20 mg/L selenocyanate 30 mg/L Fe(II) 300 mg/L H_2O_2	pH 4
			pH 6
	[PF process] Selenocyanate + Fe(II) + H_2O_2 + UV light	20 mg/L selenocyanate 30 mg/L Fe(II) 300 mg/L H_2O_2	pH 4
			pH 10
Effect of Initial EDTA Concentration	[PF process] Selenocyanate + Fe(II) + H_2O_2 + UV Light	20 mg/L selenocyanate 30 mg/L Fe(II) 300 mg/L H_2O_2 pH 4	0 mg/LEDTA
			450 mg/LEDTA
Effect of Initial Selenocyanate Concentration	[Fenton process] Selenocyanate + Fe(II) + H_2O_2	30 mg/L Fe(II) 300mg/L H_2O_2 pH 4	10 mg/L selenocyanate
			20 mg/L selenocyanate
The effect of Fe(II) Concentration	[Fenton process] Selenocyanate + Fe(II) + H_2O_2	20 mg/L selenocyanate 300 mg/L H_2O_2 pH 4	10 mg/L Fe(II)
			30 mg/L Fe(II)
			50 mg/L Fe(II)

4.5 Selenocyanate removal using 2LFh

4.5.1 2LFh synthesis

To synthesize 2LF, 500-mL of 0.2M of ferric chloride ($FeCl_3$) was prepared in 1000-mL glass beaker. Moreover, NaOH with concentration of 1M was used to maintain pH value of 6.5 while the solution was stirring vigorously. The titration with NaOH was continued dropwise till reaching pH 7-8. Furthermore, the precipitate was then centrifuged at 2500 rpm five times. The precipitate was then washed with high purity water after each time of precipitate centrifugal to clean 2LFh precipitate from any chloride impurities. After that, the solids were quickly freeze dried using FreeZone 4.5 Liter Benchtop Freeze Dry System (model 7750031, LABCONCO, USA) and stored till further analysis in fridge [21,72,73].

Figure 3 Experimental set-up for 2LFh synthesis

4.5.2 2LFh solids characterization

4.5.2.1 X-ray Diffraction (XRD) Identification

Generally, ferrihydrite is produced from rapid Fe(III) solutions hydrolysis. It can be identified by its crystallinity or the number of peaks in the XRD pattern. For instance, 2LFh shows two broad peaks. In the present work, ADX-2500 X-ray diffraction was used for XRD analysis. Diffraction pattern for 2LFh sample was obtained by a step scanning at 1°/min step with an angular range of 2Θ from 10º to 80º.

4.5.2.2 Attenuated Total Reflectance-Fourier Transform Infrared (ATR-FTIR) Spectroscopy

The solid state infrared spectra were obtained using a Perkin Elmer 16F PC FTIR spectrometer using solid potassium bromide (KBr) pellets in a region of 650-4000 cm^{-1}. In addition, resolution was 8, and number of scans were 32.

4.5.3 Adsorption of aqueous phase selenocyanate onto 2LFh experimental procedure

4.5.3.1 The effect of pH

To obtain the optimum pH conditions, the pH adsorption study of selenocyanate, single solute system, was investigated using different selenocyanate concentrations, 5, 10, 20 mg/L at pH range from 4 to 11. Procedure for adsorption experiments involves, adding 1-g/L of the produced 2LFh to the previous solutions. After that, the solutions pH was adjusted to the desired value using NaOH and HCl solutions. The mixtures were continuously mixed for 96-hr equilibrium time at room temperature using a magnetic stirrer set up. In addition, the pH was measured every 24-hr reaction time till 96 hr to investigate if there was significant pH variation or not and the final pH was reported. Finally, each

sample was centrifuged at 3000 rpm and filtered using 0.2 µm filter paper. Table 2 illustrates the experimental plan of selenocyanate adsorption using 2LFh.

4.5.3.2 Effect of Adsorbent Dosage

The effect of 2LFh amount onto selenocyanate uptake was also investigated. In this work, solutions of different selenocyanate concentration of 2.5, 10, 20, and 50 mg/L were prepared. Moreover, different 2LFh amounts of 1, 2, 3, and 5 g-L were in contact with the previous selenocyanate solution at pH 5 for 96-hr contact time.

4.5.3.3 Effect of Initial Concentration

The effect of concentration variation in the single and binary solute systems were also investigated. The optimum pH and contact time realized from pH-adsorption study were employed. Procedure for the adsorption experiments involve adding 3-g/L of 2LFh to solutions of different selenocyanate 2.5, 5, 10, 20, and 50 mg/L. It should be noted that all adsorption experiments were conducted in 125-mL Erlenmeyer flasks, and the system was kept in suspension using a magnetic stirrer set up and covered with aluminum foil. Details of the pollutants concentrations used, and other experimental parameters investigated are summarized in Table 2.

Table 2 The plan of Studying of the selenocyanate adsorption onto 2LFh metal oxide.

Variable	System	Experimental Conditions	Variation
Effect of pH	2LFh + Selenocyanate	1-g/L 2LFh, 1- 5 mg/L selenocyanate 2- 10 mg/L selenocyanate 3- 20 mg/L selenocyanate	pH 4
			pH 5
			pH 6
			pH 8
			pH 9
			pH 10
			pH 11
Effect of Adsorbent Dosage	2LFh + Selenocyanate	1- 2.5 mg/L selenocyanate 2- 10 mg/L selenocyanate 3- 20 mg/L selenocyanate 4- 50 mg/L selenocyanate pH 5	1-g/L 2LFh
			2-g/L 2LFh
			3-g/L 2LFh
			5-g/L 2LFh
Effect of Selenocyanate Concentration	2LFh + Selenocyanate	3-g/L 2LFh pH 5	2.5 mg/L selenocyanate
			5 mg/L selenocyanate
			10 mg/L selenocyanate
			20 mg/L selenocyanate
			50 mg/L selenocyanate

4.5.4 Use of 2LFh in selenocyanate Photocatalytic removal

4.5.4.1 UV-lamp light photocatalytic experimental procedure

A 1000-mL Pyrex glass batch type reactor was utilized to perform UV-light photocatalytic experiments. Lay-out of the experimental set-up is shown in Figure 2. High purity water was used to prepare batch test solutions with the desired respective chemicals concentrations. For each experiment, a1100 mL of test solution was prepared, and then a100-mL sample was taken as a blank sample. After that, 1-g/L TiO_2 was added to the remaining 1000 mL of each solution required for the selenocyanate complex destruction [50]. After this, the desired 2LFh amount was added to the mix solution. The system was kept in suspension using a magnetic stirrer set up, and initial pH was maintained to the desired value using NaOH and HCl solutions. In addition, this test solution was then transferred to the batch reactor shown in Figure 2, and was allowed to equilibrate for 30 min. The test solution was exposed to the UV-light using a 15 W UV-lamp with wavelength ~352 nm (F15T8-BLB 15W, Sankyo Denki, Japan), which was positioned at the reactor center and separated from the test solution using a glass sleeve. Samples were taken at different times. A sample was taken directly after adding both TiO_2 and 2LFh directly. Another sample was taken after 30 min time and before turning on the UV lamp to investigate the initial selenocyanate removal. The PCD reactor was fully covered with aluminum foil during experiment to cut off external source. The UV lamp was then turned on and several samples were collected via sampling port at different time intervals from 0 to 360 min. Additional samples were taken if deemed necessary. Experimental plan of using 2LFh in UV lamp light assisted photocatalysis is shown in Table 3.

Table 3 Plan of the use of 2LFh metal oxide in selenocyanate photocatalyic removal

Variable	System	Experimental Conditions	Variation
Effect of pH	UV-light + Selenocyanate	20 mg/L selenocyanate	pH 5
	Selenocyanate + UV Light + 2LFh	20 mg/L selenocyanate 1-g/L 2LFh	pH 5
	Selenocyanate + UV Light + TiO$_2$	20 mg/L selenocyanate 1-g/L TiO$_2$	pH 5
			pH 9
	Selenocyanate + UV Light + TiO$_2$ + 2LFh	20 mg/L selenocyanate 1-g/L TiO$_2$ 1-gL 2LFh	pH 5
			pH 9
	Selenocyanate + UV Light + TiO$_2$ + 2LFh	10 mg/L selenocyanate 1-g/L TiO$_2$ 1-gL 2LFh	pH 5
			pH 9
Effect of 2LFh amount	Selenocyanate + UV Light + TiO$_2$ + 2LFh	20 mg/L selenocyanate 1-g/L TiO$_2$ pH 7	0.5-g/L 2LFh
			1.5-g/L 2LFh
Effect of Initial Selenocyanate Concentration	Selenocyanate + UV Light + TiO$_2$ + 2LFh	1-g/L TiO$_2$ pH 5	10 mg/L selenocyanate
			20 mg/L selenocyanate
		1-g/L TiO$_2$ pH 9	10 mg/L selenocyanate
			20 mg/L selenocyanate

4.5.4.2 Response Surface Methodology (RSM)

The experimental design method adopted in this research for the use of 2LFh in selenocyanate photocatalytic removal was based on RSM techniques. Box-Behnken design (BBD), a three-level factorial design was employed for the experimental design and analysis. BBD design is usually described by a multidimensional cube with selected points at the mid of each edge, with a replicated center point [74]. In the present work, pH, 2LFh amount, and initial selenocyanate concentration were three independent factors that were examined in this design. Each factor was equally spaced. The pH factor was adopted to be 5, 7, and 9. The 2LFh amount was 0.5, 1, and 1.5-g/L while the initial selenocyanate concentration was 10, 15, and 20 mg/L. A total number of 13 experimental runs were adopted with a single center point per block. Design-Expert software with a one-way analysis of variance was used to analyze the response (Total selenium removal after 360 min) obtained.

4.6   Selenocyanate removal using binary oxide system Fe(III)/SiO$_2$

4.6.1   Fe(III)/SiO$_2$ system synthesis

Binary oxide system was synthesized using the combination between ferric chloride solution and powder silica gel. Powder silica gel was with BET specific surface area of 500 m^2/g. First, a 1000-mL of suspension 20-g/L SiO$_2$ was purged under nitrogen gas for 24 hr. In addition, the silica suspension was mixed with 0.1 M ferric chloride solution, and then 1M of NaOH solution was used to bring the pH to 5 and was kept mixing using magnetic stirrer for 24 hr. After that, the mixed solution was centrifuged at 3000 rpm 4 times and washed with distilled water between each centrifugal time. The precipitation was collected and quickly freeze dried using FreeZone 4.5 Liter Benchtop Freeze Dry System (model 7750031, LABCONCO, USA) and stored till further analysis in fridge [20].

4.6.2   Fe(III)/SiO$_2$ solids characterization

4.6.2.1 X-ray Diffraction (XRD) Identification and Fourier Transform Infra-Red Spectroscopy (FTIR)

This procedure was same as procedure in sections 4.5.2.1 and 4.5.2.2.

4.7   Analytical methods

0.2- µm filter papers were used to filter the collected samples from the batch experiments. Total selenium remaining for all adsorption experiments was measured using an atomic absorption spectrometer (Perkin-Elmer AAnalyst™ 700, USA) equipped with selenium lamp, type electrode-less discharge lamp (EDL) and flame accessory. The lamp operation condition were 200 mA electric current, 196.0 nm wavelength, and a spectral bandwidth of 2.0 nm. The instrument was computer-controlled via WinLab32™ software. Calibration curve was constructed before each analysis using three selenium standards. Furthermore, $SeCN^-$, SeO_4^{2-}, and SeO_3^{2-} species results were also obtained using an intelligent ion chromatograph (IC) set-up (Metrohm, Switzerland) equipped with a conductivity detector controlled by the MagIC Net^{TM} software. The composition of eluent was the same as mentioned in [55]. The eluent flow was 1mM $NaHCO_3$ and 3.2 mM Na_2CO_3 at1 ml/min.

CHAPTER 5

RESULTS AND DISCUSSION

5.1 Study of Classical Fenton/Photo-Fenton processes in selenocyanate Removal

We initially investigated use of Fe(II) only for selenocyanate removal both without and with UV light and respective results are given in Figure 4 and Figure 5, respectively. Results from experiments conducted at pH 4 and 10 indicate very small selenocyanate removal for both cases, indicating little role of Fe(II) at pH 4 and 10 only for selenocyanate removal. However adding H_2O_2 to the pH 4 system with Fe(II) only (i.e., Fenton process), we note significant selenocyanate removal as shown in Figure 6. Furthermore, Figure 6 also show 30 mg/L Fe(III) to be an optimum amount for the given Fenton reaction. Hence, using the classical Fenton process with 300 mg/L H_2O_2 and 30 mg/L, we note that selenocyanate is removed gradually with about 56% removal at time zero, and approx. 90% final removal is noted at 360 min. Typically, reaction between Fe(II) and H_2O_2 results in powerful hydroxyl radicals that will break down the selenocyanate complex, and oxidize the released elemental selenium to selenite and then to selenate [50,28]. The produced selenium species can adsorb onto produced ferric hydroxide ($Fe(OH)_3$) precipitates and get removed from the aqueous phase.

This work was further expanded to the possibility of selenocyanate species removal using the photo Fenton (PF) process. In this regard, initial batch experiments were conducted at pH 4 and 10, and respective results are shown in Figure 7. About 56% selenocyanate removal is obtained at pH 4 at time zero. However, at pH 10, selenocyanate removal is

insignificant. As Fenton reaction between ferrous species and H_2O_2 proceeds, the hydroxyl radicals are produced, with simultaneous conversion of ferrous ions to ferric ions, and reduction in total selenium removal. However, loss of Fe-species at pH 10 because of precipitation could cause the noted reduction in process efficiency.

Nevertheless, the noted constant selenocyanate removal from time zero till 360-min reaction time during pH 4 PF experiment (Figure 7) is very different from the earlier reported classical Fenton based experimental results (Figure 6). This could be attributed to autocatalytic and regenerative nature of PF process during which leads to less precipitation for soluble selenium species adsorption. To assess whether the noted selenocyanate removal transpires from its destruction, we conducted another similar experiment with addition of 450 mg/L EDTA as a hole scavenger. The respective results as given in (Figure 8) clearly show reduced selenocyanate removal in the present of EDTA, confirming that the noted selenocyanate removal is because of its destruction followed by adsorption. In any case, these results along with those without H_2O_2 (Figure 4 and Figure 5) also confirm this hypothesis. Hence, the classical Fenton process with a careful adjustment of pH and process chemicals yields better selenocyanate removal compared to PF process. However, generation of huge sludge volumes is a concern. In the coming section, we explore the other Fe-based techniques to gain further insight into such systems.

We also investigated the effect of initial selenocyanate concentration onto its removal. Figure 9 provides the respective results for 10 and 20 mg/L selenocyanate systems. The results show a notable difference between the two systems over the 360-min reaction time with > 90% removal for 20 mg/L $SeCN^-$, which is higher than the 10 mg/L selenocyanate system results. This can be attributed to higher mas transfer between the aqueous phase

selenium species and iron solid phase at higher initial SeCN⁻ amount. Another set of experiments conducted at pH 6 with 10 and 30 mg/L selenocyanate amount showed a similar trend as given in (Figure 10). Hence in general, the rate of Se removal increases with an increase in its initial selenocyanate concentration.
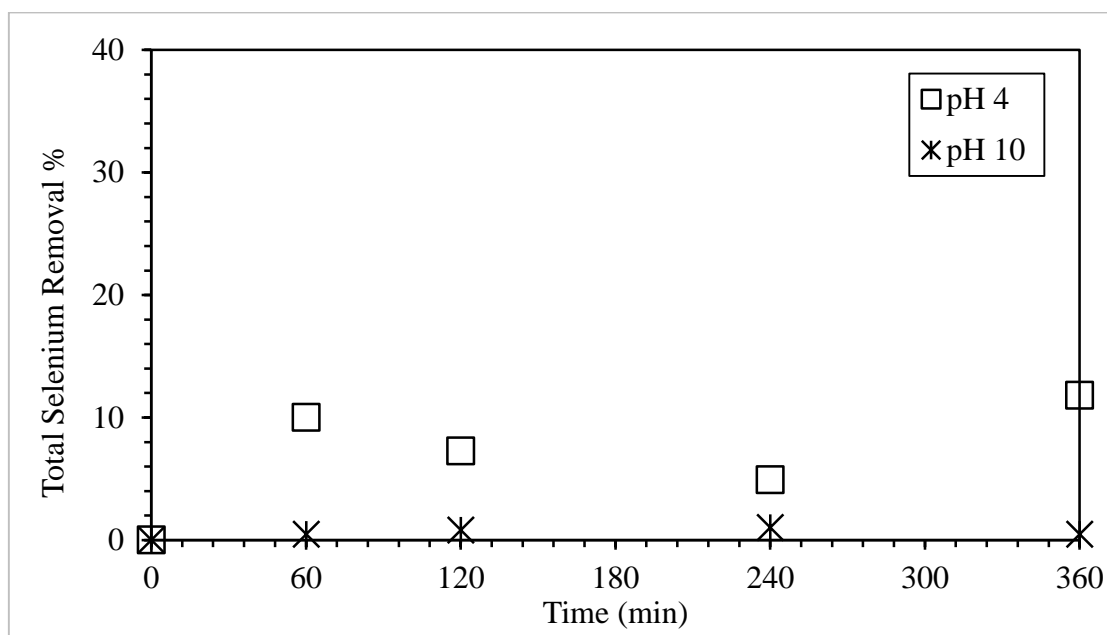
Figure 4 The effect of pH onto total selenium removal using ferrous ion (20 mg/L selenocyanate, 50 mg/L Fe(II)).
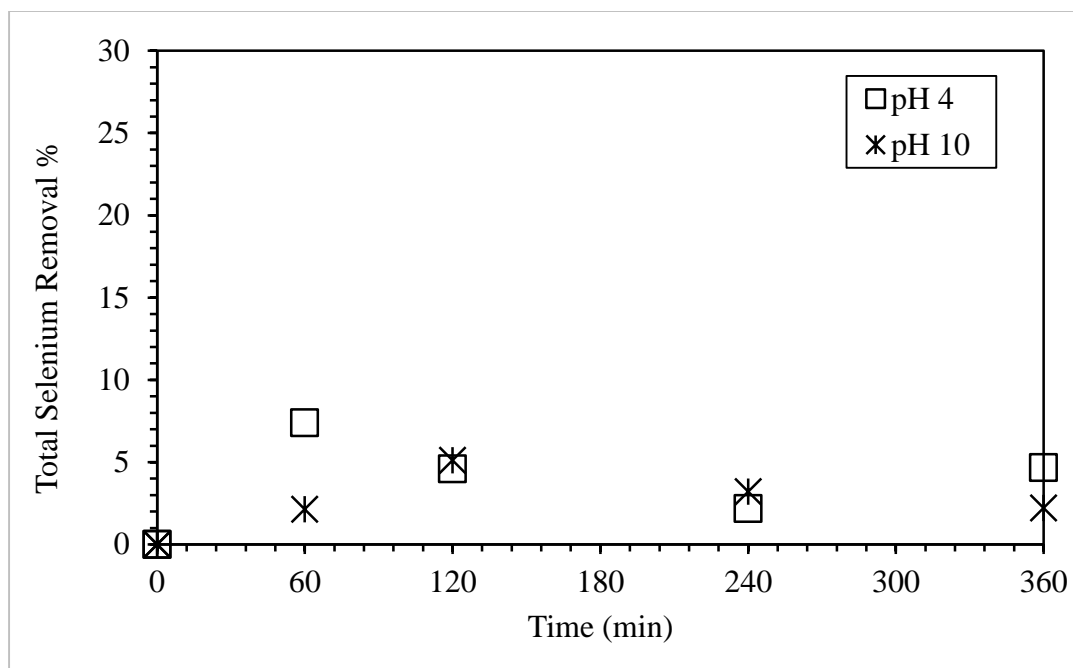
Figure 5 The effect of pH onto total selenium removal using Fe(II)/UV light (20 mg/L selenocyanate, 50 mg/L Fe(II), 15 W UV lamp).
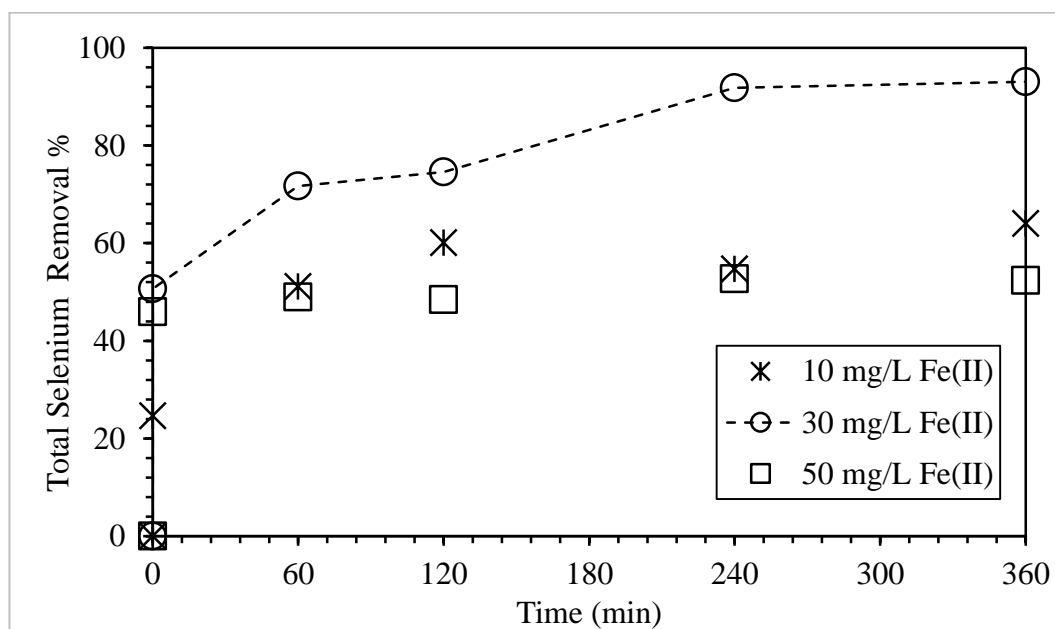
Figure 6 The effect of initial Fe(II) amount onto the removal of selenocyanate using Fenton process (20 mg/L selenocyanate, 300 m/L H_2O_2, pH4).
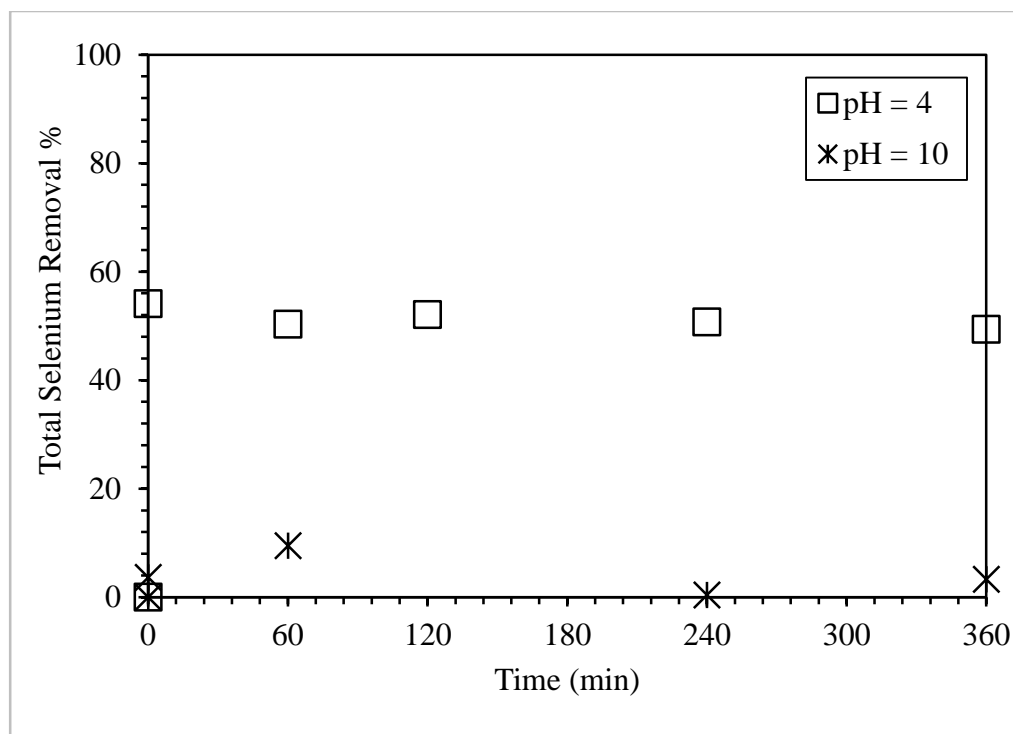
Figure 7 The effect of pH on total selenium removal using PF process (20 mg/L selenocyanate, 300 mg/LH$_2$O$_2$, 30 mg/L Fe(II), 15 W UV lamp).
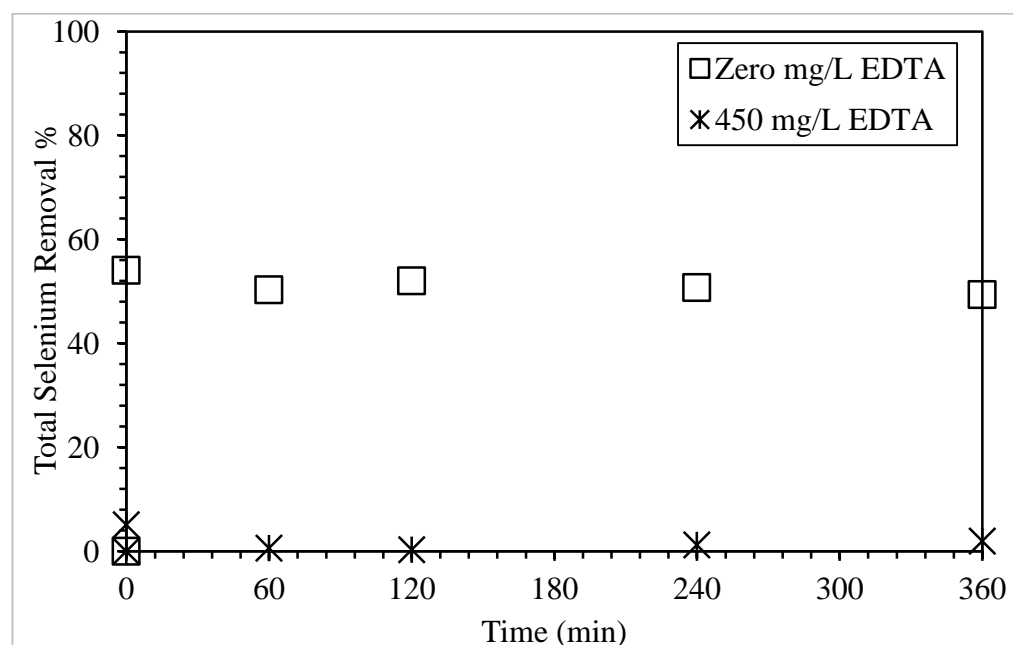
Figure 8 The Effect of EDTA concentration on total selenium removal using PF process (20 mg/L selenocyanate, pH 4, 300 mg/L H$_2$O$_2$, 30 mg/L Fe(II), 15 W UV lamp).
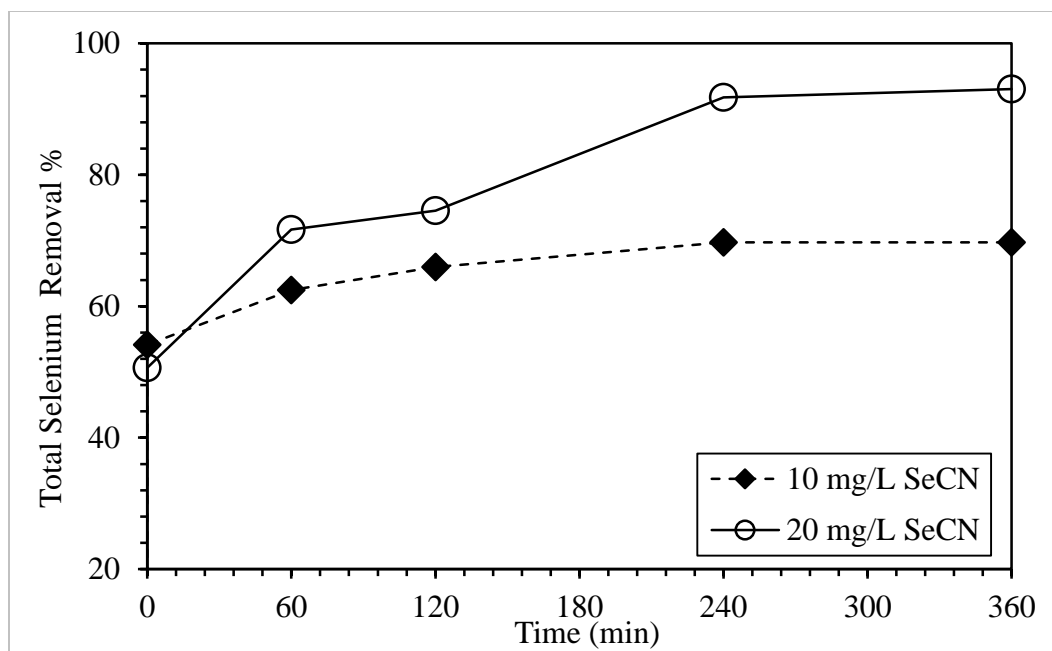
Figure 9 The Effect of selenocyanate concentration on total selenium removal using Fenton process (300 mg/L H_2O_2, 30 mg/L Fe(II), pH 4).
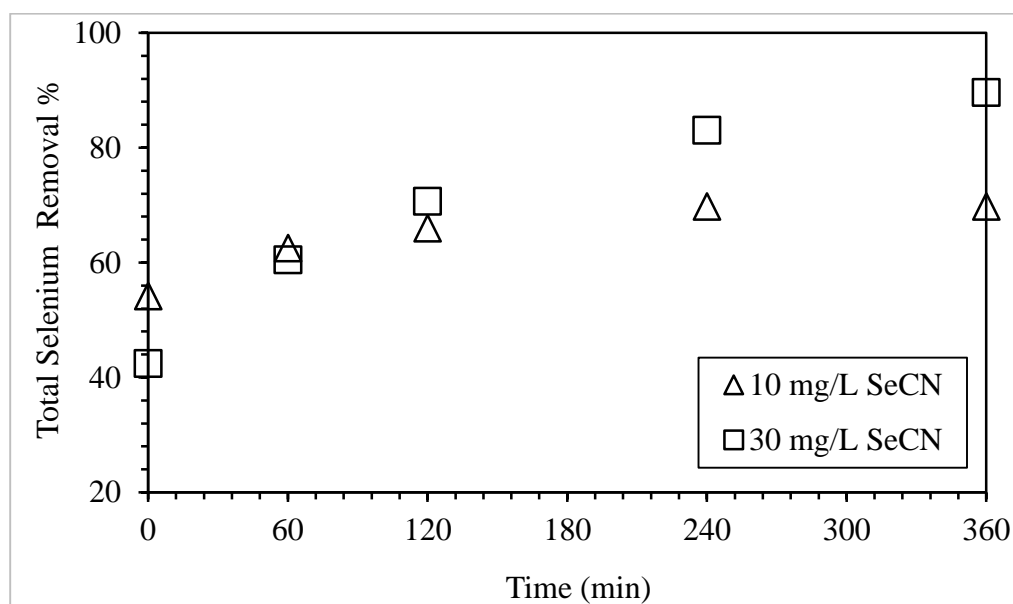
Figure 10 The effect of initial selenocyanate concentration onto its removal using Fenton process (300 mg/L H_2O_2, 30 mg/L Fe(II), pH 6).

5.2 Characterization of the prepared 2LFh

5.2.1 X-ray Diffraction Spectroscopy Results

The synthetized 2LFh product was first characterized using XRD technique. Figure 11 shows the respective XRD scans of 2LFh produced in the present work. The results reveal almost identical pattern with two broad peaks at 2Ɵ at 35º and 63º, confirming the formation of an amorphous iron oxide (2LFh) [73]. However, the peaks are somewhat placed away from the results reported for 2LFh by Das et al., (2013) [21] and by Schwertmann and Cornell (2000) [72]. Such shifting is possible in XRD scanning within a reasonable range. In any case, the given results are indicative of an amorphous phase.
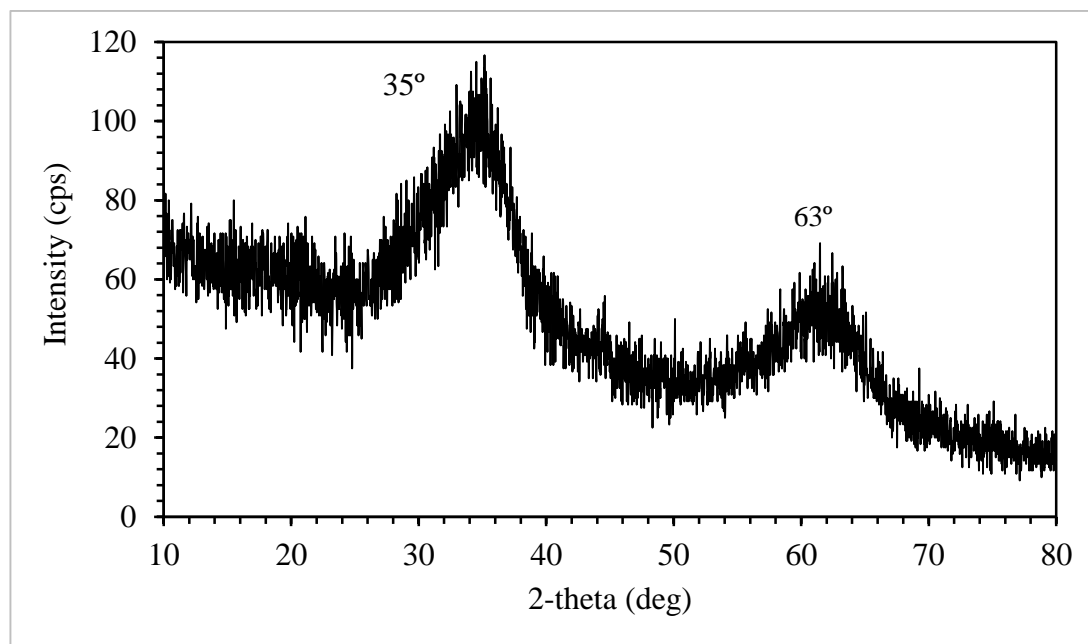
Figure 11 The XRD results for synthetized 2LFh sample

5.2.2 Attenuated Total Reflectance-Fourier Transform Infrared (ATR-FTIR) Spectroscopy results

ATR-FTIR spectra of synthetize 2LFh from 650 to 4000 cm^{-1} is shown in Figure 12. A broad peak appears at 3230 cm^{-1}, matching to the O-H stretch [75,76]. Also, Fe-OH and Fe-O are assigned at 1339, 1572 cm^{-1}, respectively [75]. Also the spectrum shows a weak band at 852 cm^{-1} which is attributed to the bending vibration of hydroxyl groups of iron hydroxides (Fe-OH) [75].
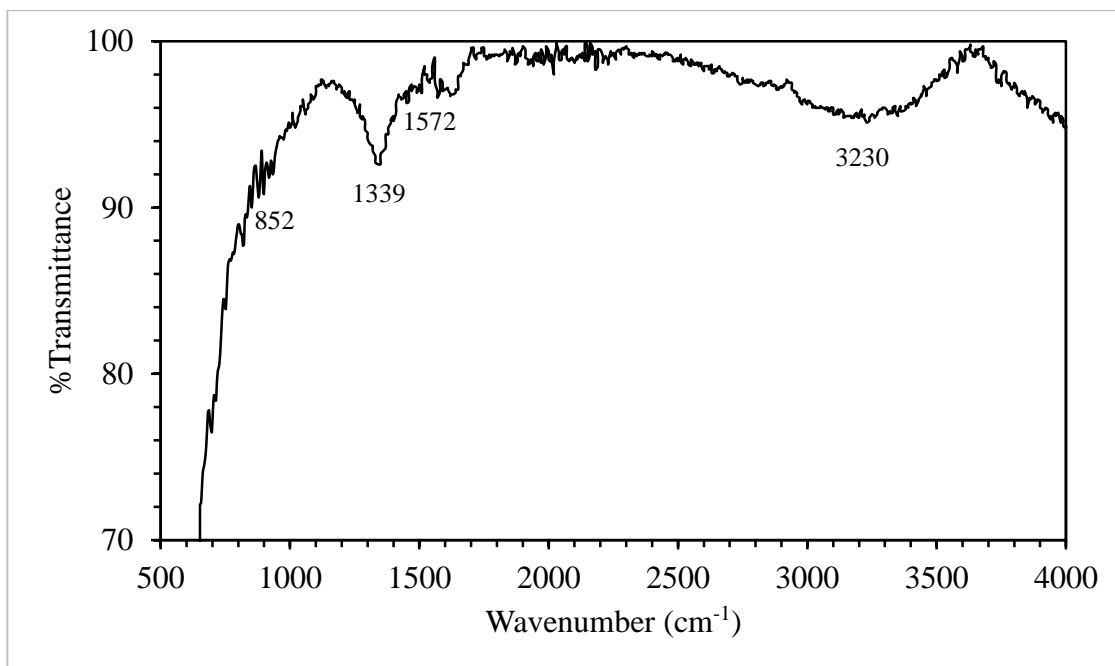
Figure 12 The ATR-FTIR spectra for 2LFh sample

5.3 Application of 2LFh for selenocyanate removal: Adsorption and Photocatalysis results

5.3.1 The adsorption of aqueous phase selenocyanate onto 2LFh

5.3.1.1 The effect of pH

Findings from adsorption of selenocyanate onto 2LFh are reported in this section. Initially, several batch experiments were conducted to examine the effect of pH onto selenocyanate adsorption and also to know the optimum pH value. Figure 13 shows the respective results for 5, 10, and 20 mg/L selenocyanate systems, under a wide range of pH between 4 to 11 at 96-hr equilibrium contact time, (it should be noted that all pH values are the final pH at equilibrium). At pH 4, we observe approx. 50% selenocyanate removal for all system, whereas at pH 5, approx. 25, 20, and 19% selenocyanate adsorption is noted for 5, 10, and 20 mg/L systems, respectively. It should however be noted that in terms of mass removal, the adsorption is still higher at higher selenocyanate concentration probably because of higher mass transfer driving force from the bulk aqueous to the bulk solid phase. Furthermore, selenocyanate adsorption decreases significantly under basic conditions (pH > 8). This could be attributed to an increase in negative charge on the solids surface with an increase in pH, resulting in electrostatic repulsion. For example, pHzpc of 2LFh is reported to be within range 5.7 and 8 [77–80]. This supports the argument that above pH 8 the surface of 2LFh will be negatively charged, thus causing electrostatic repulsion of selenocyanate anion and in turn its reduced adsorption. Furthermore, competitive adsorption of hydroxyl ions (OH$^-$) onto 2LFh surface sites will also reduce selenocyanate removal, specially at higher pH.
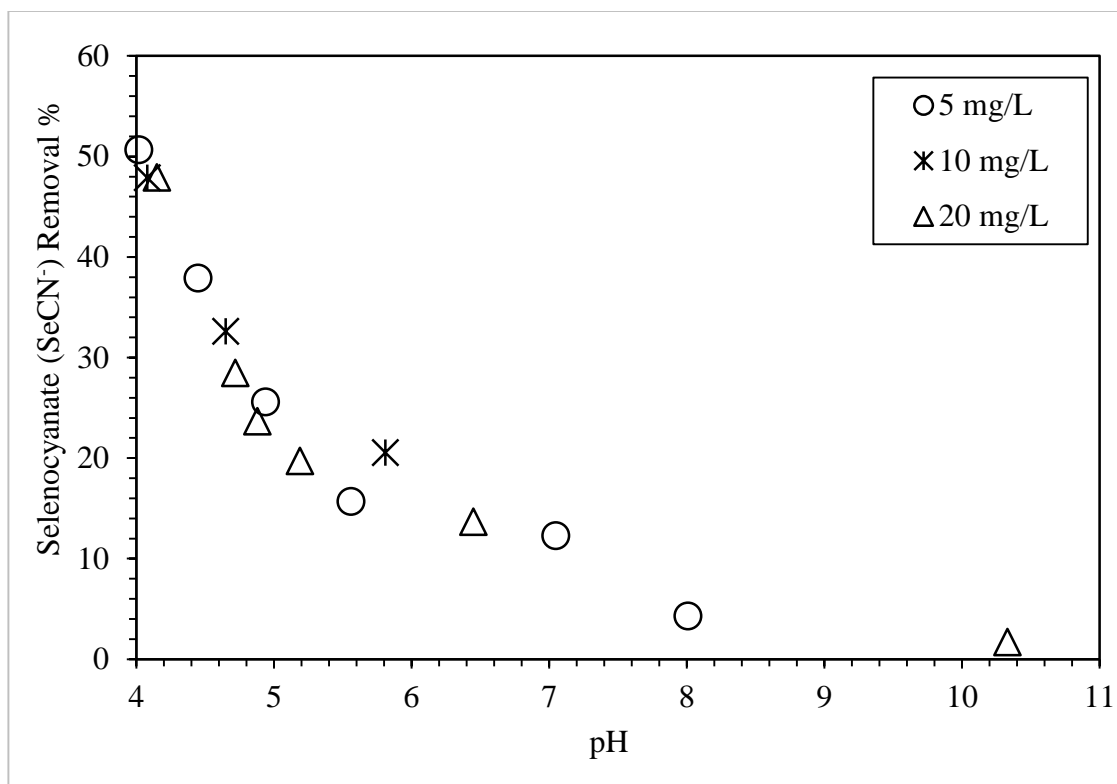
Figure 13 The effect of pH on adsorption of selenocyanate onto 2LFh (1-g/L 2LFh, 96-hr contact time).

5.3.1.2 Effect of Adsorbent Dosage

The effect of 2LFh amount onto selenocyanate uptake is given Figure 14. The initial selenocyanate concentrations tested were 2.5, 10, 20, and 50 mg/L. For the 2.5 mg/L study, we note an initial increase followed by near complete selenocyanate removal at 2-g/L 2LFh. Similarly, at higher selenocyanate concentrations of 10, 20, and 50 mg/L, its removal increases with an increase in the adsorbent amount till 3-g/L, after which adsorption reaches a plateau/saturation. Also, the percent selenocyanate removal decreases with an increase in its initial concentration. Greater percent-based adsorption at lower selenocyanate concentrations (at specific 2LFh amount) result because of comparatively higher adsorption sites availability. For example, maximum of 75, 48, and 19% selenocyanate removal transpire using 3-g/L 2LFh for the 10, 20, and 50 mg/L selenocyanate systems, respectively. Furthermore, plateau noted at adsorbent dosage more than 3-g/L may transpire because of selenocyanate in solution and at 2LFh surface reach an equilibrium. Also Figure 15 that relates the adsorption capacity (qe) to equilibrium selenocyanate concentration (Ce), shows a typical Langmuir type trend. We note a gradual increase in the adsorption capacity qe of 2LFh with an increment in Ce value, i.e., the adsorption capacity increases from 0.89 to 3 mg/g till reaching plateau (Figure 15). This supports monolayer coverage with the same surface site type, as also noted in the next section. Initially, an increase in selenocyanate adsorption with an increase in its initial concentration could result because of higher selenocyanate mass transfer driving force from bulk aqueous to bulk solid phases. Nevertheless, as the available sites reach a saturation state, the net adsorption also stabilize because of equilibra between the surface and aqueous phase selenocyanate species [77,78].
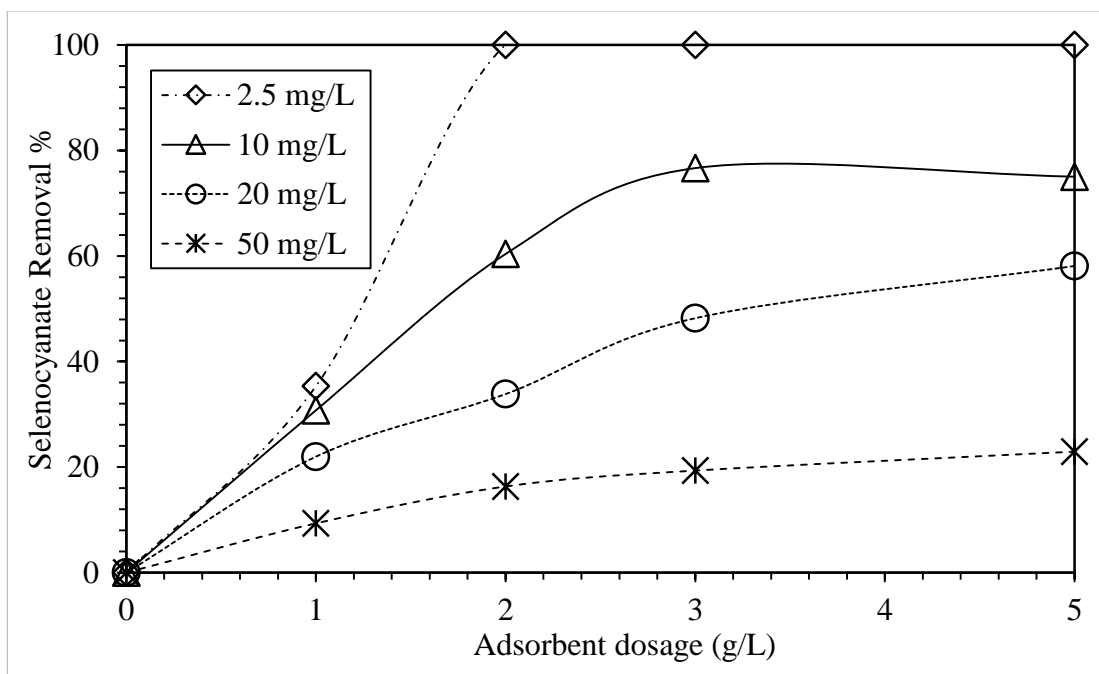
Figure 14 Effect of 2LFh dosage on the adsorption of selenocyanate at varying initial selenocyanate concentrations (pH 5, 96-hr contact time).
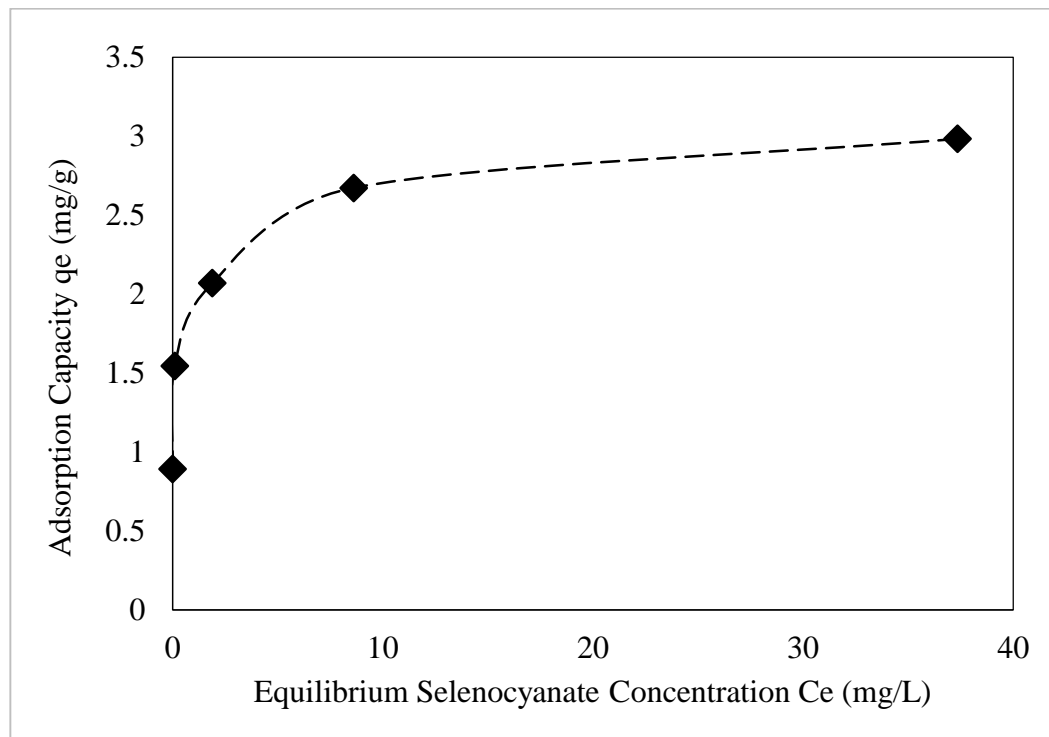
Figure 15 Adsorption isotherm of selenoyanate onto 2LFh (3-g/L 2LFh, pH 5, 96-hr contact time).

5.3.2 Application of equilibrium adsorption isotherms for the adsorption of selenocyanate onto 2LFh.

An adsorption isotherm is a quantitative relationship that describes the equilibrium between the adsorbate concentration in solution to its sorbed concentration onto a certain adsorbent surface at constant temperature [81]. The adsorption isotherm data from the present work were modeled using both Langmuir and Freundlich isotherms. There are two main assumption that the Langmuir adsorption isotherm is based on: (1) an adsorbent surface has a fixed number of surface sites, having same energy and affinity for adsorbate and (2) adsorption is reversible [81,82]. Langmuir isotherm model is presented by (6 and its linearized form is given by (7 [81,82]:

$$q_e = \frac{q_e \, K_L \, C_e}{1 + K_L C_e} \tag{6}$$

$$\frac{Ce}{qe} = \frac{1}{K_L(q_m)} + C_e \left(\frac{1}{q_m}\right) \tag{7}$$

Where,

C_e Equilibrium selenocyanate concentration (mg/L)

q_e Adsorption capacity (mg/g)

q_m The maximum adsorption capacity or Langmuir monolayer capacity (mg/g)

K_L Langmuir constant (L/mg)

Figure 16 shows the fitting of selenocyanate adsorption data according to Langmuir isotherm model by plotting Ce/q_e (g/L) versus Ce (mg/L). The resulting model parameters are given in Table 4. For the Langmuir model fitting, we note correlation coefficient equal

to 0.9993 with max adsorption capacity q_m of 3 mg/g and K_L 1.51 (L/mg). Das et al. (2012) noted a same trend for selenate species adsorption onto 2LFh surface [21].

The adsorption data were also fitted to Freundlich isotherm, which assumes a multilayer adsorption onto surface sites that may have different affinities for different adsorbates [81]. (8 and (9 give the Freundlich isotherm model and its linearized form, respectively [81,82]:

$$q_e = K_F C_e^{1/n} \tag{8}$$

$$\log(q_e) = \log(K_F) + \frac{1}{n}\log(Ce) \tag{9}$$

Where,

C_e Equilibrium selenocyanate concentration (mg/L)

q_e Adsorption capacity (mg/g)

n   Adsorption intensity ($1 \geq n \geq 10$)

K_F Freundlich capacity factor [(mg/g)(L mg^{-1})$^{1/n}$]

Figure 17 provides the fitting results, and Table 4 summarize the Freundlich isotherm parameters. The trend reported in Figure 17 shows an irregular fit. Hence, comparing the results from the Langmuir and Freundlich isotherm models indicate that selenocyanate adsorption onto 2LFh surface is well represented by the Langmuir isotherm model, as also noted previously (Figure 15). In summary based on the aforementioned finding (Figure 15) and also adsorption isotherm results (Figure 16), selenocyanate adsorption onto 2LFh can be represented by the Langmuir isotherm.
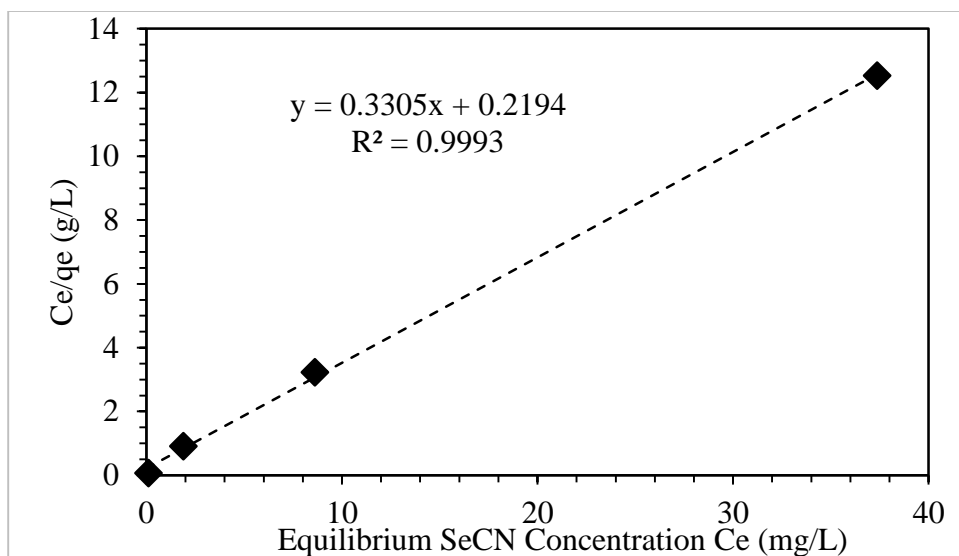
Figure 16 Langmuir adsorption isotherm for Selenocyanate adsorption using 2LFh at pH 5 for 96-hr contact time.
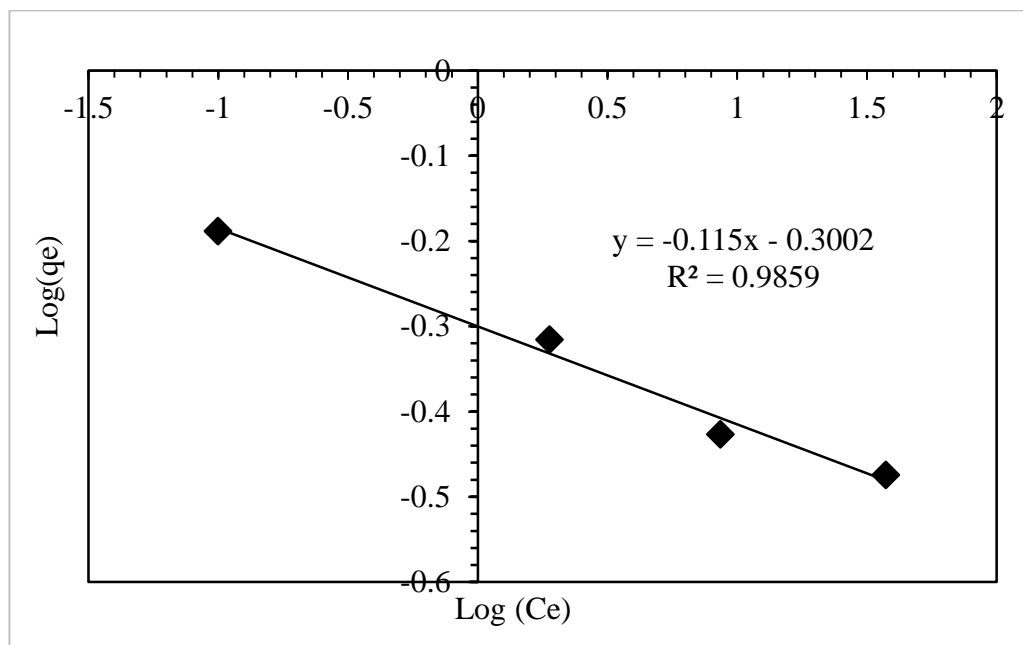
Figure 17 Freundlich adsorption isotherm for Selenocyanate adsorption using 2LFh at pH 5 for 96-hr contact time.

Table 4 Adsorption isotherm constants for Langmuir and Freundlich isotherms for the adsorption of aqueous phase selenocyanate onto 2LFh surfaces.

Langmuir Isotherm Parameters			Freundlich Isotherm Parameters		
q_m (mg/g)	K_L (L/mg)	R^2	K_F [(mg/g)(L/mg)$^{1/n}$]	n	R^2
3	1.51	0.9993	0.501	9.09	0.9859

5.3.3 Adsorption kinetics for selenocyanate adsorption onto 2LFh

Generally, the design of adsorption systems requires a better understanding of process kinetics for optimum design of a full scale reactor [83]. Hence, the kinetics of selenocyanate adsorption onto 2LFh was also studied. In this regard, results from batch experiments carried out at different selenocyanate concentrations of 5, 10, and 20 mg/L and 3-g/L 2LFh are given in Figure 18. For the 5 and 10 mg/L selenocyanate systems, we note an initial sharp uptake followed by a gradual uptake, whereas for the 20 mg/L selenocyanate system, only a gradual uptake is noted. Data shown in Figure 18 was fitted to the first and second order kinetic models as given below by (10 and (11, respectively [81,84].

$$\ln(C_t/C_0) = -K_1.t \qquad\qquad (10)$$

$$^1\!/_{C_t} = K_2.t + ^1\!/_{C_o} \qquad\qquad (11)$$

Where,

K_1 The rate constant of first order kinetics (min^{-1})

K_2 The rate constant of second order kinetics (L/mg.min)

C_o Initial selenocyanate concentration (mg/L)

C_t Selenocyanate concentration at time t, (mg/L)

Figure 19 and Figure 20 present plots for the first and second order kinetics, and their rate constants values are given in Table 5. The rate constant varies between 0.0031 min^{-1} for 5 mg/L to 0.0039 min^{-1} for 20 mg/L systems. For the second order kinetics model, Table 5 and Figure 20 illustrate that order rate constant decreases with an increase in the initial selenocyanate concentration; for 5, 10, and 20 mg/L selenocyanate systems, the second order rate constants are 0.008, 0.004, 0.003 L/mg.min, respectively. Overall, the results show that adsorption kinetics of selenocyanate is described well by second order kinetics model.

Table 5 Kinetic parameters for selenocyanate adsorption of selenocyanate onto the 2LFh

Selenocyanate Concentration (mg/L)	First-order Parameters		Second-order Parameters	
	Rate constant K_1 (min^{-1})	R^2	Rate constant K_2 (L/mg.min)	R^2
5	0.0031	0.8554	0.0008	0.8927
10	0.0027	0.9252	0.0004	0.9459
20	0.0039	0.9906	0.0003	0.9738
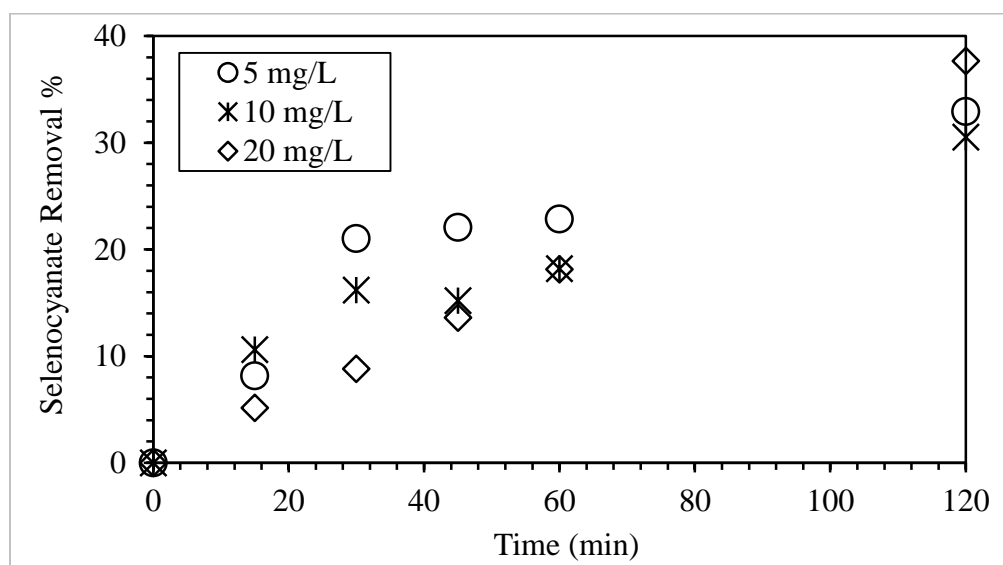
Figure 18 Adsorption of selenocyanate onto 2LFh with respect to time (3-g/L 2LFh, pH 5).
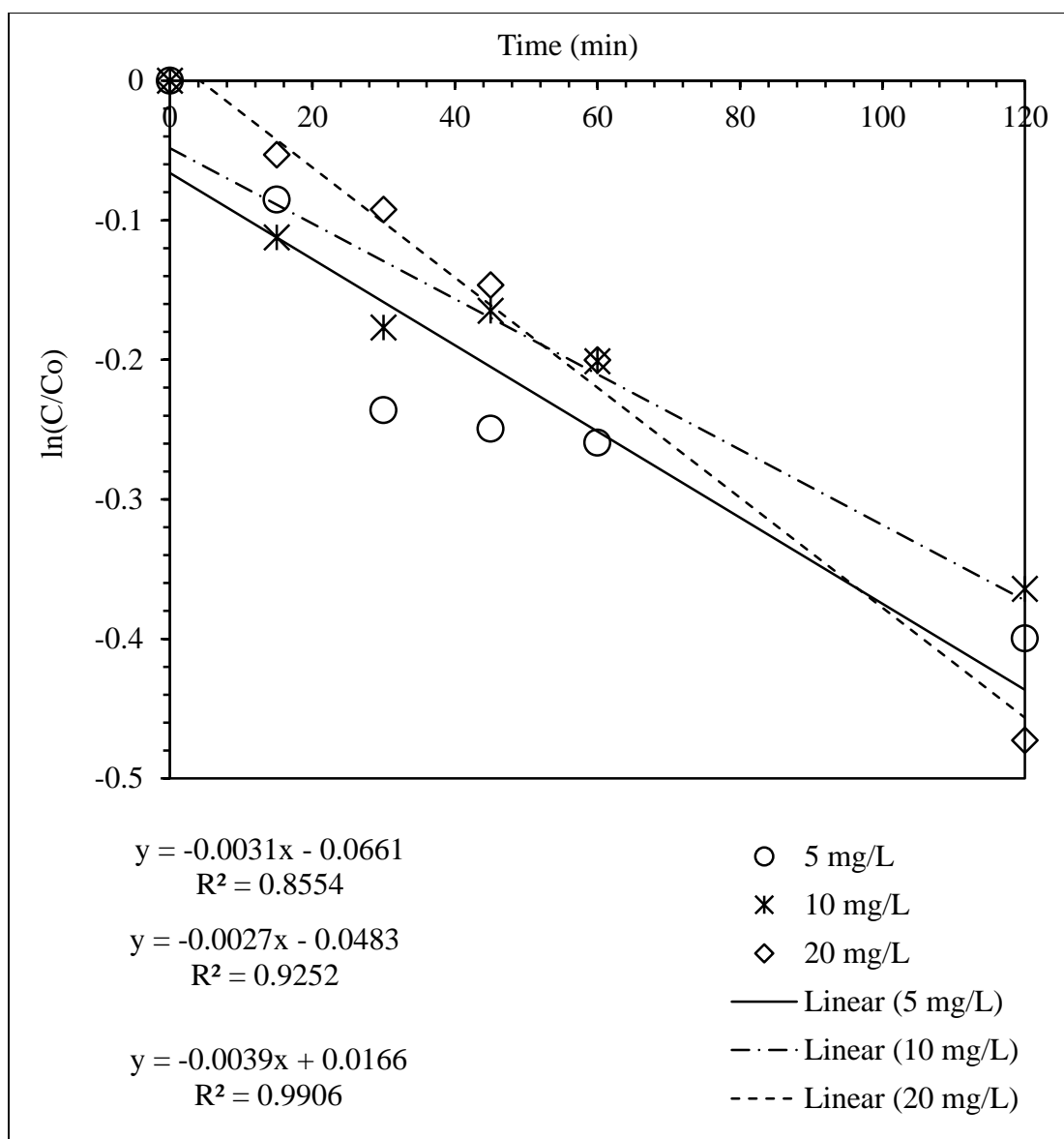
Figure 19 First-order kinetic plot for selenocyanate adsorption onto 2LFh (3-g/L 2LFh, pH 5).
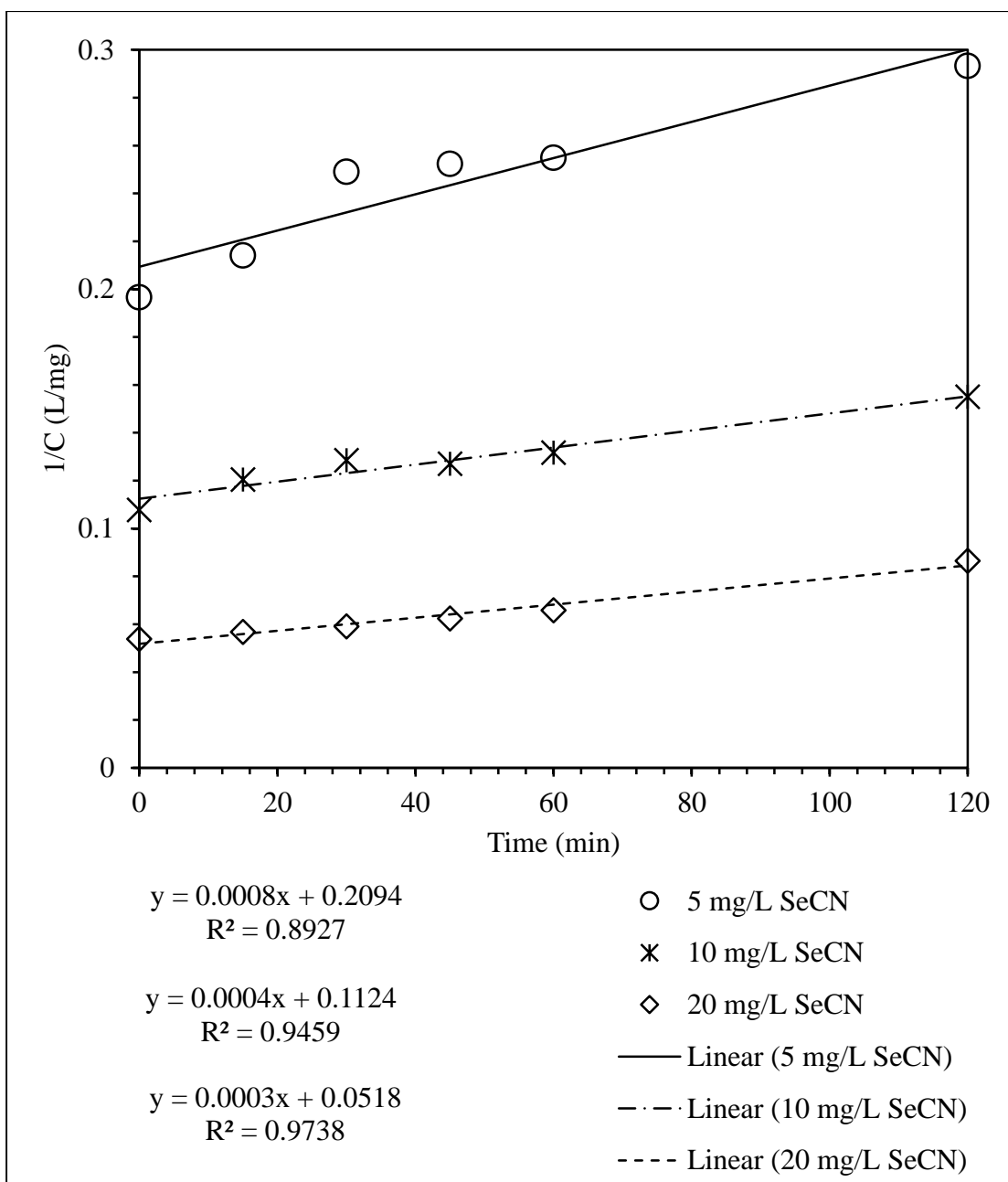
Figure 20 Second-order kinetic plot for selenocyanate adsorption onto 2LFh (3-g/L 2LFh, pH 5).

5.3.4 The removal of selenocyanate species using photocatalysis

5.3.4.1 Results from batch experiments

Selenocyanate species removal using photocatalysis based advanced oxidation process was also studied in this work. The photocatalytic experimental details were described earlier in chapter 4. Initially, several 20 mg/L selenocyanate photocatalysis batch experiments were conducted under different conditions, i.e., use of only UV light, use of a combination of UV light and 2LFh, and use of a combination of UV radiation and TiO_2. This was to investigate the possibility of using metal oxide 2LFh as a photocatalyst for selenocyanate removal. Figure 21 that shows the respective experimental results indicates no selenocyanate removal with only UV exposure over 360-min. These findings are similar to those noted by Vohra (2015) [50]. Similarly, it is also observed that using UV with 2LFh also yields only a negligible decrease in selenocyanate species at 360-min reaction time. It should be noted that the earlier reported selenocyanate adsorption based removal using 2LFh provided a long equilibrium time of 96 hr that did yield the reported adsorption and removal, whereas in the photocatalysis experiments the contact time is very small. On the other hand for the third experiment using TiO_2 gives complete selenocyanate complex destruction in 120 min as shown in Figure 21. Hence, the destruction of the selenocyanate complex is successfully initiated by hydroxyl-radicals ($\bullet$OH) that are produced during photocatalytic degradation (PCD) process [50]. Hoffmann et al., (1995) [85] elucidated use of TiO_2 during photocatalysis and the respective reaction mechanism are represented by (12 and (13;

$$TiO_2 + h\nu \rightarrow e^- + h^+ \tag{12}$$

$$Ti - OH^- + h^+ \rightarrow Ti - OH\bullet \tag{13}$$

(12 shows that when a TiO_2 particle is exposed to UV radiation (~352 nm), it adsorbs the light energy, leading to excitation of the valence band (VB) electrons/e^-. Consequently, the electrons are transferred to the conduction band (CB) of respective TiO_2 particle. This reaction produces in turn an electron/hole pair (e^-/h^+). Moreover, the h^+ species in VB is considered as electron deficient that scavenges an electron from the hydroxyl species (OH^-) adsorbed onto surface of TiO_2 and generates powerful hydroxyl radicals ($\bullet OH$), which break down the selenocyanate complex, eventually converting it to oxidized selenite (SeO_3^{2-}) and then to selenate species (SeO_4^{2-}) along the reaction as shown in Figure 22. We further investigated the use of 2LFh metal oxide along withTiO_2 as explained in the following sections.
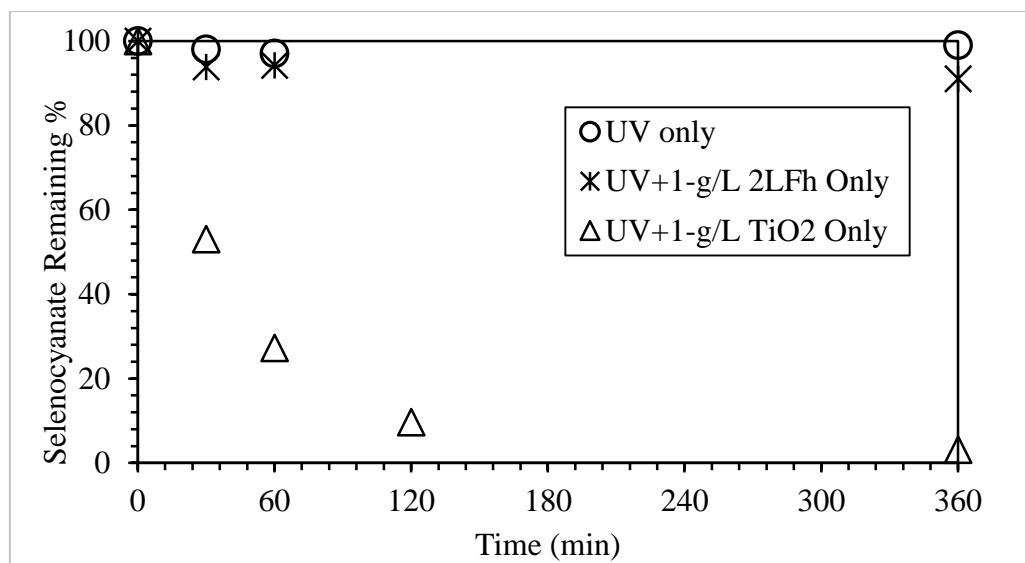
Figure 21 The destruction of selenocyanate complex under varying experimental conditions: 1) in the presence of UV light only, 2) in the presence of UV light with 2LFh only, and 3) in the presence of UV light with TiO_2 only (20 mg/L selenocyanate, 1-g/L 2LFh, 1-g/L TiO_2, 15 W UV lamp, pH 5)
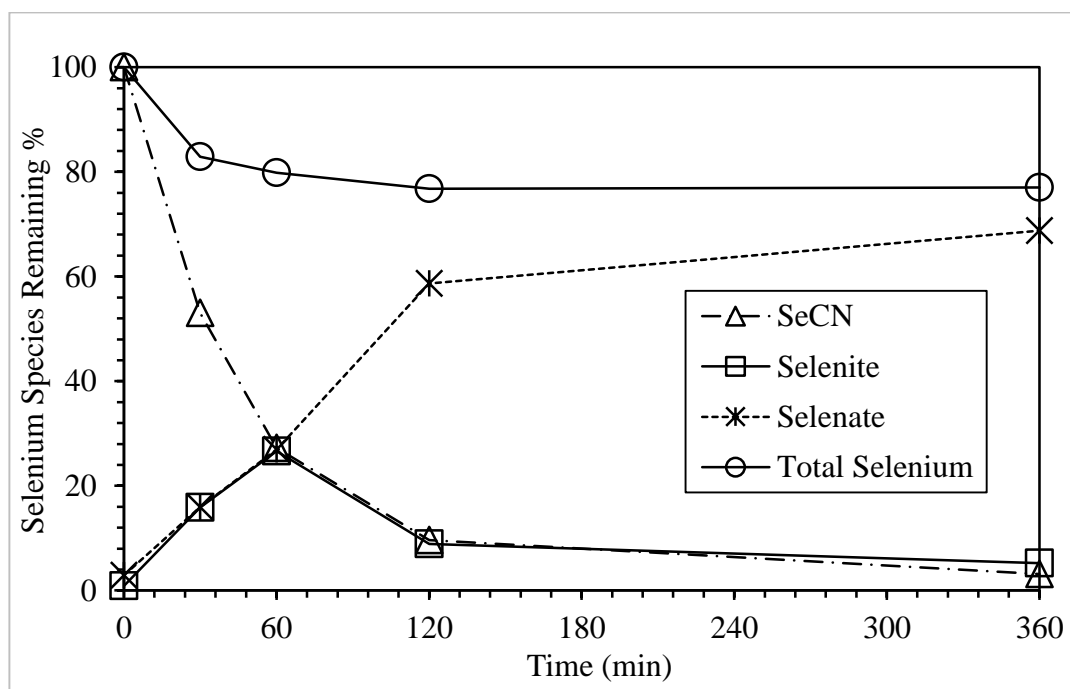
Figure 22 Destruction of selenocyanate complex and formation of other selenium species (selenite and selenate) using photocatalysis using TiO_2 (20 mg/L selenocyanate, 1-g/L TiO_2, 15 W UV lamp, pH 5).

5.3.4.2 Use of 2LFh for the removal of different selenium species produced during photocatalysis selenocyanate complex

In the previous section (5.3.4.1), we noted that using only 2LFh metal oxide with UV lamp light did not remove selenocyanate species. We thus investigated the use of 2LFh along with TiO_2 for selenocyanate removal to know the possibility of achieving complete selenium species removal, via a two-path way reaction, i.e. breaking down of selenocyanate complex by the TiO_2 photocatalysis followed by the adsorption of released selenium species onto 2LFh. Please note that previous TiO_2-based system has reported use of reducing agents such as formate to initiate reduction of selenite/selenate to elemental selenium that follows removal of selenium via precipitation. However in the present case, the produced oxidized Se-species can be eventually removed by adsorption onto 2LFh, as reported earlier by Das et al., (2013) [21].

5.3.4.3 Initial adsorption results

Before starting photocatalysis experiments, adsorption of selenocyanate onto TiO_2 only and 2LFh/TiO_2 was first examined via 30-min pre-adsorption time because of its importance during photocatalysis of selenium species. The respective results as presented in Figure 23 show the effect of pH on initial selenocyanate adsorption onto TiO_2 only and 2LFh/TiO_2 surfaces. Though we note negligible selenocyanate adsorption onto TiO_2 only at pH 5 and 9; about 7% selenocyanate removal is obtained using 2LFh/TiO_2 at pH 5, but its adsorption at pH9 is neglected. (It should be noted that details of selenocyanate adsorption onto 2LFh using longer equilibrium time has been discussed in section 5.3.1.1).
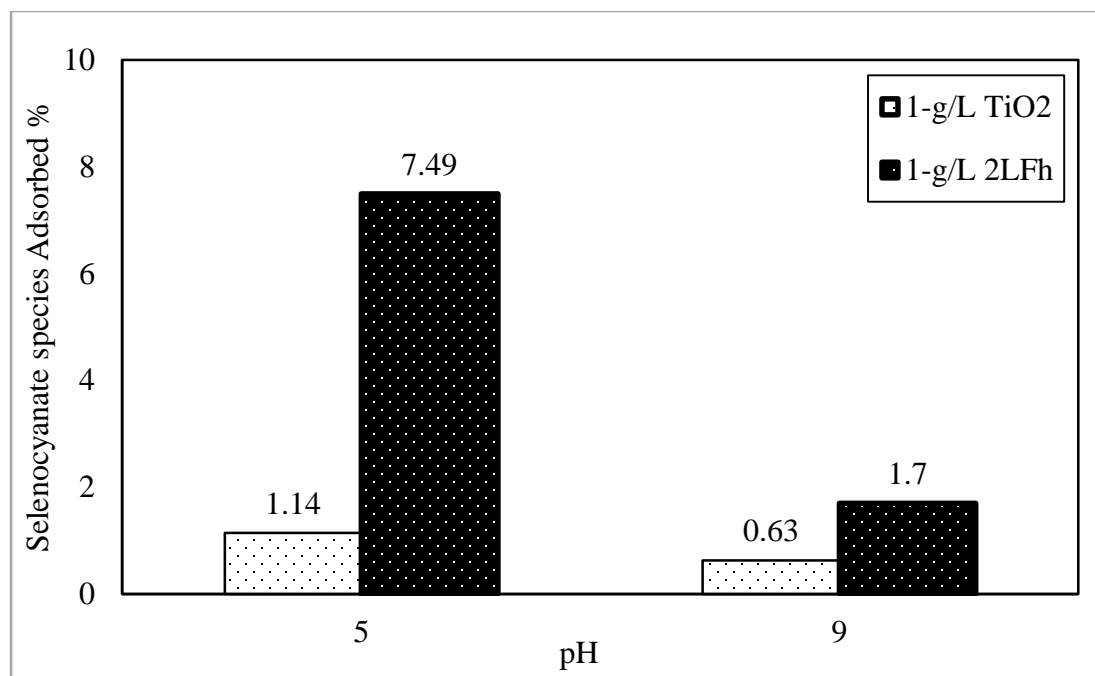
Figure 23 Initial adsorption of selenocyanate before explosure to UV-light during PCD experiments (20 mg/L selenocyanate, 30 min contact time, 1-g/L TiO₂, 1-g/L 2LFh)

5.3.4.4 Effect of pH onto photocatalytic removal of selenocyanate

In this section, we examine the effect of pH during 2LFh/TiO$_2$ based photocatalytic selenocyanate removal. Figure 24 shows that selenocyanate species disappears gradually over 360-min reaction time with approx. 85% of selenocyanate removal noted at 2 hr and near complete removal at 6 hr. Furthermore, Figure 25-(a) that provides the total selenium results in the absence and presence of 2LFh, showing that in the absence of 2LFh, approx. 20% of total selenium is removed, whereas using TiO$_2$ with 2LFh during photocatalysis causes a gradual decrease in the total selenium over 6-hr remediation time until its near complete removal. Also, Figure 25-(b) compares the selenite trends during the destruction of selenocyanate complex both without and with 2LFh (the results are given as percent of total initial selenium). In the absence of 2LFh, selenite anions buildup at an earlier stage to reach 25% at 60 min. Thereafter, the selenite species decrease to a complete disappearance. However in the presence of 2LFh, the selenite species builds only to 4% at 60 min and then disappears completely. Also, Figure 25-(c) that compares the selenate trends shows a clear difference between the two systems, i.e., in absence and presence of 2LFh. For the former case, selenate species progressively continues to build reaching 65% selenate. On the other hand, in the presence of 2LFh, we note only 7% selenate species at 360 min.

Two more batch experiments were conducted at pH 9 to further investigate the above noted degradation trends for selenocyanate to elucidate on the main removal mechanisms. The results are shown in Figure 26 and Figure 27. Figure 26 presents the removal of selenocyanate species using PCD in the absence of 2LFh. It is evident that though the general trends at pH 9 are almost similar to trends at pH 5, but at pH 9 selenocyanate is removed at 120 min. Moreover, a significant buildup of selenite species along with a

gradual selenate increase is noted, i.e., about 65 and 28% selenite and selenate species, respectively (at 2 hr). After 120 min, the selenite species starts to decrease gradually while getting oxidized to selenate. But, the results indicate negligible total selenium removal over 6-hr reaction time. On the other hand as shown in Figure 27 and Figure 28-(a), adding 1-g/L 2LFh to the system results in about 40% total selenium removal in 360 min, and a clear difference is evident between the two systems at higher pH value. Also, the removal of selenite species (for the above two systems) formed during the selenocyanate destruction is given in Figure 28-(b). It is observed that about only 10% selenite species remains in the aqueous phase at 360-min reaction time. Figure 28-(c) shows about 40% selenate remaining in the solution with greater removal noted for the combined $2LFh/TiO_2$ system. Hence, we can clearly see the role of using 2LFh metal oxide on the removal of all selenium species during selenocyanate destruction along with the effect of pH on the total removal efficiency, i.e., reduced overall selenium removal noted at pH 9 because of reduced adsorption, as also discussed earlier.

We also further looked into what really causes high total selenium removal using 2LFh during the PCD process. In this regard, additional adsorption experiments were conducted to find out the removal of single solute selenite and selenate species using only 2LFh. For single 20 mg/L selenite and 20 mg/L selenate systems at pH values of 5, 7, and 9, we note the following details: for the selenite system, approx. 96% selenite removal is noted at pH 5, whereas approx. 56% removal transpires at pH 7 that further reduces to 22% at pH 9 (Figure 29). Similar to selenite findings, selenate removal also decreases with an increase in the initial pH; approx. 95% and 45% selenate removal transpires at pH 5 and 7 respectively as shown in Figure 29 and negligible at pH9, which could be attributed to an

increased electrostatic repulsion due to 2LFh tuning anion at pH above pH_{zpc}, as also discussed previously in section (5.3.1.1). Hence, though 2LFh has a special affinity for selenite and selenate species, however it decreases with an increase in pH. These findings are similar to those reported in previous studies [21,86,87]. Hence, we could explain the higher selenium removal using 2LFh during PCD destruction selenocyanate. While selenocyanate complex gets destroyed due to hydroxyl radicals generated by excitation of TiO_2, significant selenite and selenate species buildup starts increasing in the absence of 2LFh. However in the presence of 2LFh, these species get simultaneously adsorbed onto 2LFh, which is a better adsorbent. This eventually yields near complete total selenium species removal at acidic pH 5 (Figure 29).

Figure 24 The removal of removal of all dissolved selenium associated species during the destruction of the selenocyanate complex using photocatalysis with 2LFh (20-mg/L selenocyanate, 1-g/L 2LFh, 1-g/L TiO_2, 15 W UV lamp, pH 5).

Figure 25 Comparison between use of TiO$_2$ only and TiO$_2$/2LFh during selenocyanate photocatalysis-adsorption based treatment: (a) total selenium trends, (b) selenite trends, and (d) selenate trends (20 mg/L selenocyanate, 1-g/L TiO$_2$, 1-g/L 2LFh, 15 W UV lamp, pH 5).

Figure 26 Destruction of selenocyanate complex and formation of other selenium species (Selenite and Selenate) using photocatalysis using only 1-g/L TiO$_2$ at pH 9 (20 mg/L selenocyanate, 15 W UV lamp).

Figure 27 The removal of removal of all dissolved selenium associated species during the destruction of the selenocyanate complex using photocatalysis with 2LFh (20-mg/L SeCN$^-$, 1-g/L 2LFh, 1-g/L TiO$_2$, 15 W UV lamp, pH 9).
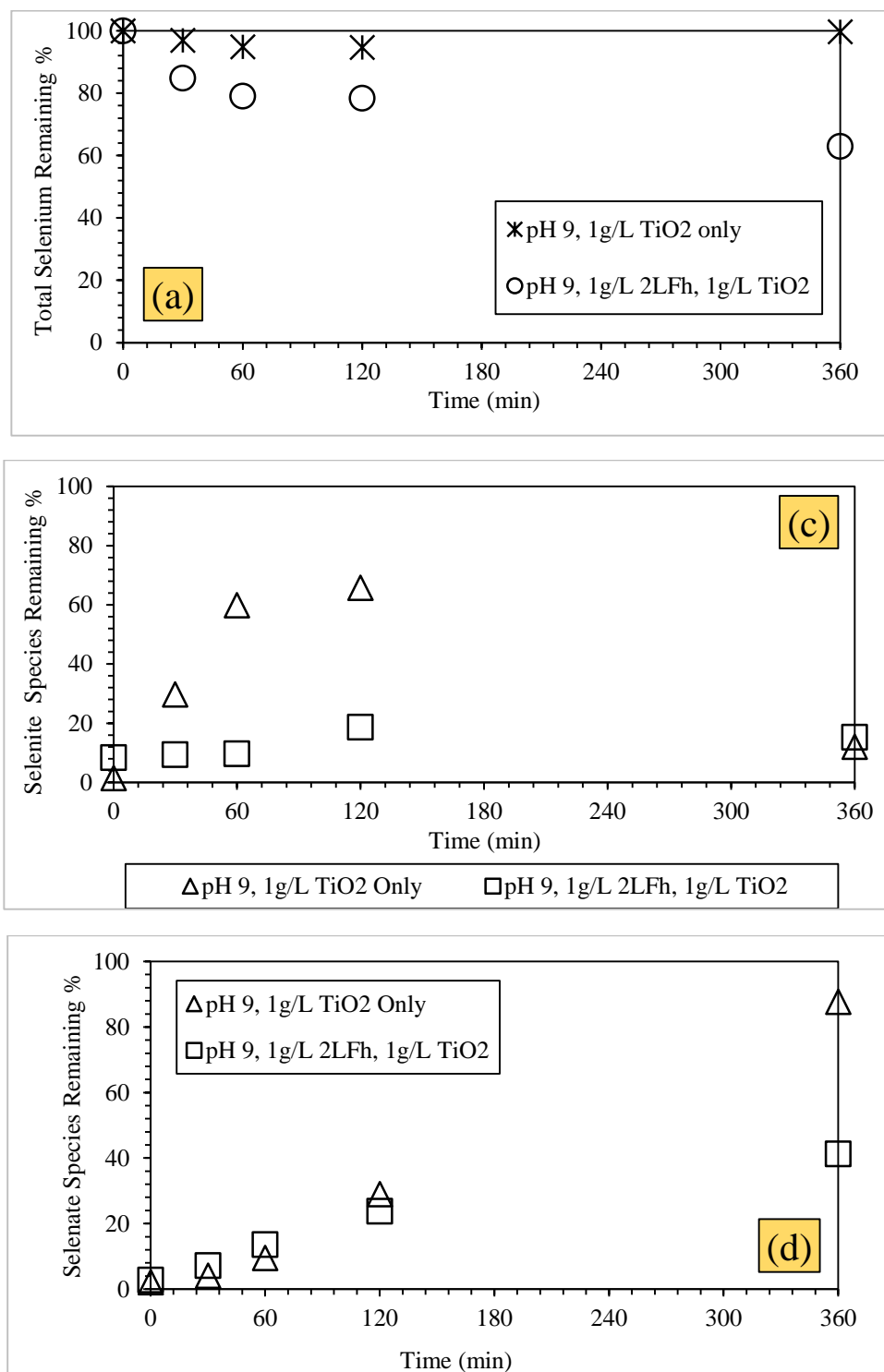
Figure 28 Comparison between use of TiO$_2$ only and TiO$_2$/2LFh during selenocyanate photocatalysis-adsorption based treatment: (a) total selenium trends, (b) selenite trends, and (d) selenate trends (20 mg/L selenocyanate, 1-g/L TiO$_2$, 1-g/L 2LFh, 15 W UV lamp, pH 9).
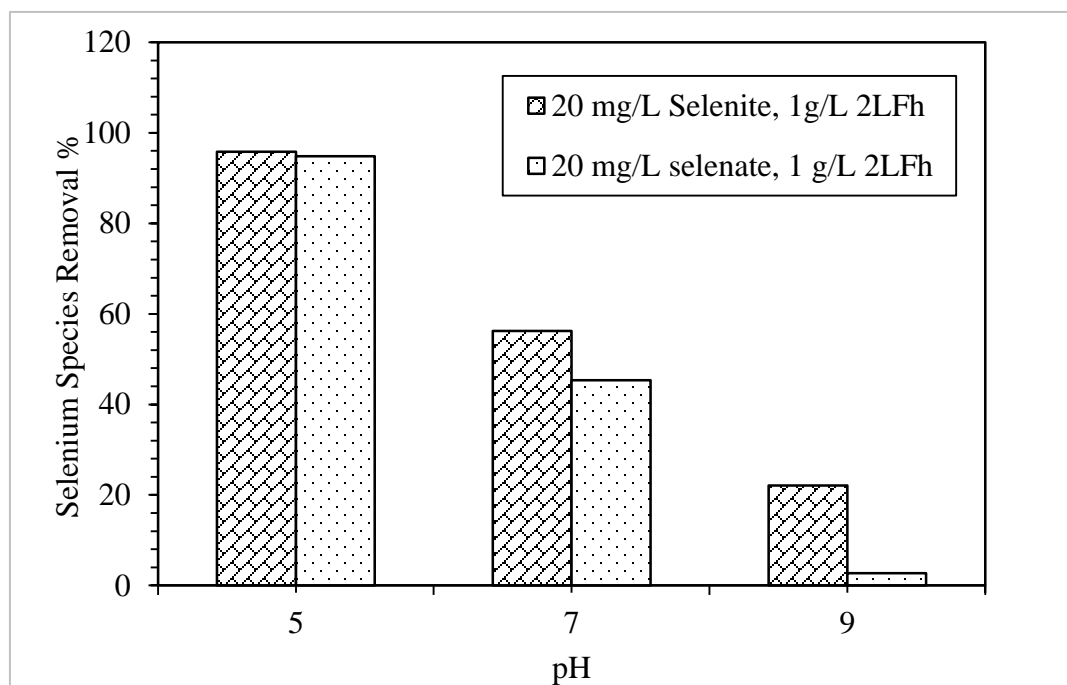
Figure 29 The effect of pH on adsorption of single solute systems selenite and selenate onto 2LFh surface (20 mg/L selenite, 20 mg/L selenate, 1-g/L 2LFh, 24-hr equilibrium time).

5.3.4.5 Effect of 2LFh amount onto photocatalysis

In the previous section, we noted the removal of total selenium during the destruction of selenocyanate complex due to TiO_2 based and 2LFh based adsorption of different selenium species. Taking this into consideration, we further examined the effect of 2LFh amount onto the removal of respective selenium species. In this regard, two additional experiments were conducted at 0.5 and 1.5 g/L 2LFh with (20 mg/L selenocyanate, 1-g/L TiO_2, UV light, pH 7). Figure 30 and Figure 31 show the respective results of these experiments, whereas Figure 32 summarizes the comparison between two systems. The results clearly show the effect of 2LFh amount onto the gradual removal of total selenium (Figure 32-(a)). For example, about 30% total selenium removal is obtained at 60-min reaction time when only 0.5-g/L 2LFh is used, after which the reaction reaches a plateau. However, the total selenium remaining decreases gradually when we use 1.5 g/L 2LFh, achieving approx. 90% removal in 360-min treatment period (Figure 32-(a)). In contrast, the amount of 2LFh has no significant effect onto selenocyanate complex destruction as illustrated in Figure 32-(b). The selenite results, as shown in Figure 32-(c), show small amounts, for both 2LFh amounts. It should be noted at lower 2LFh of 0.5-g/L, 2LFh gets saturated in the first 30 min due to adsorption of selenite and some of selenate species in the earlier stages, which could also be the reason for higher selenate buildup (approx. 65%) (Figure 32-(d)). On the other hand at higher 2LFh amount of 1.5-g/L, both selenite and selenate species are simultaneously adsorbed onto 2LFh at higher rate, showing near complete removal as shown in Figure 32-(c-d).
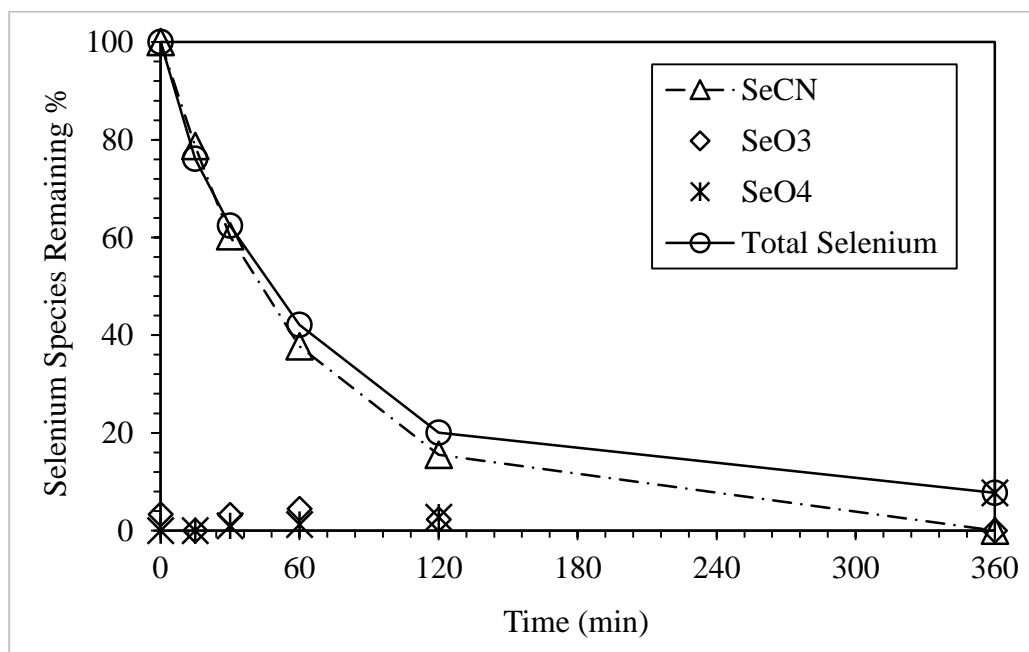
Figure 30 The removal of removal of all dissolved selenium associated species during the destruction the selenocyanate complex using photocatalysis with 2LFh (20 mg/L selenocyanate, 0.5-g/L 2LFh, 1-g/L TiO_2, , 15 W UV lamp, pH 7).
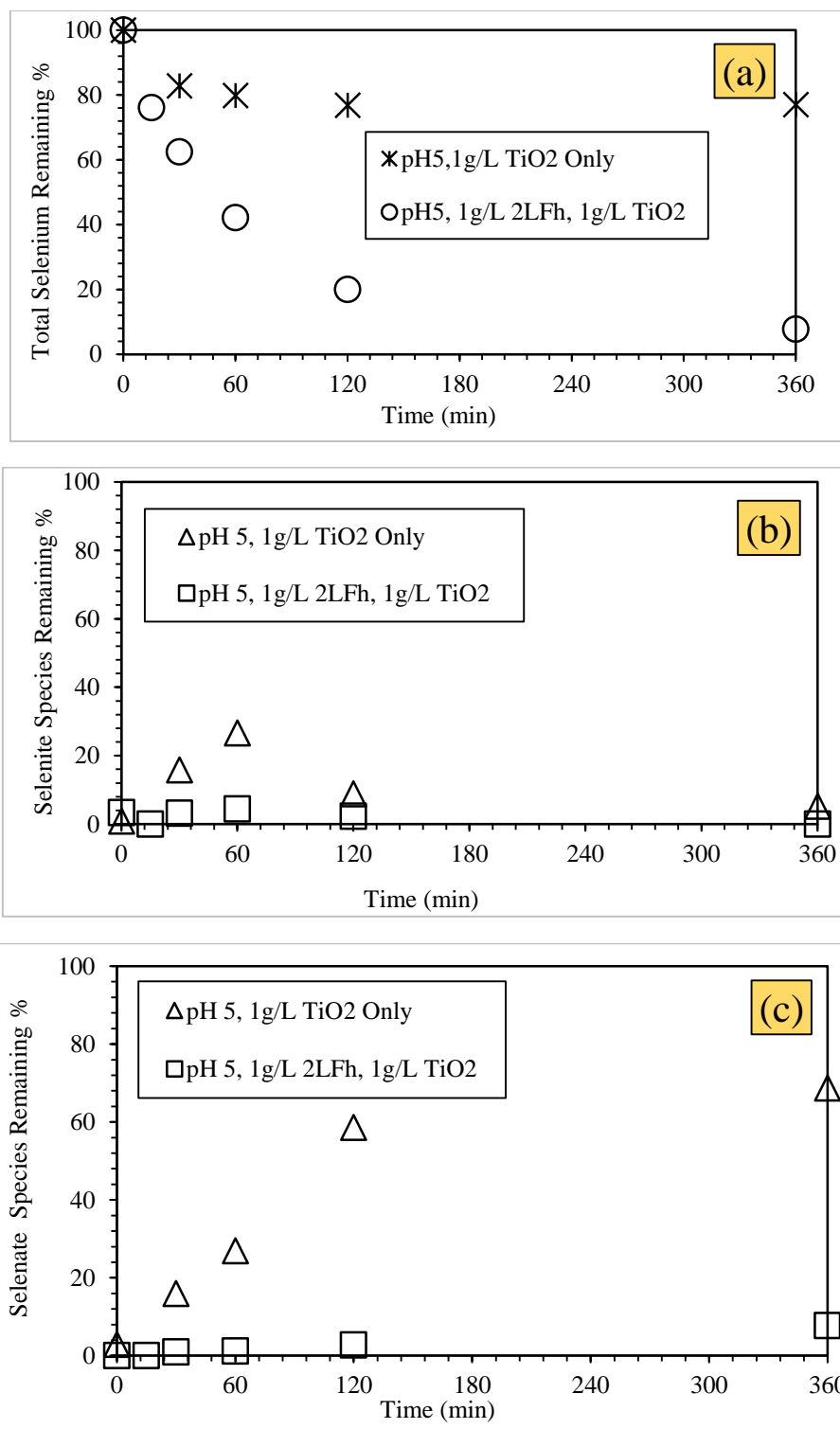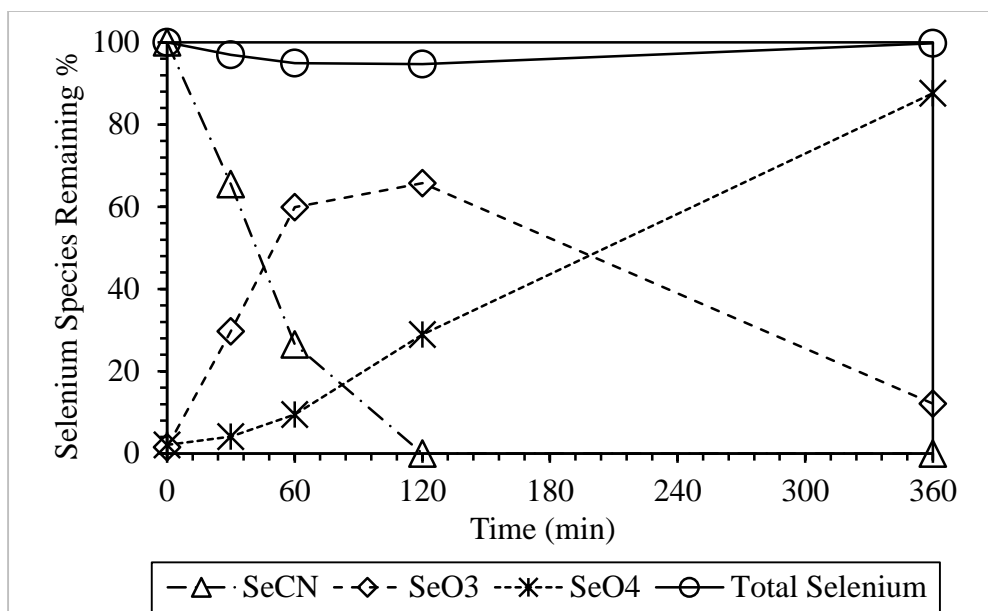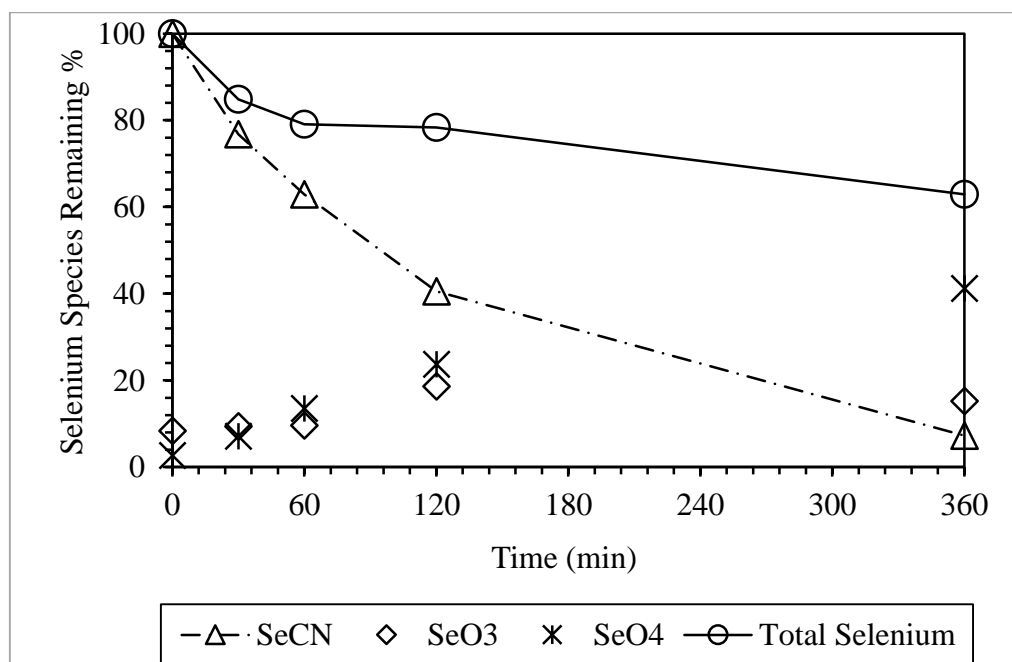
Figure 31 The removal of removal of all dissolved selenium associated species during the destruction of selenocyanate complex using photocatalysis with 2LFh (20 mg/L selenocyanate, 1.5-g/L 2LFh, 1-g/L TiO_2, , 15 W UV lamp, pH 7).

Figure 32 The effect of 2LFh amount onto the removal of (a) total selenium remaining, (b) selenocyanate remaining, (c) selenite remaining, and (d) selenate remaining associated species during destruction of selenocyanate complex using photocatalysis (20 mg/L selenocyanate, 1-g/L TiO_2, 15 W UV lamp, pH 7).

5.3.4.6 Effect of initial selenocyanate concentration onto photocatalysis

We also investigated the influence of selenocyanate concentration onto removal of different selenium species during selenocyanate removal. Two additional experiments were carried out at 10 mg/L initial selenocyanate concentration and pH 5 and 9. The respective results of the two experiments are given in Figure 33-(A&B), whereas Figure 34 and Figure 35 compare these results to respective 20 mg/L selenocyanate results. It is noted that at pH 5 the total selenium removal decreases with an increase in the initial selenocyanate concentration as shown in Figure 34-(a), i.e., approx. 90% and 80% removal are observed at 120-min reaction time from 10 to 20 mg/L selenocyanate systems (Figure 34-(a)). We also observe similar trends for selenocyanate species (Figure 34-(b)). Figure 34-(c) that shows the selenite results indicates that selenite species generated during photocatalysis is instantaneously adsorbed onto 2LFh. On the other hand for selenate species, near complete removal is obtained in 360 min with no significant effect of initial selenocyanate concentration (Figure 34-(d)), which could be attributed to its simultaneous adsorption onto 2LFh. We also observe qualitatively similar trends at pH 9 as illustrated in Figure 35, though adsorption of selenite and selenate is lower as noted before as well. In summary, the above results show that the use of TiO_2/2LFh particles during photocatalysis causes destruction of selenocyanate complex with simultaneous adsorption of reaction intermediates (selenite and selenate) at acidic pH of 5 that can be successfully removed from the respective wastewater streams. Hence, use of 2LFh along with TiO_2-PCD offers a viable process for the treatment of selenocyanate contaminated waters.
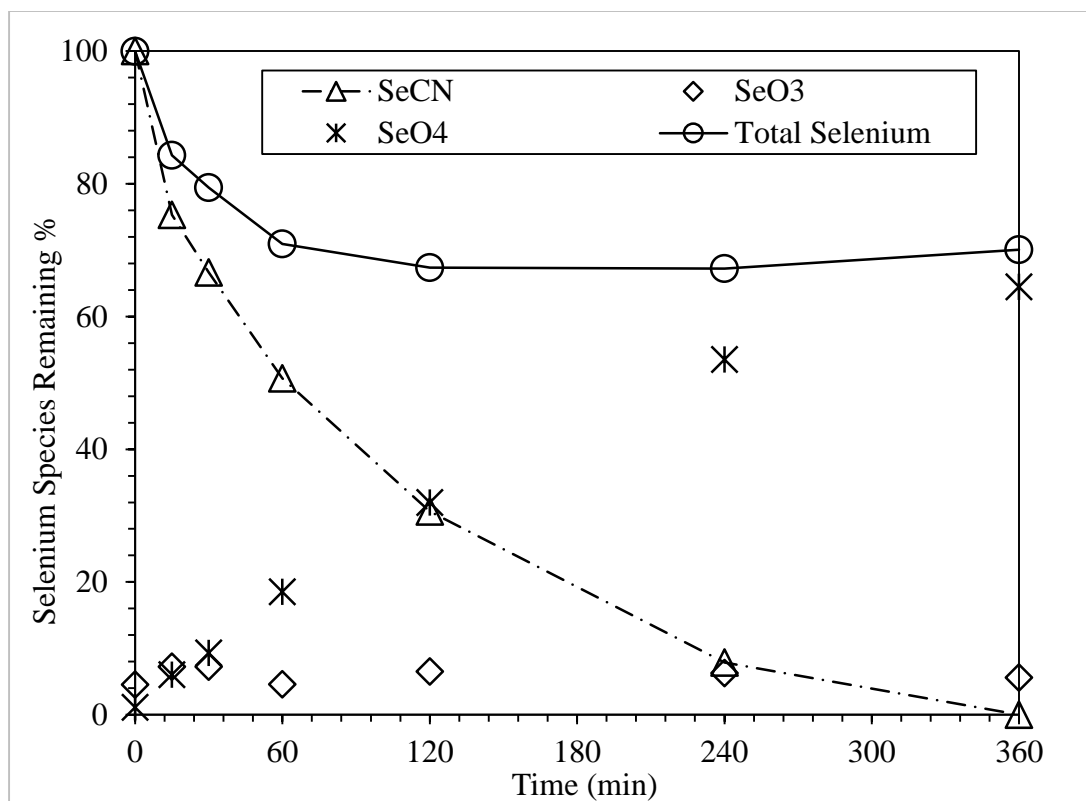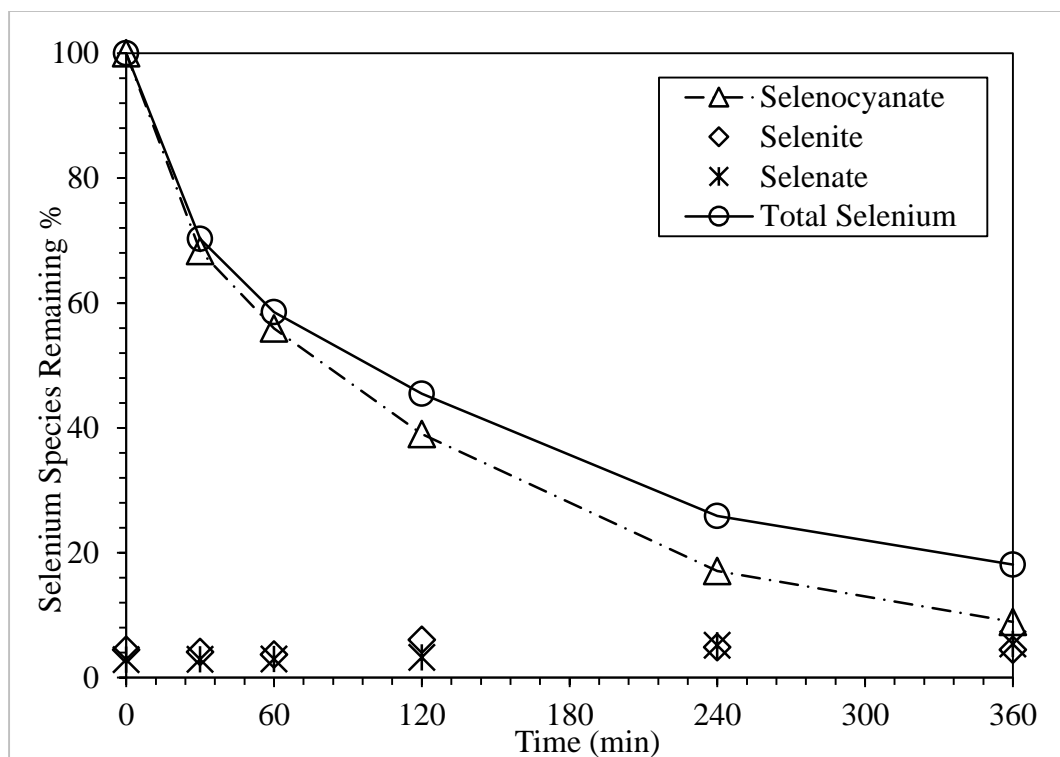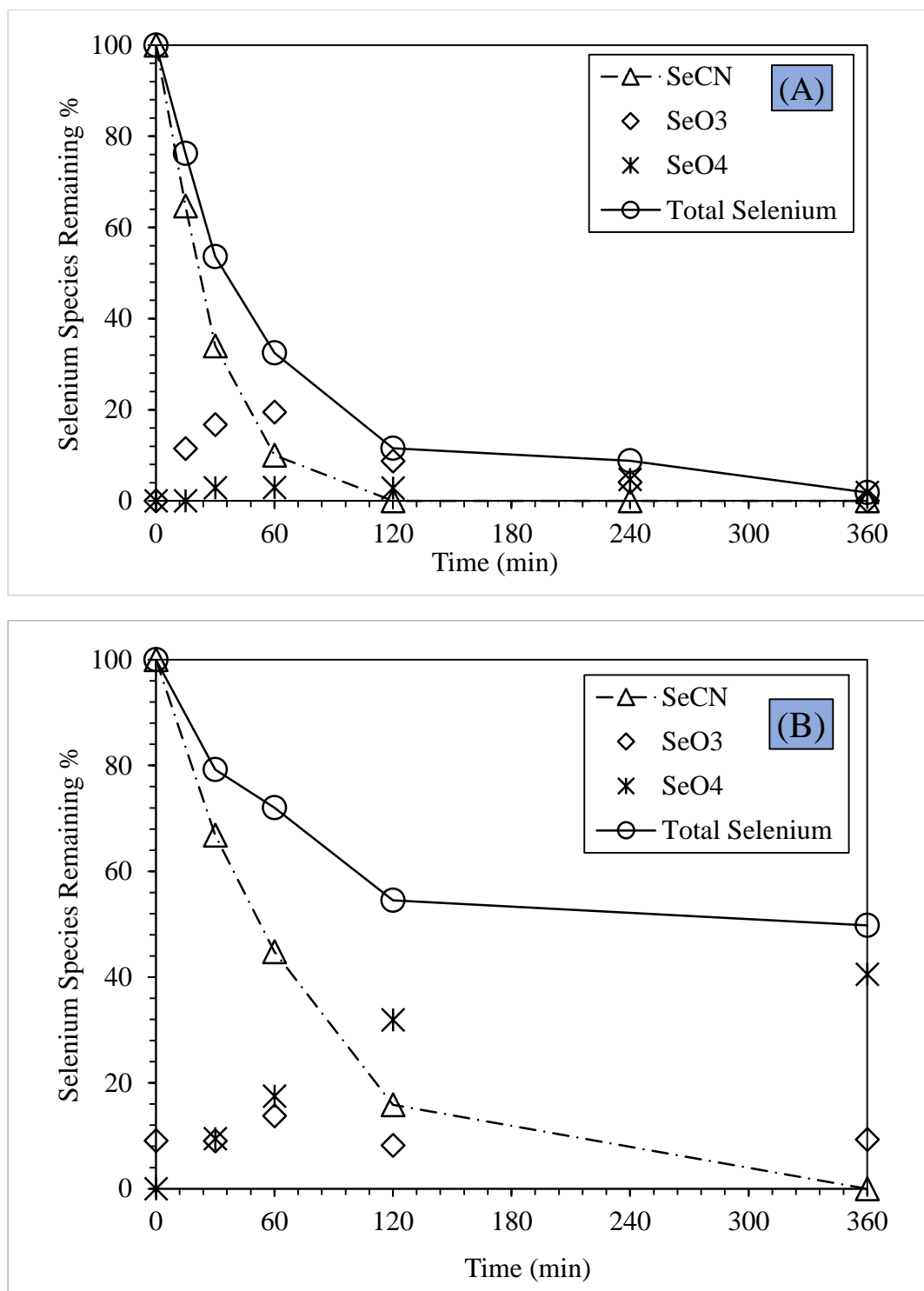
Figure 33 (A&B) The removal of removal of all dissolved selenium associated species during the destruction of se;enocyanate complex using photocatalysis with 2LFh (10 mg/L selenocyanae, 1-g/L 2LFh, 1-g/L TiO_2, 15 W UV lamp, (A): pH 5, (B): pH 9).
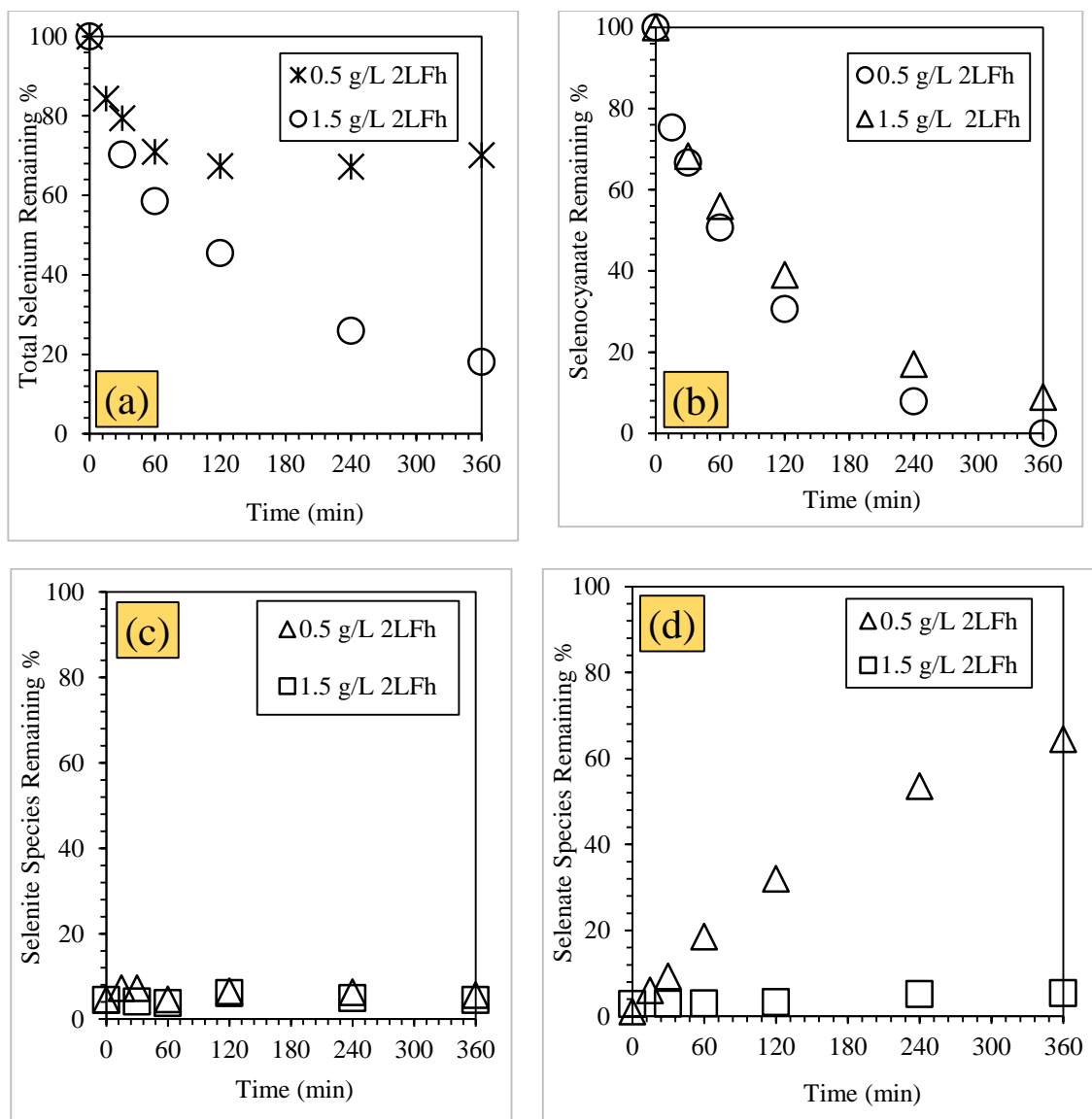
Figure 34 The effect of initial selenocyanate concentration onto the removal of (a) total selenium remaining, (b) selenocyanate remaining, (c) selenite remaining, and (d) selenate remaining during the destruction of selenocyanate complex using photocatalysis (1-g/L 2LFh, 1-g/L TiO_2, 15 W UV lamp, pH 5).
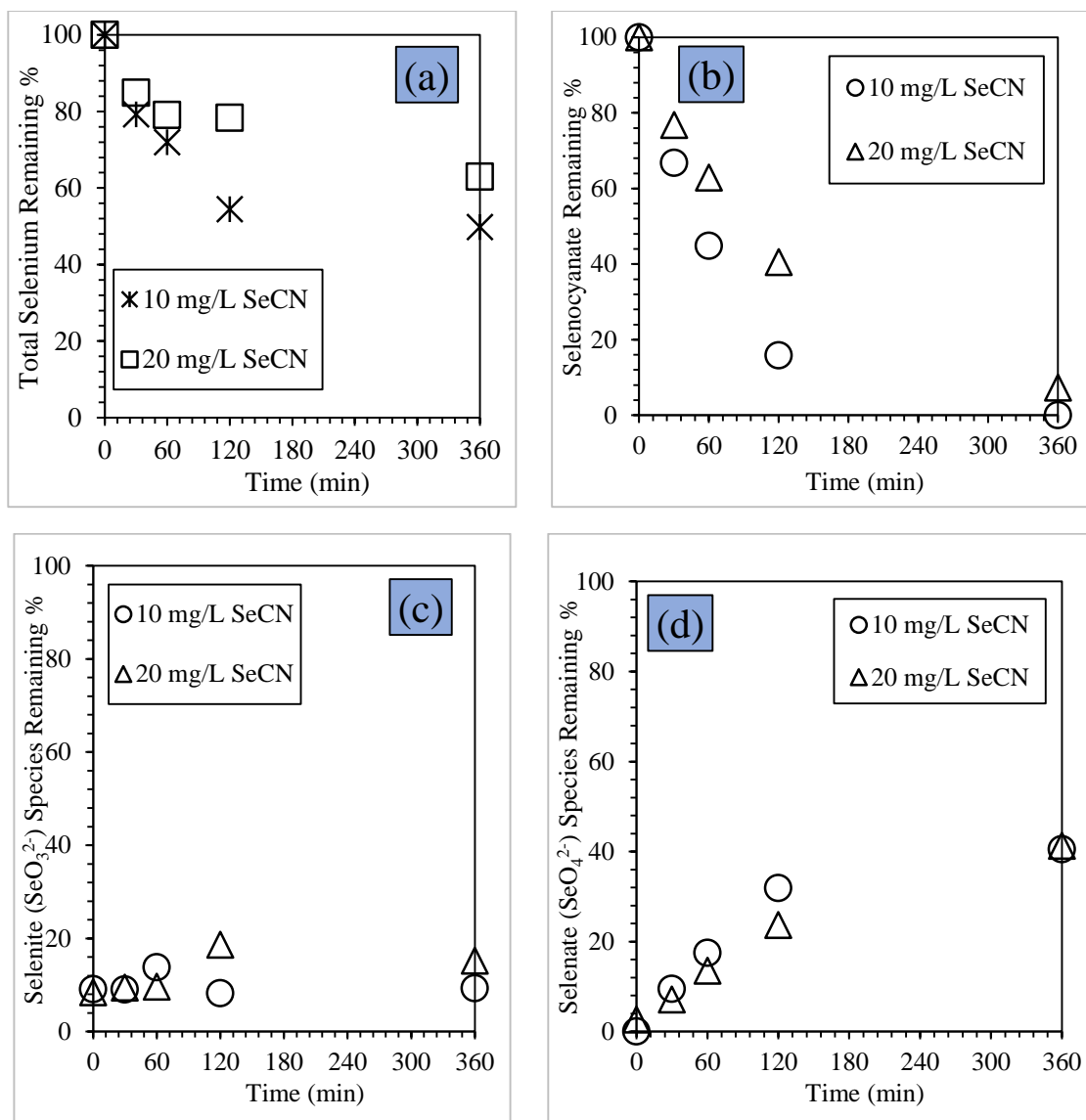
Figure 35 The effect of initial selenocyanate concentration onto the removal of (a) total selenium remaining, (b) selenocyanate remaining, (c) selenite remaining, and (d) selenate remaining during the destruction of selenocyanate complex using photocatalysis (1-g/L 2LFh, 1-g/L TiO$_2$, 15 W UV lamp, pH 9).

5.3.4.7 RSM modeling

Recently, RSM has been use in many optimization studies [74]. It is a combination of statistical and mathematical methods to study the response of a process under varying conditions to optimize this response [74]. In this work, we used BBD, which is a special type of RSM techniques that consider three factors with three equally spaced levels, for the experimental design and response analysis. In this design, we examined the effect of three independent factors, which were 2LFh amount, initial selenocyanate amount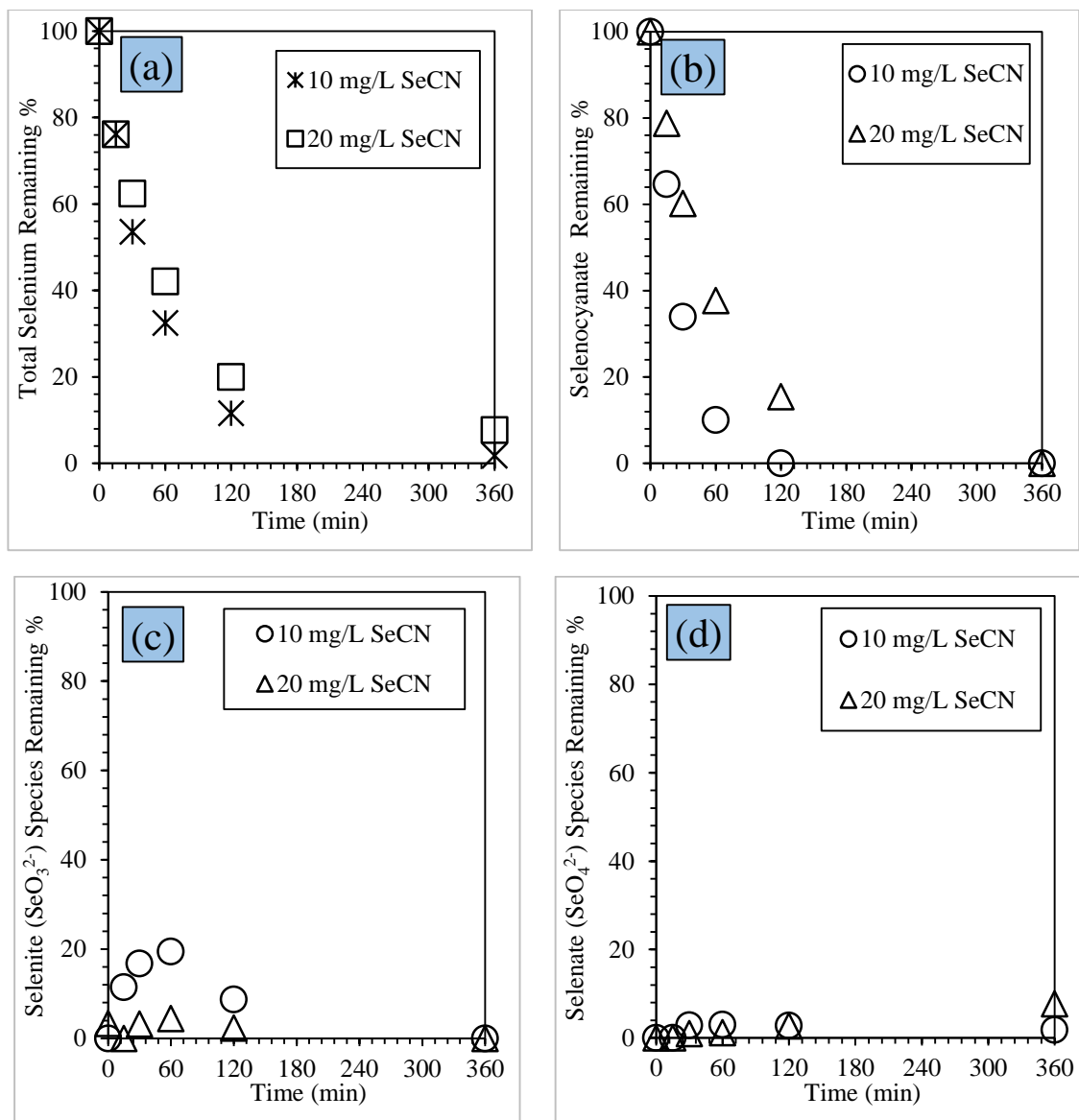, and pH, onto the total selenium removal during the destruction of the selenocyanate complex using photocatalysis (1-g/L TiO$_2$, 15 W UV lamp) at 360-min reaction time. BBD considers three equally spaced level coded as, low (-1), medium (0), and high (+1), as presented in Table 6. For this design, thirteen randomized experimental runs were performed, and Design-Expert® Software v.10 was used in the analysis. The software employs the least square regression method in fitting the experimental data to the selected polynomial function. The responses values used for the analysis were based on total selenium removal % at 360-min reaction time, and also the complete design layout is illustrated in Table 6. (14 explains the model equation for total selenium removal in terms of coded factors. It should be noted that the factors were designated as A, B, and C, which 2LFh amount (-1 = 0.5 g/L, 0 = 1 g/L, and +1 = 1.5 g/L), SeCN$^-$ concentration (-1 = 10 mg/L, 0 = 15 mg/L, and +1 = 20 mg/L), and pH (-1 = pH 5, 0 = pH 7, and +1 = pH 9), respectively. Moreover, Table 7 provides analysis of variance (ANOVA), which provides the significance level of the model and model parameters.

Table 7 also shows the significance level of each model and its term based on the probability value (p-value) and the F-statistic value. Values of "Prob > F" less than 0.05

indicate model terms are significant in predicting the experimental response. Otherwise, values greater than 0.1000 denote the model terms are not significant.

$$\text{Total selenium removal \%} = +66.61 + 15.73 \times A - 4.46 \times B - 21.79 \times C \qquad (14)$$

Typically, the model presented a p-value of 0.0094 which is less than 0.05. Thus, it implies that model is significant. Additionally, model terms A and C were both statistically significant. It is noted from (14 that the removal of total selenium increases with an increase in the amount of 2LFh. Higher 2LFh amount increases the number of available sites required for simultaneous selenium species adsorption, and this was previously discussed in section (5.3.4.5). In contrast, total selenium removal decreases, as initial pH increases. Also, this could be attributed to the same reason mentioned in sections (5.3.1.1) and (5.3.4.4), which is that above pH 5.7, the 2LFh will be negatively charged and thus, an electrostatic repulsion will exist between the 2LFh and different selenium species formed. Nevertheless, the 2LFh surface has positive charge below pH 7.8, which will attract the negative selenium species to 2LFh surface. Also, we look into the model factor B, initial selenocyanate concentration. The model term B shows p-value of 0.4677 greater than 0.05, and this term has no significant effect onto the total selenium removal because the removal process is a function of the rate of selenocyanate complex destruction as confirmed in section (5.3.4.6). In addition, important model characteristics are shown in Table 8. Figure 36, Figure 37 and Figure 38 show three-dimensional representation for the effect of the above mentioned factors (A: 2LFh amount, B: initial selenocyanate concentration, and C: pH) individually.

The model shows R^2, about 0.7040 (Table 8). However, adjusted and the predicted R^2 of the models were found to be in good agreement with values of 0.6054, and 0.4472, respectively as their difference in is less than 0.2. Larger R^2 values, close to 1, imply a good fit model regression. However, there may be some errors between the model and the real results, causing that the model is totally insignificant. The average absolute deviation value (AAD), which indicates the predictive capability of the developed model, could eliminate these errors. (15 [74] represents the AAD,

$$AAD = \left\{ \left[\sum_{i=1}^{p} \left(|y_{i,exp} - y_{i,cal}| / y_{i,exp} \right) \right] / p \right\} \times 100 \qquad (15)$$

Where,

$y_{i,exp}$	The experimental responces
$y_{i,cal}$	The calculated responses
p	Number of experimental runs

AAD should be as small as possible[74]. However, AAD obtained for this model is about 21.7% (Table 8). Also, adequate precision indicates signal-to-noise ratio, which is acceptable with value more than 4. Adequate precision the value of 8.123 is obtained for the present model (Table 8). These results show that the model is adequate signal and can be used for predicting the experimental data to some extent. In summary, the above argument reveals that RMS modeling could be used to anticipate total selenium removal using 2LFh during photocatalytic selenocyanate complex destruction with TiO_2.

Table 6 Experimental design and the total selenium removal, according to BBD

Run	Factor 1 A: 2LFh (g/L)	Factor 2 B: selenocyanate amount (mg/L)	Factor 3 C: pH	Response: Total selenium removal % at 360 min
1	1	10	9	50.21
2	0.5	20	7	29.6
3	1.5	15	9	44.35
4	0.5	15	9	46.81
5	1	10	5	98.18
6	1.5	20	7	81.88
7	1.5	10	7	93.6
8	1	20	9	37.03
9	0.5	15	5	72.68
10	1	15	7	95.25
11	1.5	15	5	89.6
12	1	20	5	92.28
13	0.5	10	7	34.52

Table 7 Statistical significance level of the model and the model parameters at 5% ($p < 0.05$)

Response	Model	A	B	C
Total selenium removal% at 360 min	0.0094	0.0256	0.4677	0.0049

Table 8 Pertinent model characteristics established using the RSM method.

Response	Response transformation	Adequate precision	R^2	Adjusted R^2	Predicted R^2	AAD (%)
Total selenium removal% at 360 min	None	8.123	0.7040	0.6054	0.4472	21.7%

Figure 36 3D graph presenting the effect of 2LFh amount(A) and initial selenocyanate concentration (B) on removal of total selenium during selenocyanate complex destruction using photocatalysis (1-g/L TiO$_2$, pH 7).
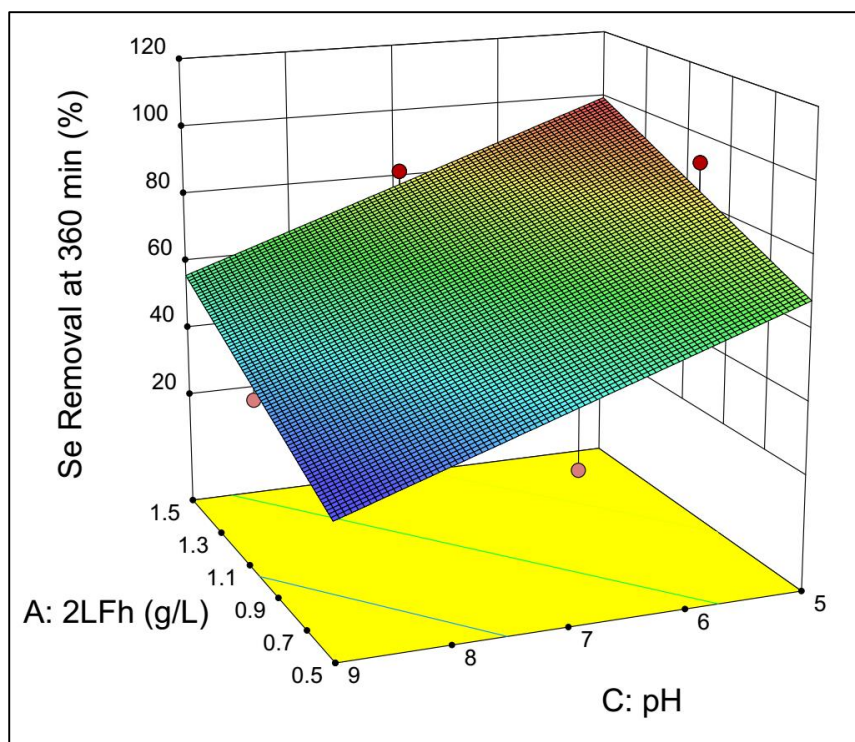
Figure 37 3D graph presenting the effect of 2LFh amount (A) and pH (C) on removal of total selenium during selenocyanate complex destruction using photocatalysis (20 mg/L seleocyanate, 1-g/L TiO$_2$, pH 7).
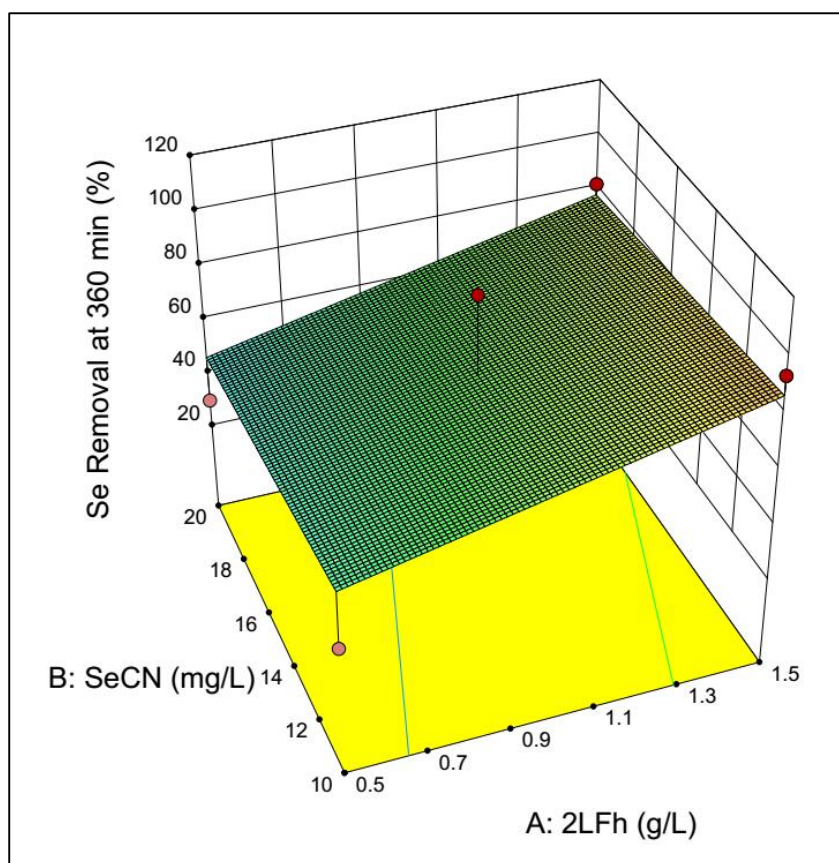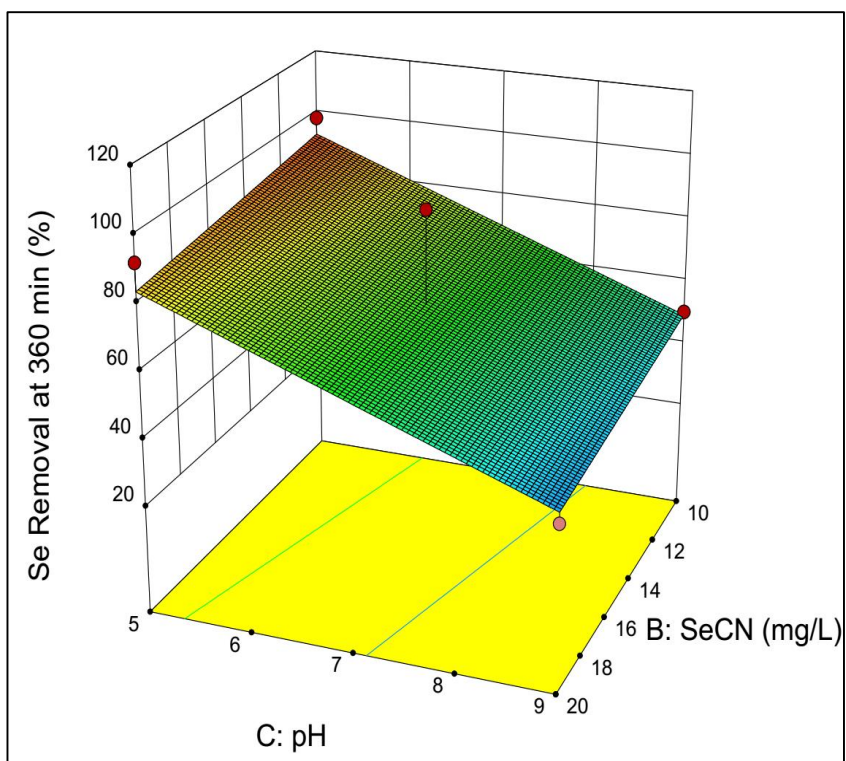
Figure 38 3D graph presenting the effect of initial selenocyanate concentration (B) and pH (C) on removal of total selenium during selenocyanate complex destruction using photocatalysis (1-g/L TiO$_2$, 1-g/L 2LFh).

5.4 Characterization of the prepared binary oxide system [Fe(III)/SiO$_2$]

5.4.1 X-ray Diffraction Spectroscopy Results

X-ray diffraction patterns was use for the produced Fe(III)/SiO$_2$ binary oxide system. The respective characterization is given in Figure 39. XRD study shows no evidence to support formation of crystalline Fe-oxide phase. XRD results in our work show that Fe(III)/SiO$_2$ are X-ray noncrystalline mixed oxides at pH 5.0. One broad peak is shown at 2Ө of 23° as presented in Figure 39. Similar findings were reported by Brigante et al., (2013 [88], Gervasini et al., (2009)[89], and Ennas et al., (1998) [90]. Shift in the XRD peaks from the previously reported by Kamal et al., (2008) [91], could be attributed to the stabilization of the amorphous Fe$_2$O$_3$ nanophase due to preventive role of the silica matrix [92].
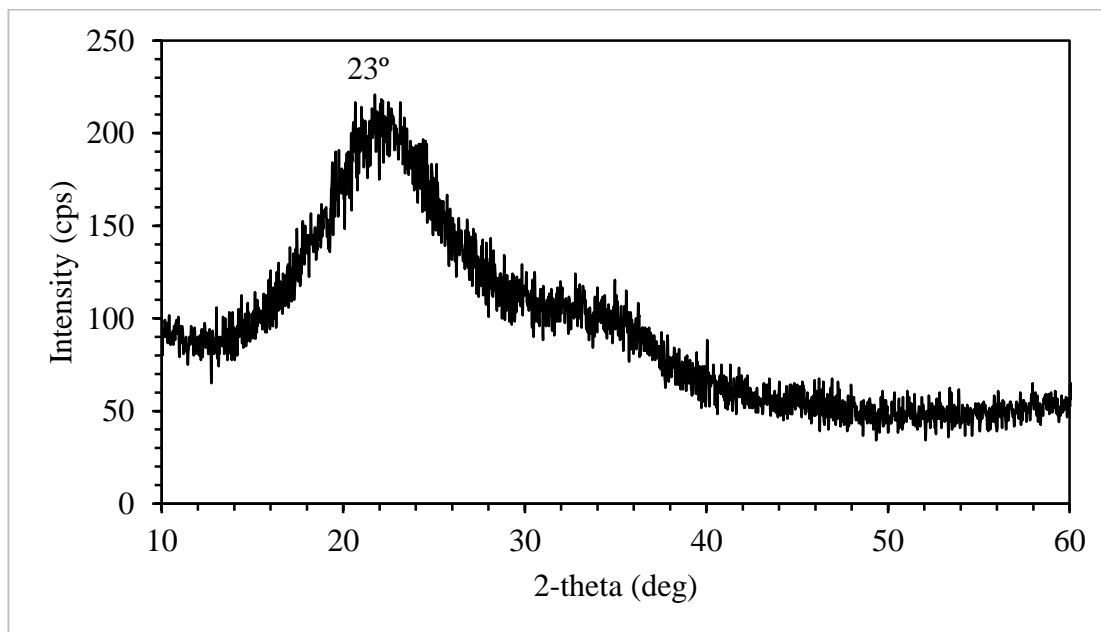
Figure 39 XRD spectra for binary oxide system [Fe(III)/SiO$_2$]

5.4.2 Attenuated Total Reflectance-Fourier Transform Infrared (ATR-FTIR) Spectroscopy

FTIR spectra is considered as an important feature to identify Fe(III)/SiO2 binary oxide (Figure 40). We observe a broad band centered at 3232 cm^{-1}, which associated to OH stretching of surface hydroxyls bound to silicon (Si-OH) [88,93]. In addition, a peak at about 1630 cm^{-1} due to the OH bending mode of water molecules [88,93]. Also, broad peaks located at 1050 and 790 cm^{-1} are attributed to asymmetric and symmetric Si-O-Si vibrations, respectively [93].
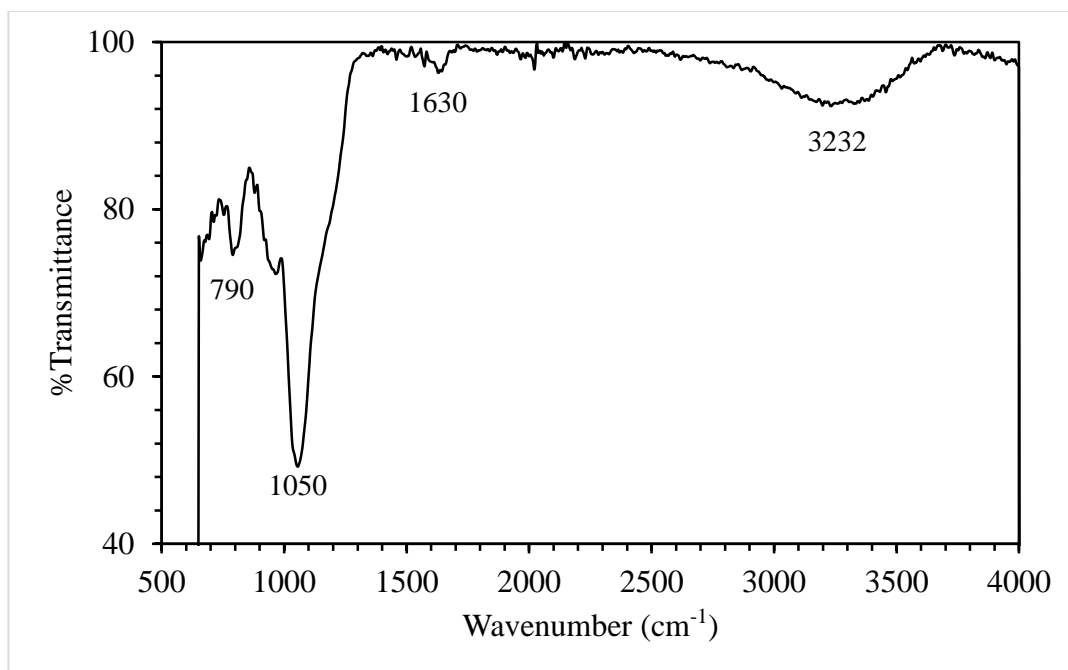
Figure 40 ATR-FTIR spectra of binary oxide system [Fe(III)/SiO₂].

5.5 Application of binary oxide system [Fe(III)/SiO₂] for selenocyanate removal

5.5.1 The adsorption of aqueous phase selenocyanate onto Fe(III)/SiO₂

5.5.1.1 The effect of pH

The influence of pH on adsorption process is an important parameter because it determines the ionization of the adsorbate in the aqueous phase as well as the surface charge of the adsorbent being employed. Hence, the effect of pH on the single solute adsorption of selenocyanate onto Fe(III)/SiO$_2$ was investigated at pH range between 4 to 11. Batch adsorption experiments were conducted at 10 and 20 mg/L selenocyanate and 1-g/L Fe(III)/SiO$_2$. The respective results are given in Figure 41. It should be noted that those results were obtained at equilibrium time 96 hr. It is observed that selenocyanate adsorption increases with a decrease in pH. Approx. 6% and 2% selenocyanate adsorption transpires for 10 and 20 mg/L selenocyanate, respectively at pH 6. However, selenocyanate removal decreases gradually, as pH increases, showing negligible removal at higher pH. This phenomenon is attributed to the lower pHzpc of binary oxide system. Chan et al., (2009) [20] reported pHzpc of 6.5 for Fe(III)/SiO$_2$. At pH above pHzpc, the adsorbent surface will be predominantly negatively charged, resulting in electrostatic repulsion between the solid phase and the selenocyanate aqueous phase. In addition, an increase in pH also increases the hydroxyl ions (OH$^-$), which in turn compete with selenium oxyanions for fixed surface adsorption sites, causing decrease in selenocyanate adsorption.
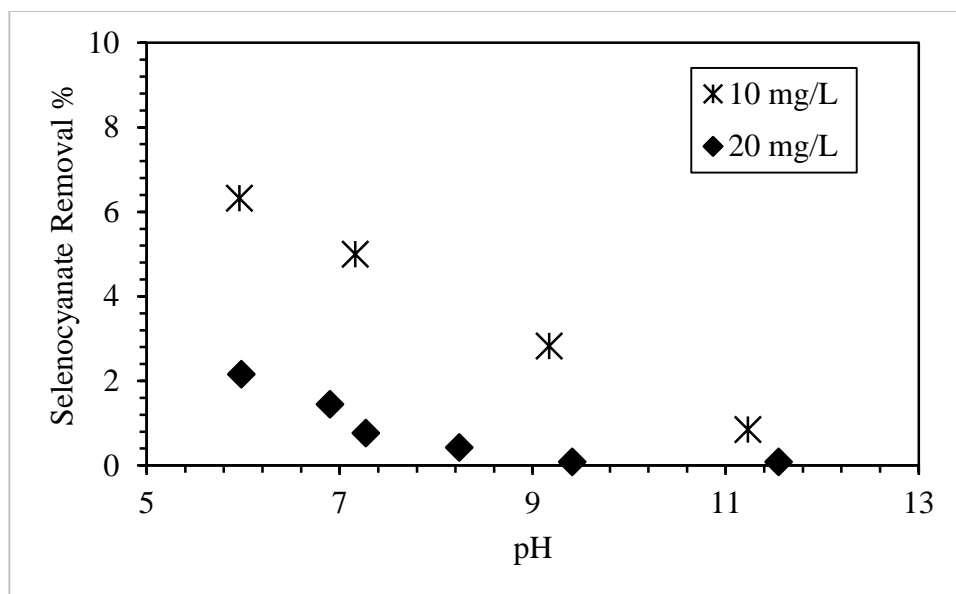
Figure 41 The effect of pH on selenocyanate adsorption onto binary oxide system [Fe(III)/SiO$_2$], (10-20 mg/L selenocyanate, 1 g/L Fe(III)/SiO$_2$, 96-hr contact time).

5.5.1.2 The effect of adsorbent dosage

The effect of Fe(III)/SiO$_2$ amount onto selenocyanate adsorption was also assessed. In this regard, two additional experiment were carried out at 20 and 50 mg/L selenocyanate and different Fe(III)/SiO$_2$ amount at pH 5. Figure 42 shows the respective results. It is noted that selenocyanate adsorption increases with an increment in adsorbent dosage. About 50% removal is obtained at 5-g/L Fe(III)/SiO$_2$ for 20 mg/L selenocyanate system. Similarly, the removal of 50 mg/L selenocyanate increases, as the adsorbent amount increases till 5-g/L. Thereafter, the adsorption reaches a plateau. Increasing the adsorbent amount increases the available adsorption sites, which in turn increases removal efficiency. Also, Figure 43 gives the adsorption capacity of Fe(III)/SiO$_2$ with respect to equilibrium selenocyanate concentration. We note that the adsorption capacity increases with increasing Ce from 1.6 to 2.65 mg/g. these results a very low affinity of Fe(III)/SiO$_2$ for selenocyanate adsorption.
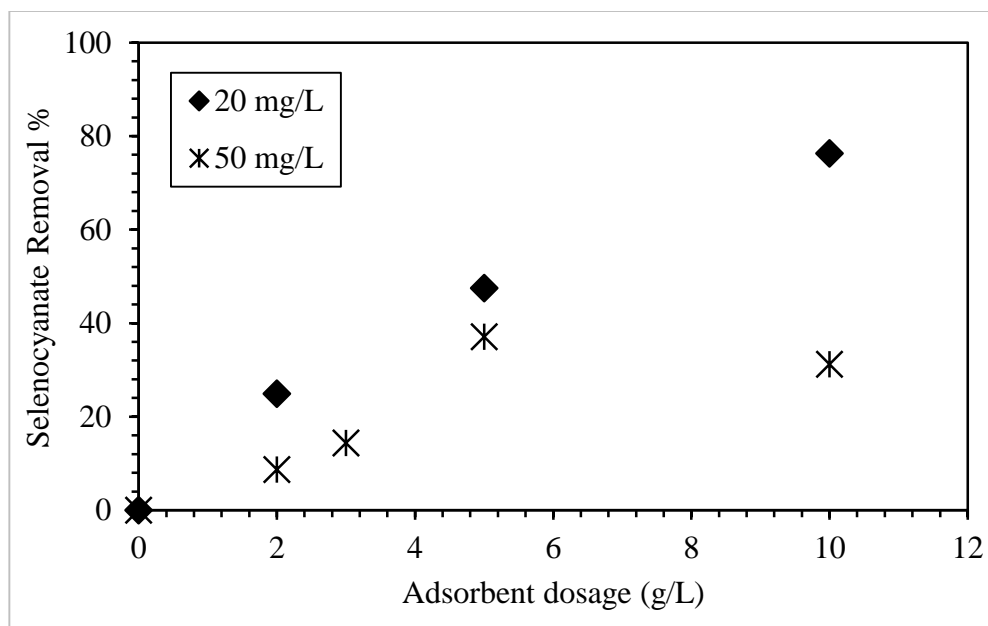
Figure 42 The effect of Fe(III)/SiO$_2$ amount on the adsorption of selenocyanate (pH 5, 96-hr contact time).
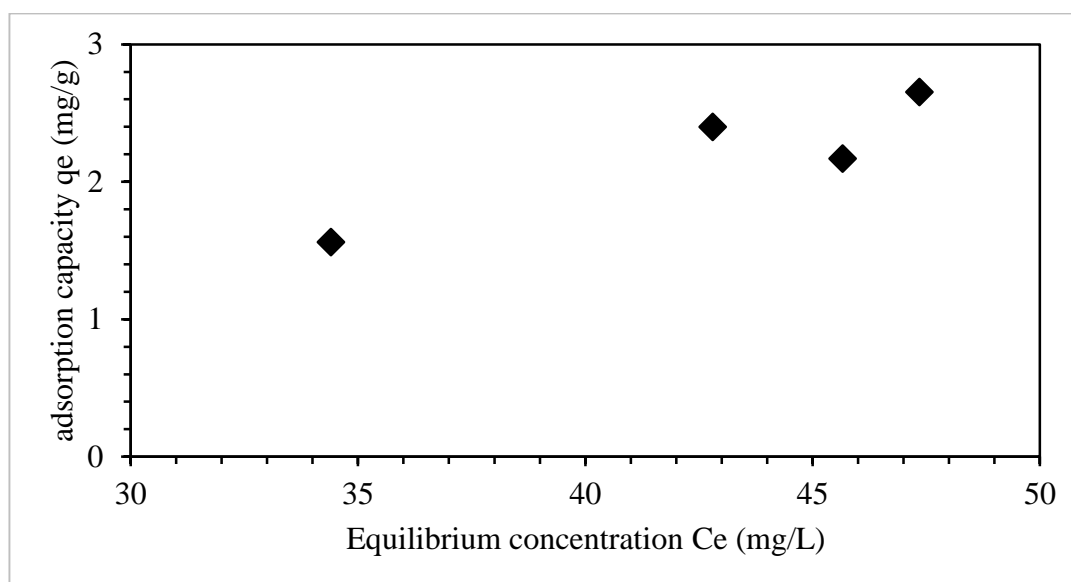
Figure 43 Adsorption isotherm of selenocyanate onto Fe(III)/SiO$_2$ (50 mg/L selenocyanate, 1-10 g/L Fe(III)/SiO$_2$, pH 5, 96-hr contact time).

5.5.1.3 Application of equilibrium adsorption isotherms for selenocyanate adsorption onto binary oxide system [Fe(III)/SiO$_2$]

To investigate the adsorption capacity of Fe(III)/SiO$_2$ binary oxide, batch adsorption experiment at 50 mg/L selenocyanate were completed at different Fe(III)/SiO$_2$ amounts (1, 2, 3, 5, and 10 g/L Fe(III)/SiO$_2$). The respective results are presented in Figure 42 and Figure 43. Adsorption data are fitted to Langmuir isotherm (Figure 44), and also the Freundlich isotherm as explained earlier in section (5.3.2).

Along with the trends noted in Figure 43, and from those for Freundlich isotherm suggest that the Freundlich isotherm model is suitable for describing the adsorption equilibrium of selenocyanate the binary oxide systems. The fitting data shows that Freundlich constant (K$_F$) and (n) for selenocyanate by Fe(III)/SiO$_2$ are 0.0079 and 0.6673, respectively.
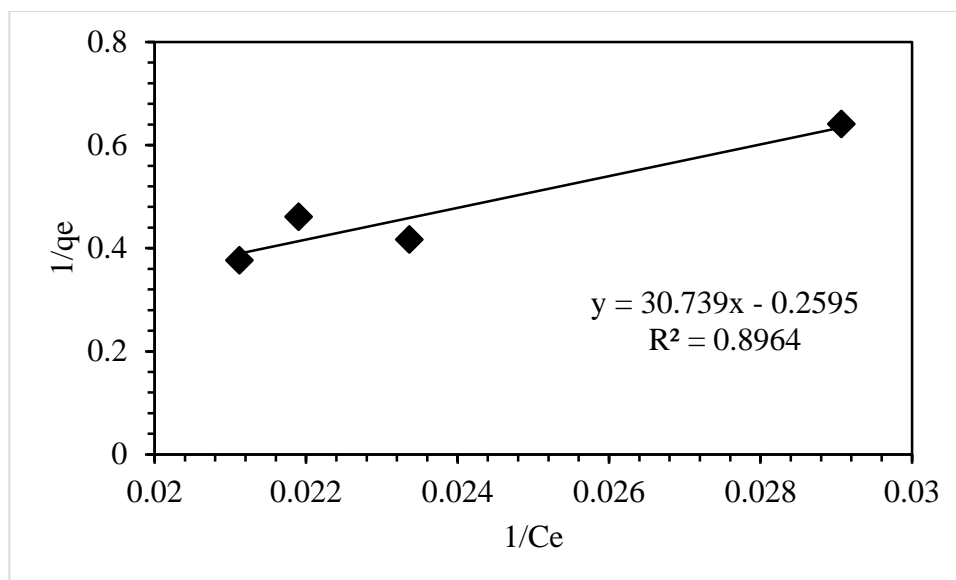
Figure 44 Langmuir adsorption isotherm for selenocyanate adsorption using Fe(III)/SiO$_2$ at pH 5 for 96-hr contact time.
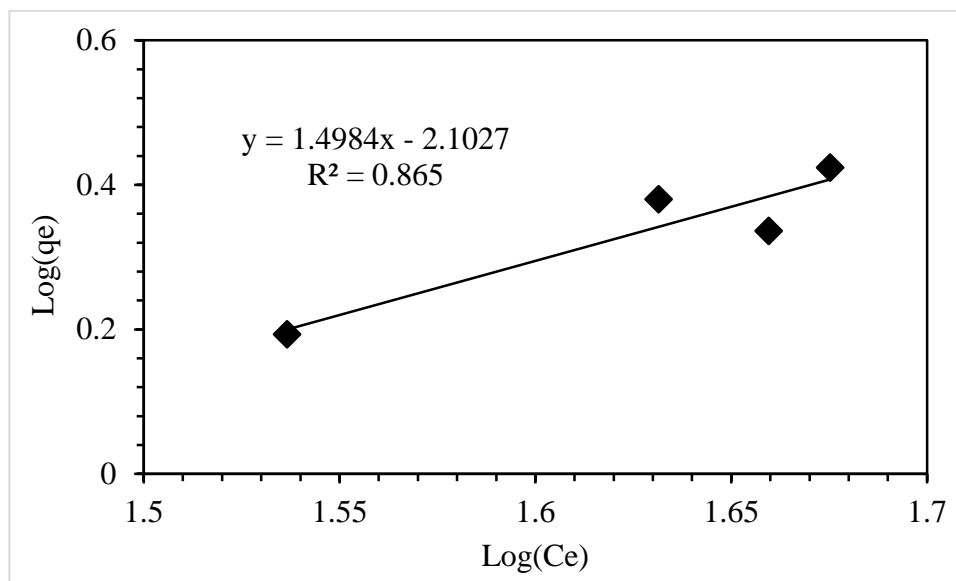
Figure 45 Freundlich adsorption isotherm for selenocyanate adsorption using Fe(III)/SiO$_2$ at pH 5 for 96-hr contact time.

5.5.1.4 Adsorption kinetics for selenocyanate adsorption onto Fe(III)/SiO$_2$

The selenocyanate adsorption kinetics onto Fe(III)/SiO$_2$ is also investigated. Two batch experiments were conducted to examine the rate of selenocyanate uptake at 20 and 50 mg/L initial selenocyanate concentrations. The respective results are given in Figure 46. We observe a negligible selenocyanate removal during the first 2 hr. Thus, the binary oxide system shows a very slow selenocyanate uptake. Nevertheless, given higher equilibrium time, as reported earlier, noticeable adsorption does transpire.
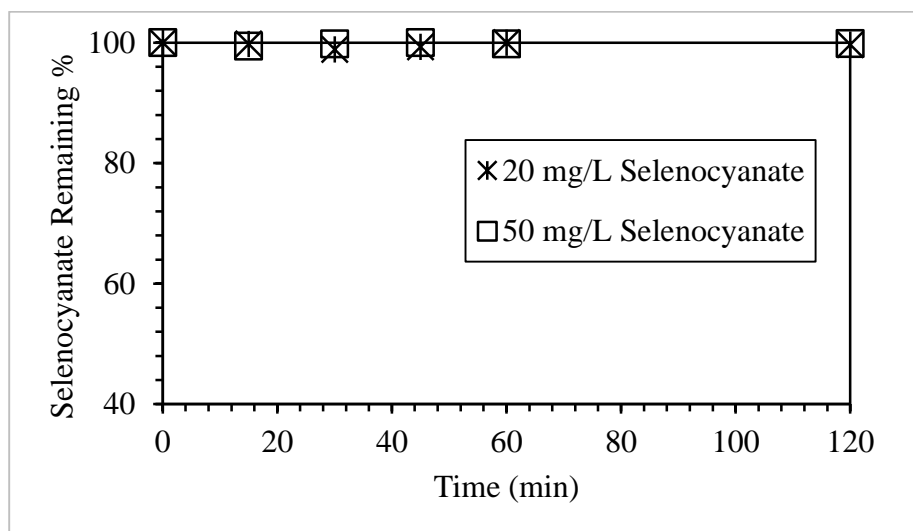
Figure 46 Adsorption of selenocaynate onto Fe(III)/SiO$_2$ with respect to time (5-g/L Fe(III)/SiO$_2$)

5.5.2 The removal of selenocyanate species using photocatalysis process

5.5.2.1 Results from batch experiments

Removal of selenocyanate using $Fe(III)/SiO_2$ binary oxide based photocatalysis was also investigated in this study. Photocatalysis using $Fe(III)/SiO_2$ only showed insignificant change in selenocyanate species over 360-min reaction time as shown in Figure 47. Hence, $Fe(III)/SiO_2$ binary oxide is not effective as a photocatalyst. However, adding TiO_2 yields near complete selenocyanate removal as also mentioned earlier in this thesis. Therefore, (as also noted earlier for 2LFh system) mixed system with TiO_2-photocataysis breaking down the selenocyanate complex into intermediates including selenite and selenate, followed by the adsorption of these species by $Fe(III)/SiO_2$ system was also investigated. Hence as a first step, we examined the adsorption of selenocyanate, selenite, and selenate in single adsorption systems using the binary oxide at different pH values. Three batch experiments were conducted using 1-g/L $Fe(III)/SiO_2$ added to individual 20 mg/L selenite, selenate, and selenocyanate systems at pH 5, 7, and 9. The respective results are given in Figure 48. It is observed that the adsorption of selenium species decreases with an increase in pH. For example, although $Fe(III)/SiO_2$ adsorbent shows approx. 30% selenate removal at pH 5, a negligible selenate adsorption (0.5%) is observed at pH 9. Similarly, about 82, 30, and 14% selenite removals are noted at pH 5, 7, and 9, respectively. Though very small, however selenocyanate adsorption also decreases with pH increasing. Similar findings are reported by Chan et al., (2009) [20], who attributed this to the lower pH_{zpc} of 6.5 for $Fe(III)/SiO_2$. Above pH_{zpc}, the surface of the adsorbent will be negatively charged, leading to electrostatic repulsion of selenium oxyanions. This along with higher hydroxyl ions that can compete with selenium oxyanions for fixed surface adsorption sites will cause reduced

selenite and selenate adsorption [20]. Nevertheless, the above findings show successful application of Fe(III)/SiO$_2$ for the removal of selenium species. Hence, the Se-species produced during selenocyanate complex destruction using TiO$_2$ PCD process can be adsorbed onto Fe(III)/SiO$_2$ binary oxide and potentially removed from the aqueous phase. The respective experiment findings are reported in the next section.
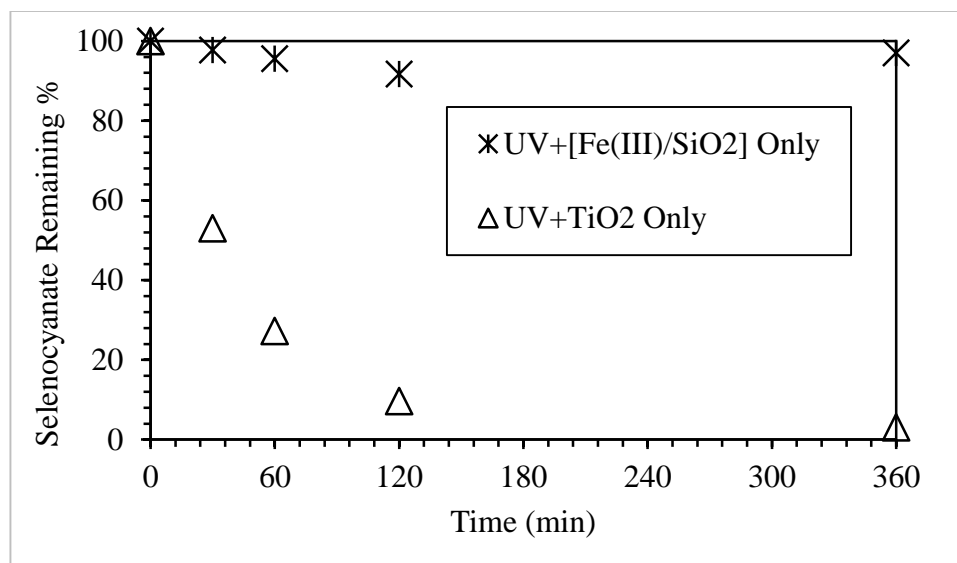
Figure 47 Destruction of selenocyanate complex using photocatalytic process under varying experimental conditions: 1) in the presence of UV light with 1-g/L Fe(III)/SiO$_2$, and 2) in the presence of UV light with 1-g/L TiO$_2$ (20 mg /L selenocyanate, pH 5)
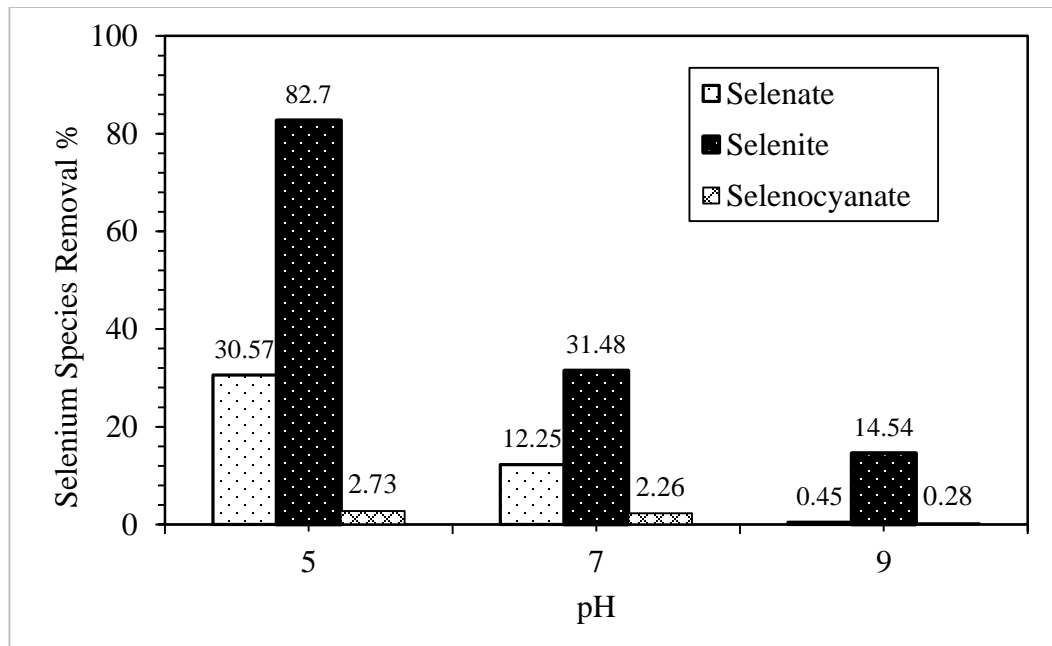
Figure 48 The effect of pH on adsorption of single solute system selenate, selenite, and selenocyanate onto Fe(III)/SiO$_2$ surface (20 mg/L selenate only, 20 mg/L selenite only, 20 mg/L selenocyanate only, 1-g/L Fe(III)/SiO$_2$).

5.5.2.2 Effect of pH onto photocatalytic removal of selenocyanate

The effect of pH onto selenocyanate removal using combination of TiO_2 photocatalysis and $Fe(III)/SiO_2$ adsorption based system was also studied in the present work. Figure 49 (A&B) show the trends for 20 mg/L selenocyanate photocatalysis at pH 5 and 9, and Figure 50 compares the respective species trends at pH 5 and 9. At pH 5, 90% total selenium removal is noted at 240 min, whereas at pH 9 this reduces to 40% Figure 50-(a).

Furthermore, a qualitatively similar trend is noted for selenocyanate that shows about 85% removal in 60 min (followed by near complete removal after 120 min), whereas at pH 9 we note approx. 50% of selenocyanate species removal at 60 min (Figure 50-(b)). Vohra (2015) also reported reduced PCD selenocyanate complex destruction with an increase in pH [50]. Now comparing the removal of reaction intermediates selenite and selenate, we note near complete selenite removal at both pH 5 and 9 (Figure 50-(c)), however selenate remaining at pH 5 and 9 is about 15% and 60 %, respectively as shown in Figure 50-(d). That also accounts for the total selenium remaining in the system. This would be attributed to lower selenate adsorption at pH 9, as also noted in Figure 48.

We also examined the effect of pH onto removal of 10 mg/L selenocyanate with respective results are given in Figure 51 (A&B) and Figure 52-(a)-(d), with trends similar to those noted for the 20 mg/L selenocyanate system. At pH 5, total selenium removal transpires at 120 min, whereas at pH 9, we note about 45% total selenium removal at 240 min (Figure 52-a). Also, the selenocyanate removal rate is higher at pH 5 (Figure 52-b). Additionally, though near complete selenite removal is obtained at both pH 5 and 9 (Figure 52-c), however selenate shows incomplete removal at pH 9 (Figure 52-c). These trends are qualitatively very similar to those noted earlier for the 20 mg/L selenocyanate system.

Hence, though the PCD process breaks down the selenocyanate complex to oxidized selenite and to selenate form, nevertheless, it is only upon the addition of $Fe(III)/SiO_2$ that the produced selenite and selenate species are adsorbed and removed from the aqueous phase. However, the affinity of $Fe(III)/SiO_2$ specifically for selenate decreases significantly at basic pH. Hence, the above results indicate acidic pH to be the optimum for total selenium removal.

Figure 49 (A&B) The removal of dissolved selenium associated species during the destruction of selenocyanate complex using photocatalysis with Fe(III)/SiO$_2$ system (20-mg/L selenocyanate, 1-g/L Fe(III)/SiO$_2$, 1-g/L TiO$_2$, 15 W UV lamp, (A): pH 5, (B): pH 9).

Figure 50 The effect of pH onto the removal of selenium species: (a) total selenium, (b) selenocyanate, (c) selenite, and (d) selenate, remaining during selenocyanate complex destruction using photocatalysis with Fe(III)/SiO$_2$ system (20-mg/L selenocyanate, 1-g/L Fe(III)/SiO$_2$, 1-g/L TiO$_2$, 15 W UV lamp).
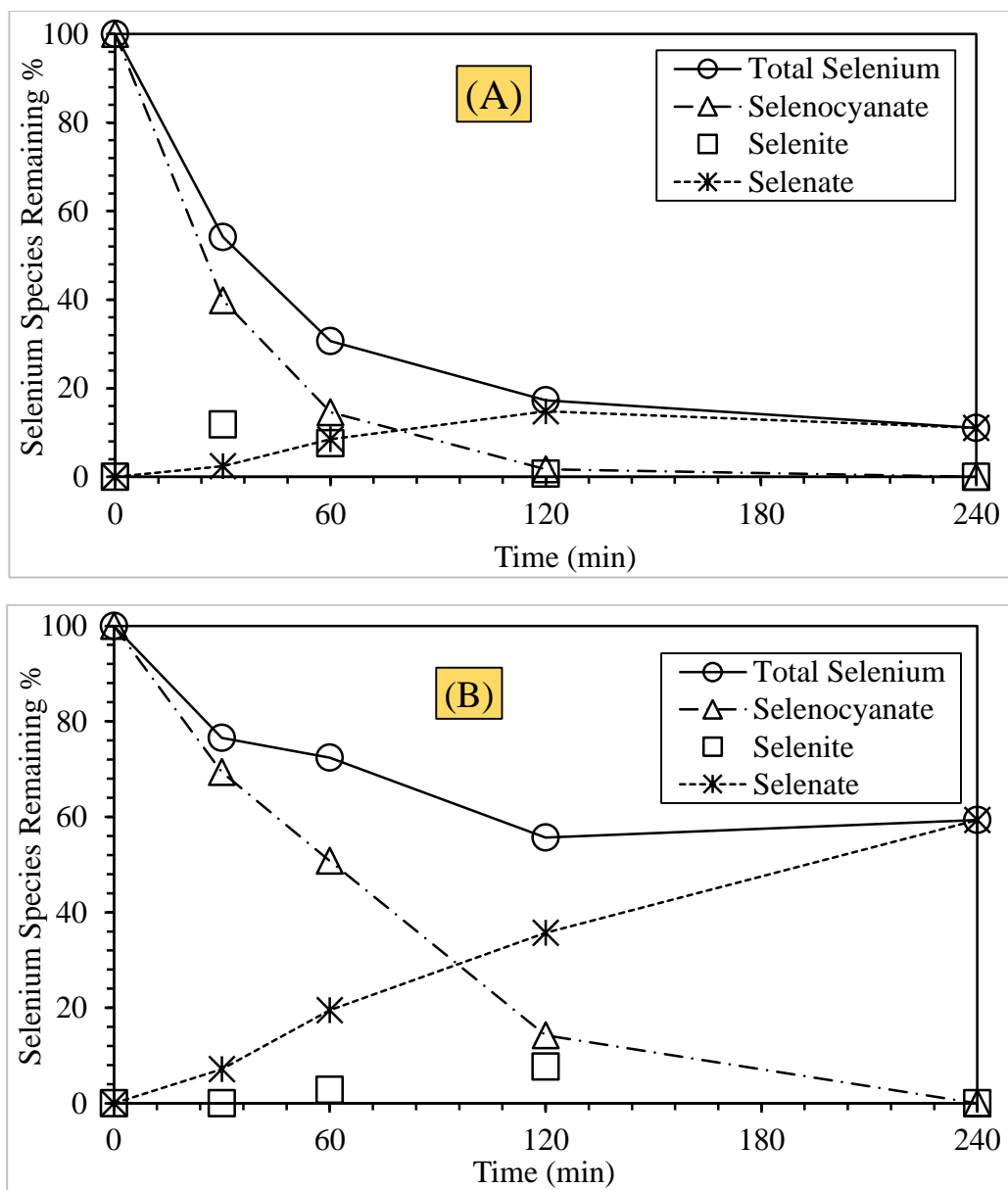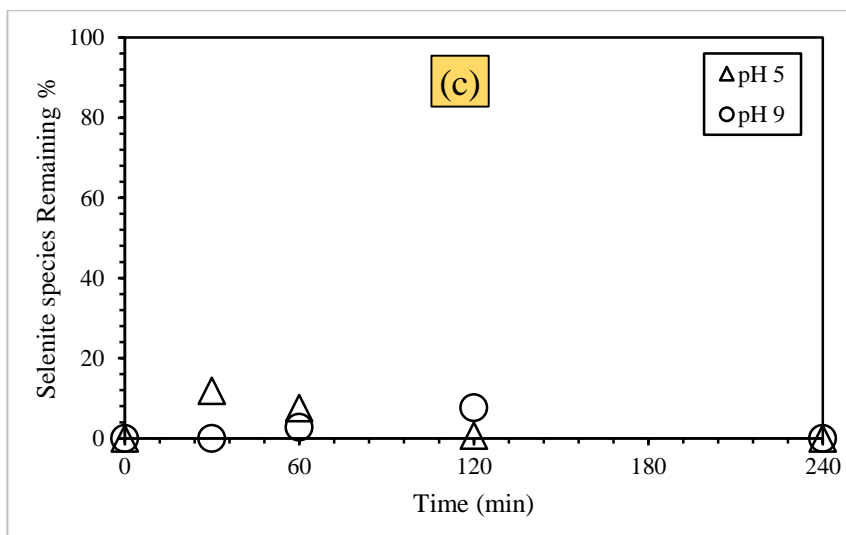
Figure 51 (A&B) The removal of dissolved selenium associated species during the destruction of selenocyanate complex using photocatalysis with Fe(III)/SiO$_2$ system (10 mg/L selenocyanate, 1-g/L Fe(III)/SiO$_2$, 1-g/L TiO$_2$, 15 W UV lamp, (A): pH 5, (B): pH 9).

Figure 52 The effect of pH onto the removal of selenium species: (a) total selenium, (b) selenocyanate, (c) selenite, and (d) selenate, remaining during the selenocyanate complex destruction using photocatalysis with Fe(III)/SiO$_2$ system (10-mg/L selenocyanate, 1-g/L Fe(III)/SiO$_2$, 1-g/L TiO$_2$, 15 W UV lamp).

5.5.2.3 Effect of Fe(III)/SiO$_2$ amount onto photocatalysis

The effect of Fe(IIII)/SiO$_2$ amount onto the removal of respective selenium species during the mixed photocatalysis-adsorption treatment was also assessed. We initially conducted two experiments at 0.5 and 1.5 g/L Fe(III)/SiO$_2$ for 20 mg/L selenocyanate removal at pH 7, and respective findings are given in Figure 53 (A&B). Though we do not observe any difference in selenocyanate species removal (Figure 54-b). However, we note maximum of 30 and 65% total selenium removal at 120 min for the 0.5 and 1.5 g/L Fe(III)/SiO$_2$ systems, respectively (Figure 54-a). Similarly out of selenite and selenate removal trends, it is only selenate species for which we note higher removal at higher Fe(III)/SiO$_2$ amount (Figure 54-c and Figure 54-d, respectively).For example, about 40% selenate removal is noted for the 0.5 g/L system at 240 min, whereas approx. 65% removal transpires at 1.5 g/L Fe(III)/SiO$_2$.

Furthermore, two more experiments were conducted at pH 5 and 15 mg/L selenocyanate, with respective results shown in Figure 55-(A&B) and Figure 56-a-d. The Total selenium removal increases with an increase in the binary oxide amount, i.e., approx. 40 and 96% removals are noted for 0.5 and 1.5 systems, respectively (Figure 56-a). Though qualitatively the total selenium, selenocyanate, and selenite removal trends (Figure 56-a-d) are similar to those reported in Figure 54-a-d, however, it is the selenate removal trends that unlike the previous results show significant removal at increased Fe(II)/SiO$_2$ amount and pH. Higher adsorbent amount added to the system increases the available sites to adsorb selenium associated species, and hence increasing the overall total selenium removal efficiency. Figure 52 that reports uses of 1-g/L Fe(III)/SiO$_2$ at pH 5 for 10 mg/L selenocyanate removal also shows near complete total selenium and selenate removals,

whereas Figure 50 that reports results at higher 20 mg/L selenocyanate shows incomplete removals. The findings indicate that along with pH, the optimum $Fe(III)/SiO_2$ amount will also define the total selenium removal efficiency depending on the initial selenocyanate amount.
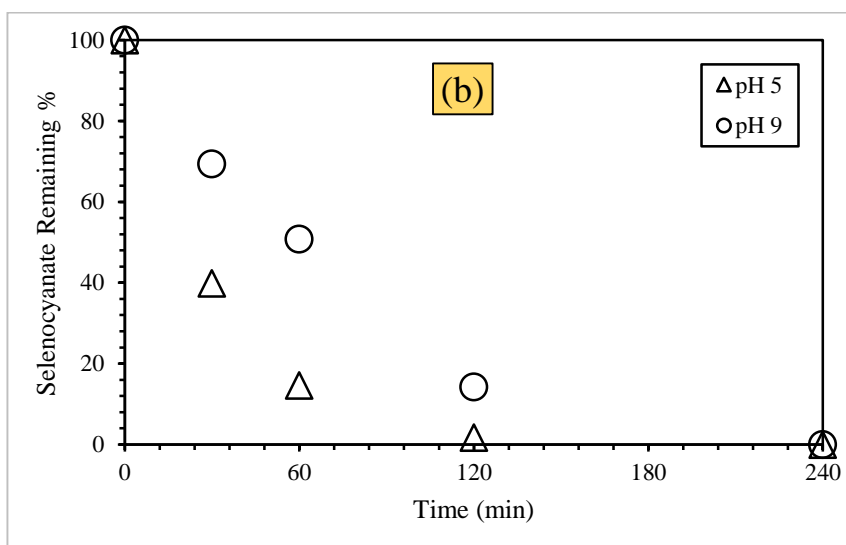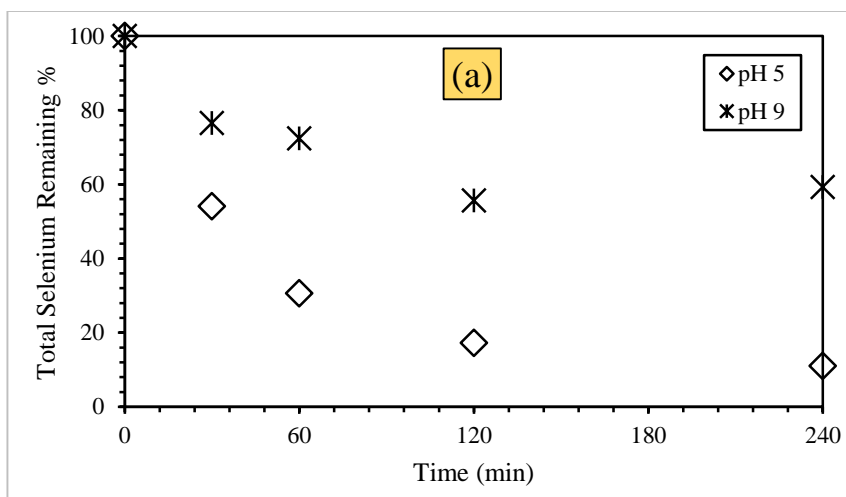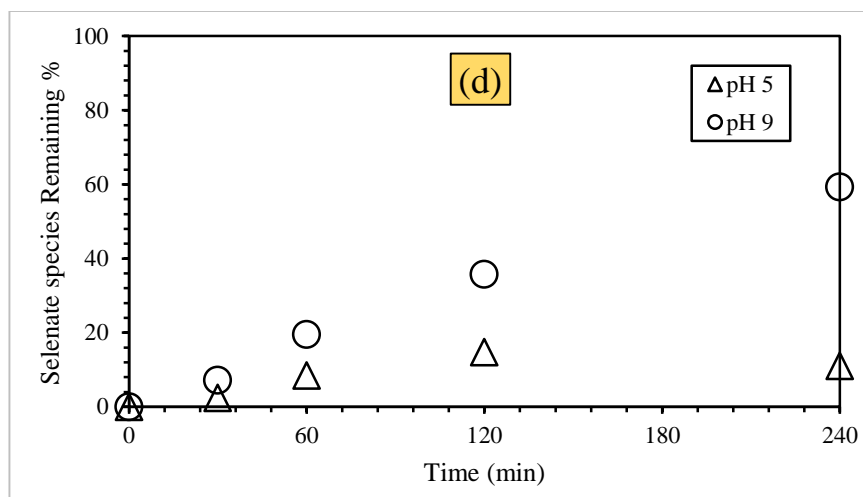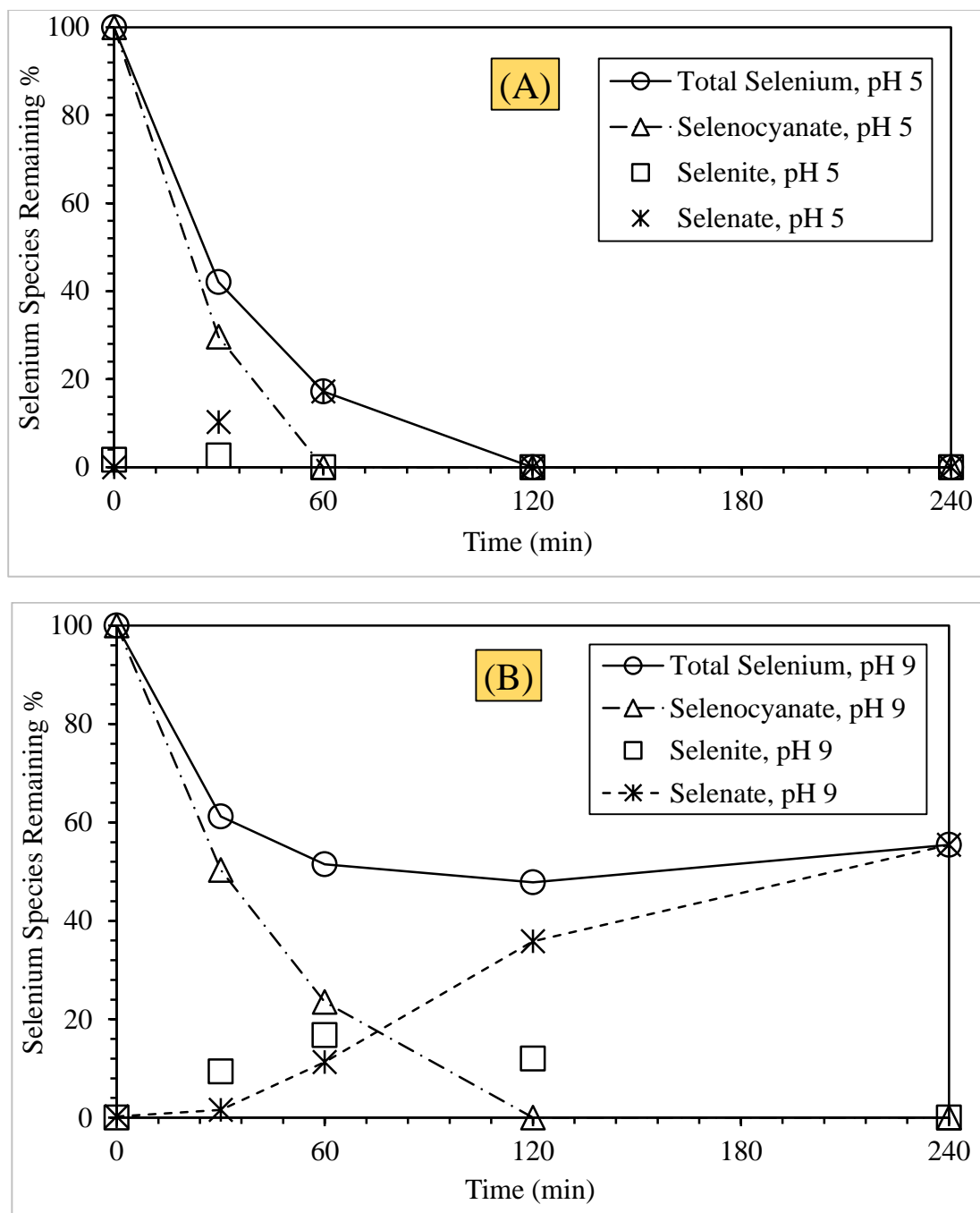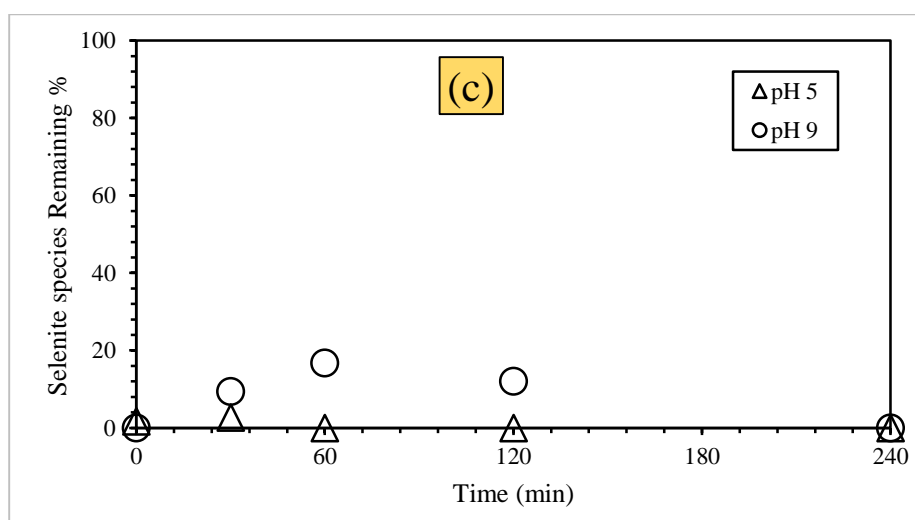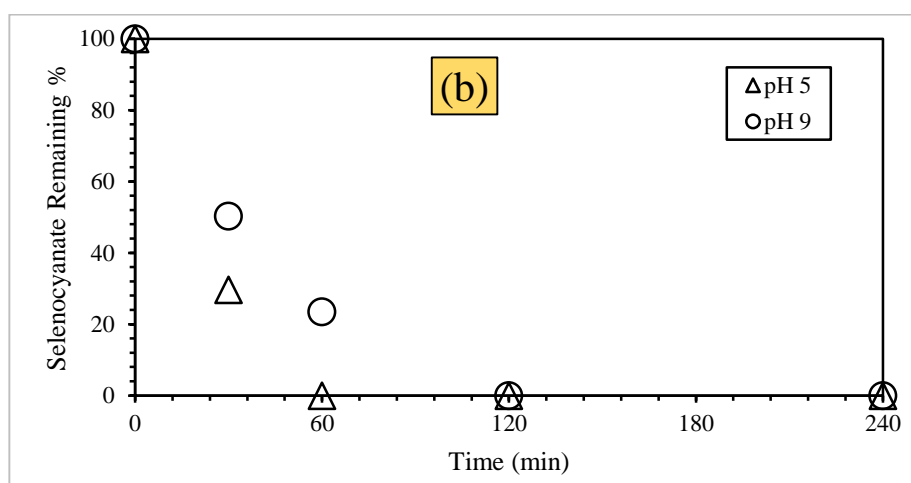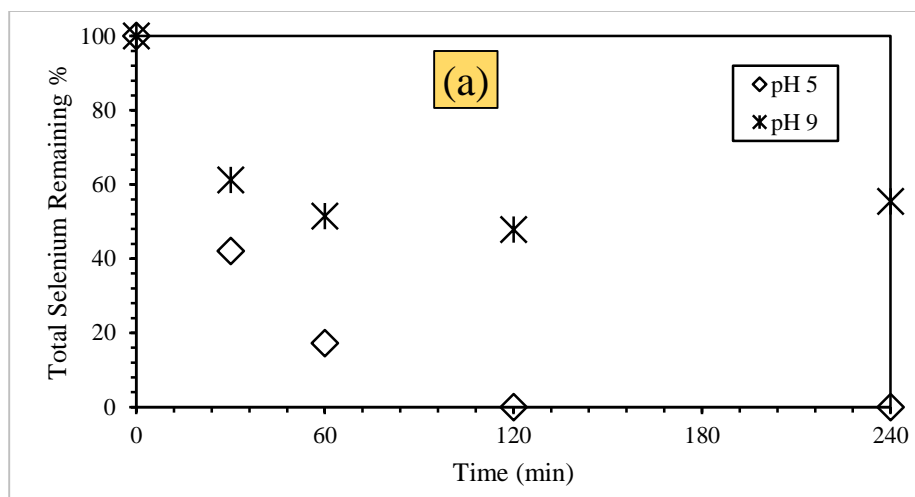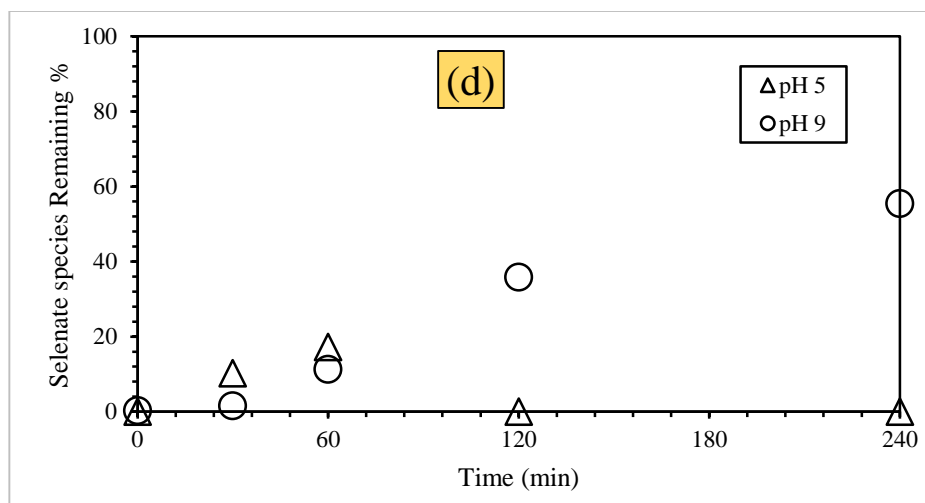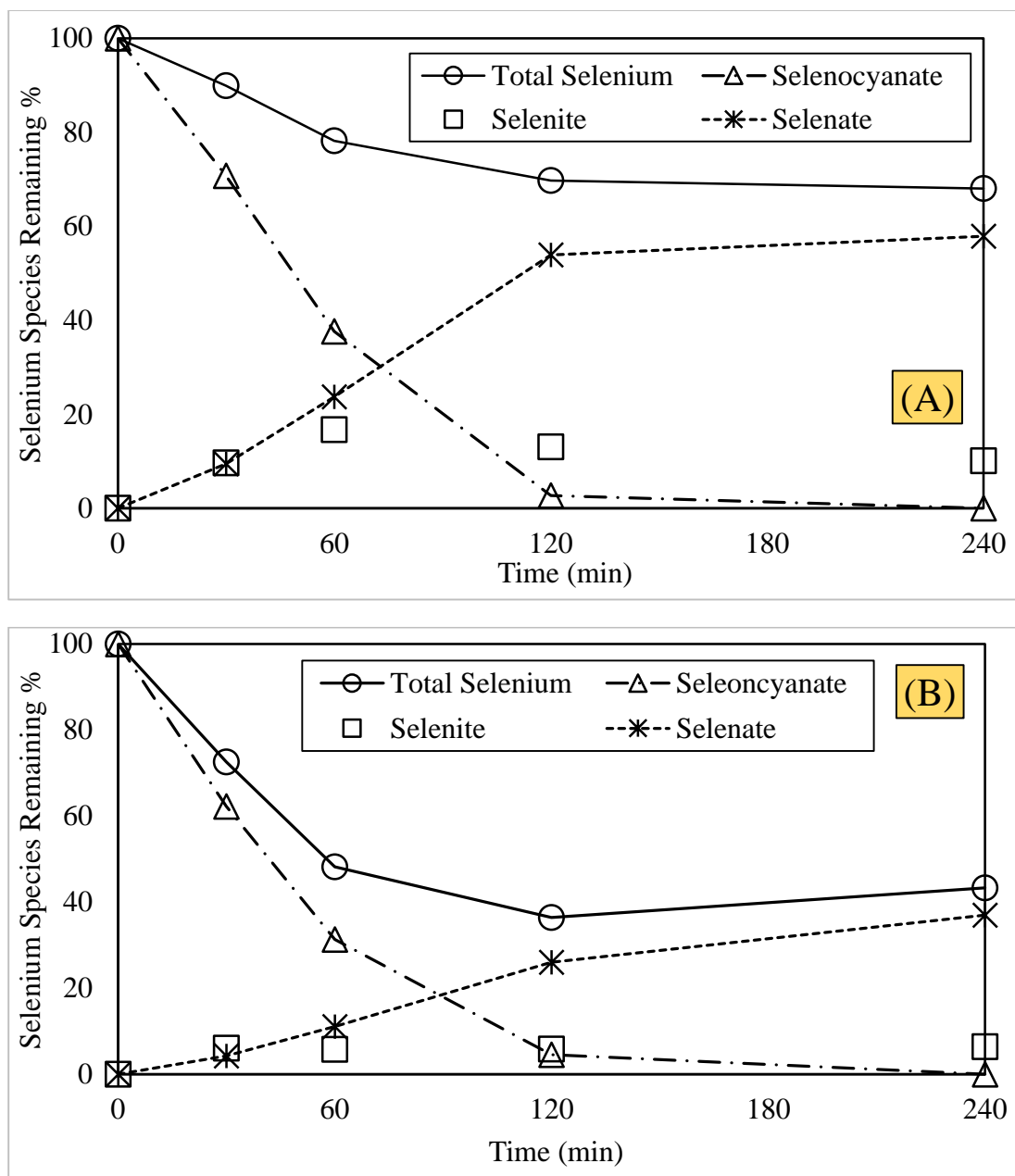
Figure 53 (A&B) The removal of dissolved selenium associated species during the destruction of selenocyanate complex using photocatalysis with Fe(III)/SiO$_2$ system (20 mg/L selenocyanate, 1 g/L TiO$_2$, pH 7, 15 W UV lamp, (A): 0.5 g/L Fe(III)/SiO$_2$, (B): 1.5 g/L Fe(III)/SiO$_2$).
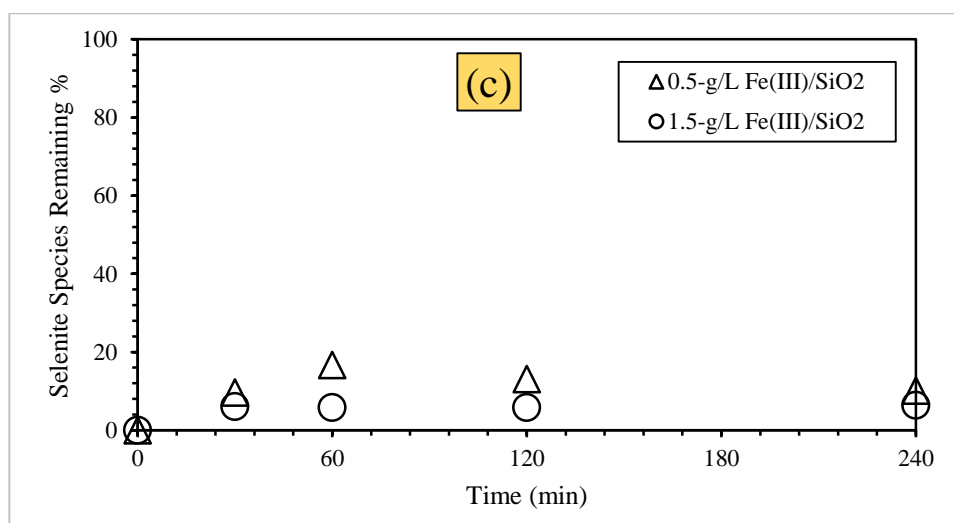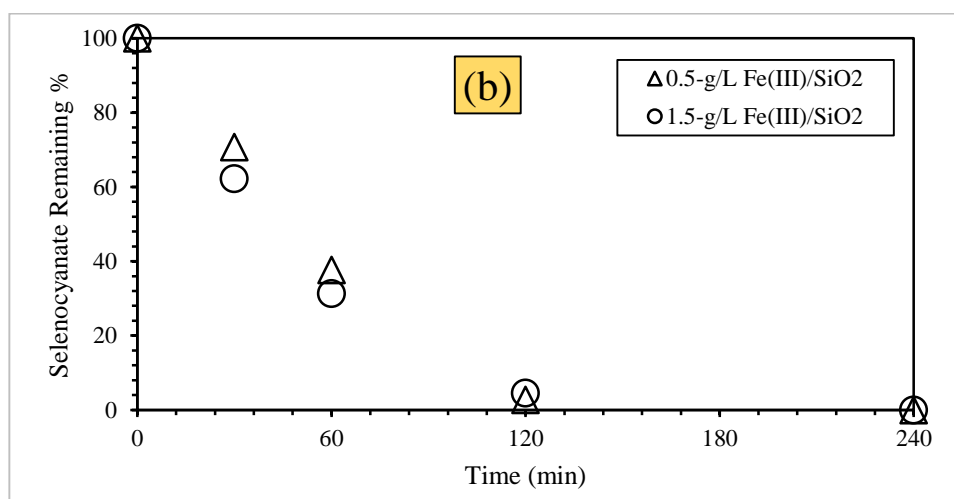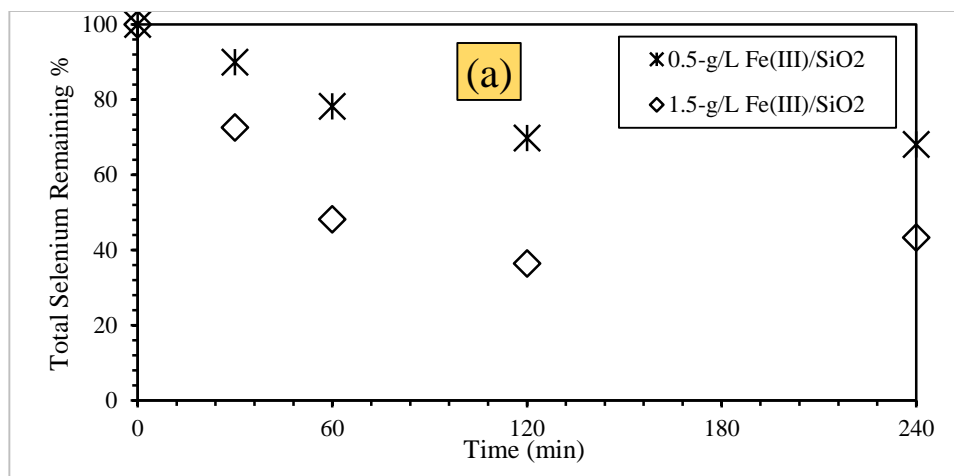
Figure 54 The effect of Fe(III)/SiO$_2$ amount onto the removal of selenium species: (a) total selenium, (b) selenocyanate, (c) selenite, and (d) selenate, remaining during the selenocyanate complex destruction using photocatalysis with Fe(III)/SiO$_2$ system (20 mg/L selenocyanate, 1-g/L TiO$_2$, 15 W UV lamp, pH 7).
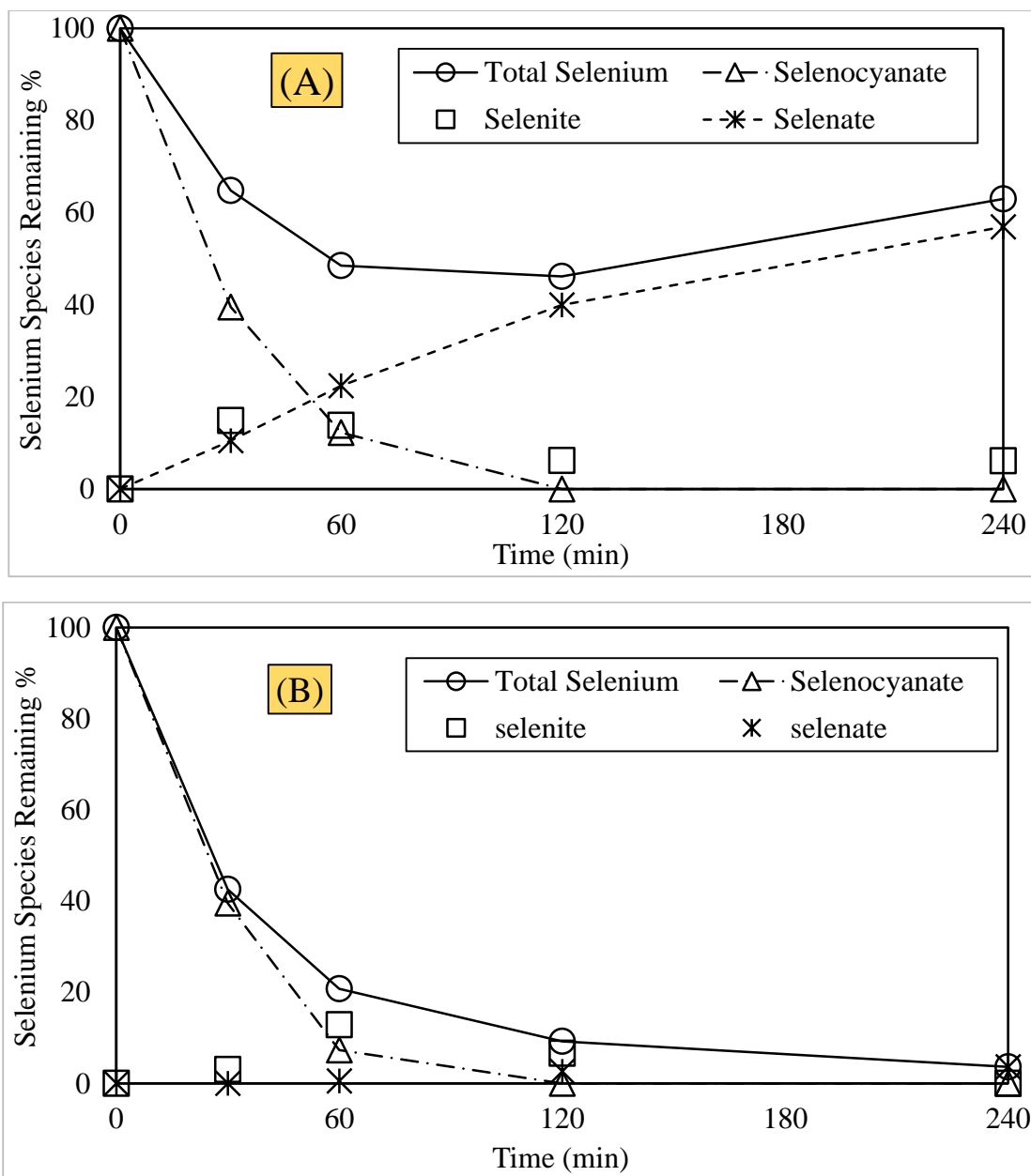
Figure 55(A&B) The removal of removal of all dissolved selenium associated species during the destruction of selenocyanate complex using photocatalysis with Fe(III)/SiO$_2$ system (15 mg/L selenocyanate, 1 g/L TiO$_2$, pH 5, 15 W UV lamp, (A): 0.5 g/L Fe(III)/SiO$_2$, (B): 1.5 g/L Fe(III)/SiO$_2$).
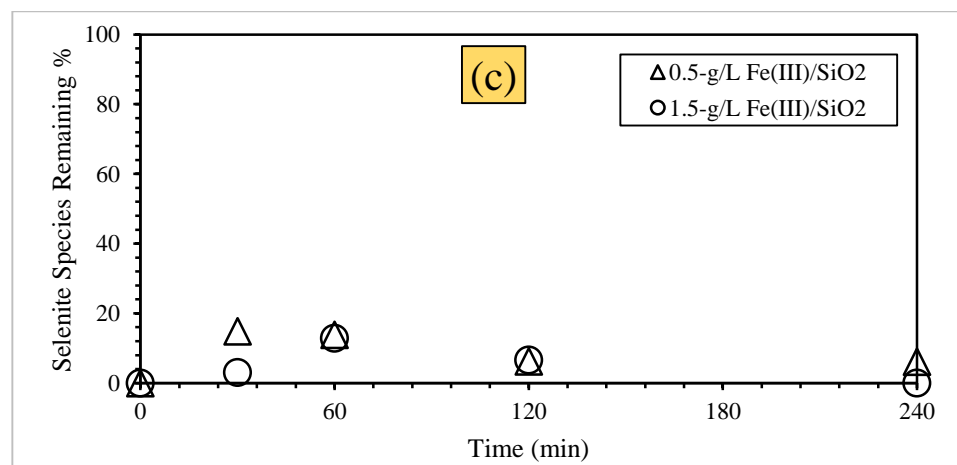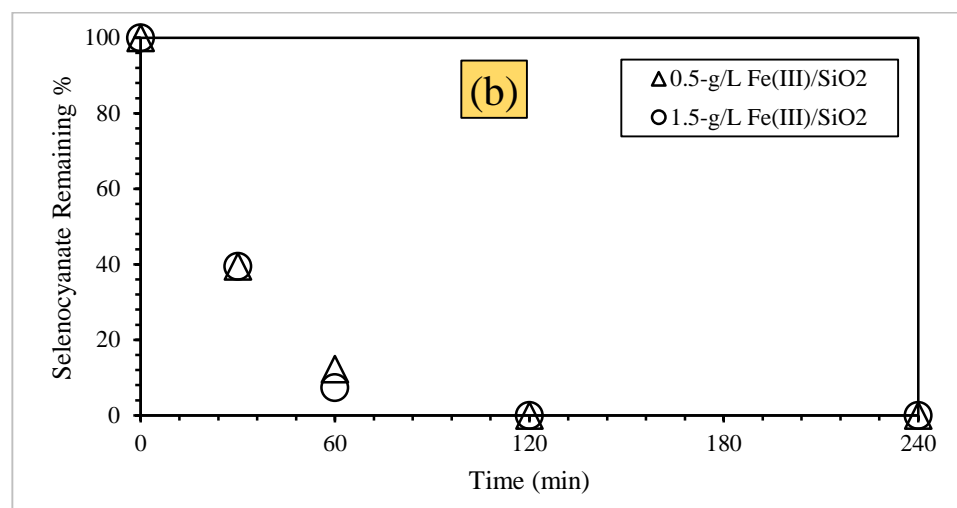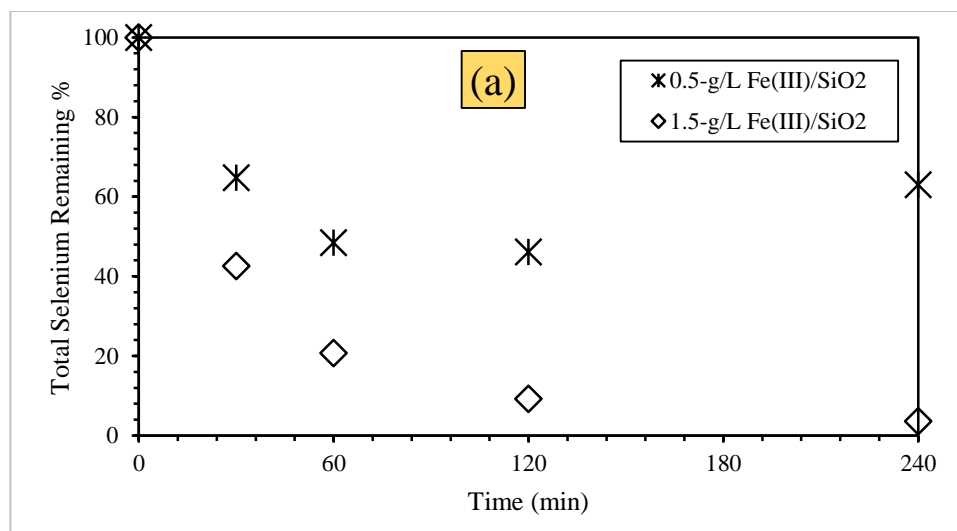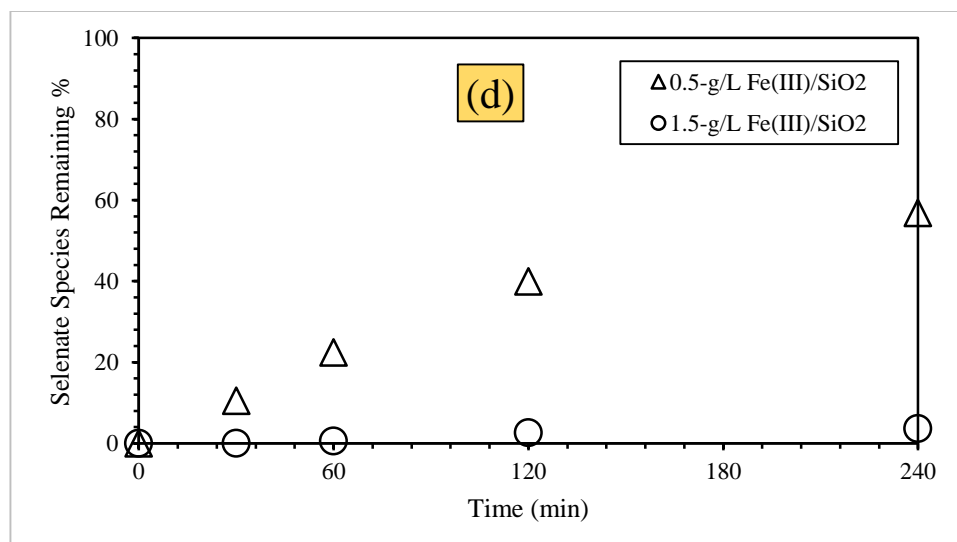
Figure 56 The effect of Fe(III)/SiO$_2$ amount onto the removal of selenium species: (a) total selenium, (b) selenocyanate, (c) selenite, and (d) selenate, associated during the selenocyanate complex destruction using photocatalysis with Fe(III)/SiO$_2$ system (15 mg/L selenocyanate, 1-g/L TiO$_2$, 15 W UV lamp, pH 5).

5.5.2.4 Effect of initial selenocyanate concentration onto photocatalysis

The previously reported, results from Figure 49 and Figure 51 are re-arranged in Figure 57 and Figure 58 to compare the effect selenocyanate amount onto its removal. We note small changes in the respective selenium species removal with an increase in initial selenocyanate concentration, at both pH 5 and 9. In summary, the TiO_2 photocatalysis based selenocyanate complex destruction, and simultaneous adsorption of selenium oxyanions (selenite and selenate) by $Fe(III)/SiO_2$ at acidic pH is a viable option for treatment of respective waste streams.
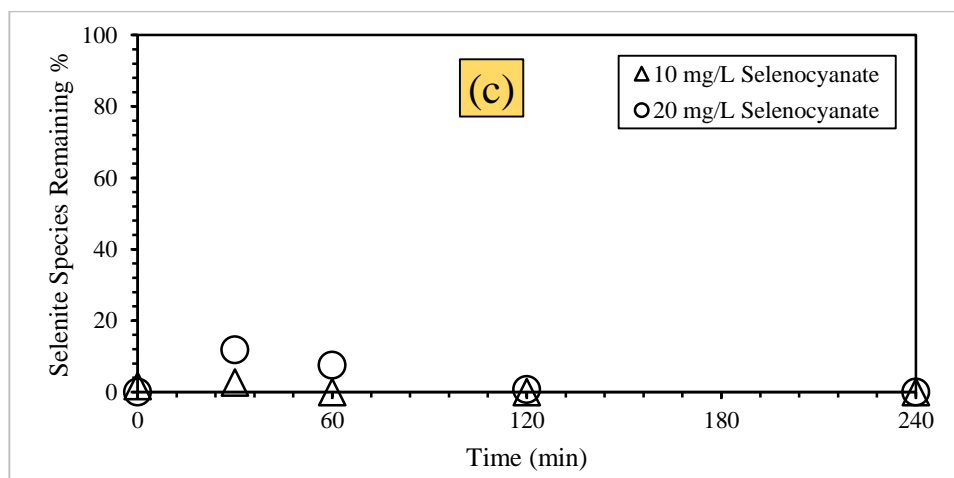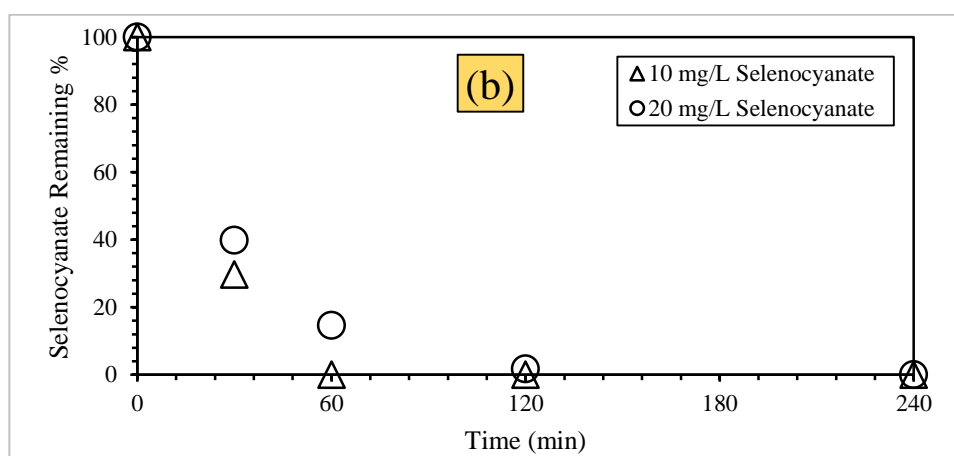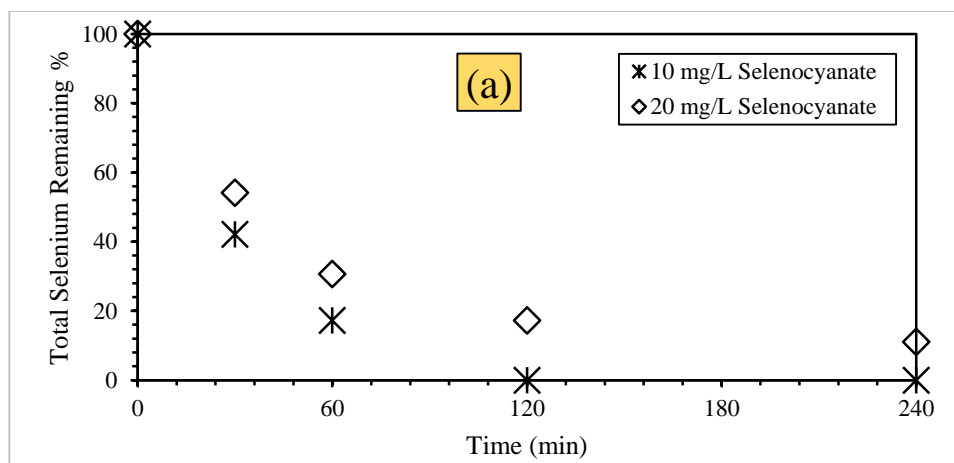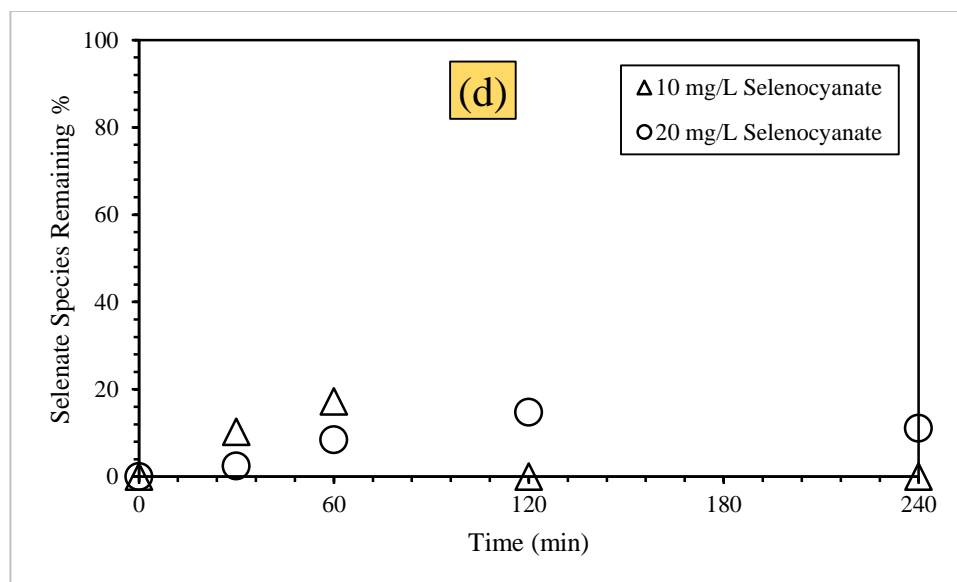
Figure 57 The effect of initial selenocyanate concentration onto the removal of selenium species: (a) total selenium, (b) selenocyanate, (c) selenite, and (d) selenate, associated during the selenocyanate complex destruction using photocatalysis with Fe(III)/SiO$_2$ system (1 g/L Fe(III)/SiO$_2$, 1 g/L TiO$_2$, 15 W UV lamp, pH 5).
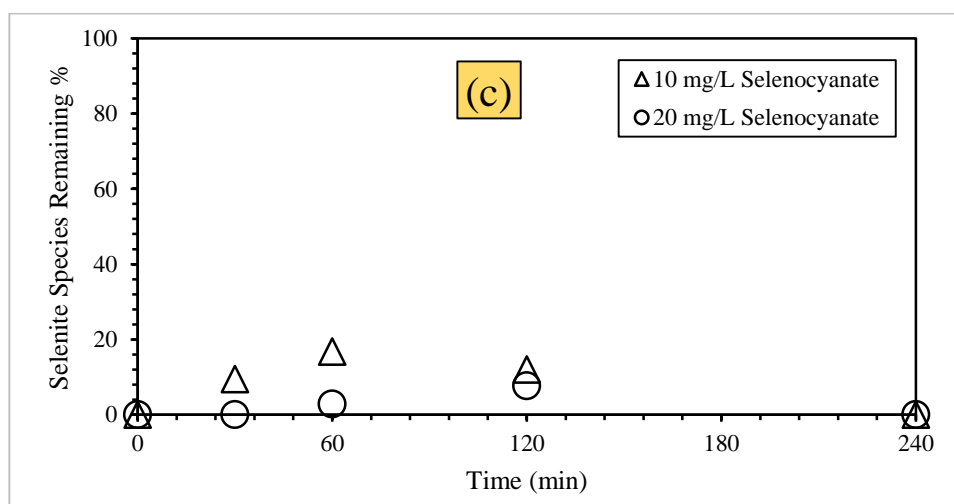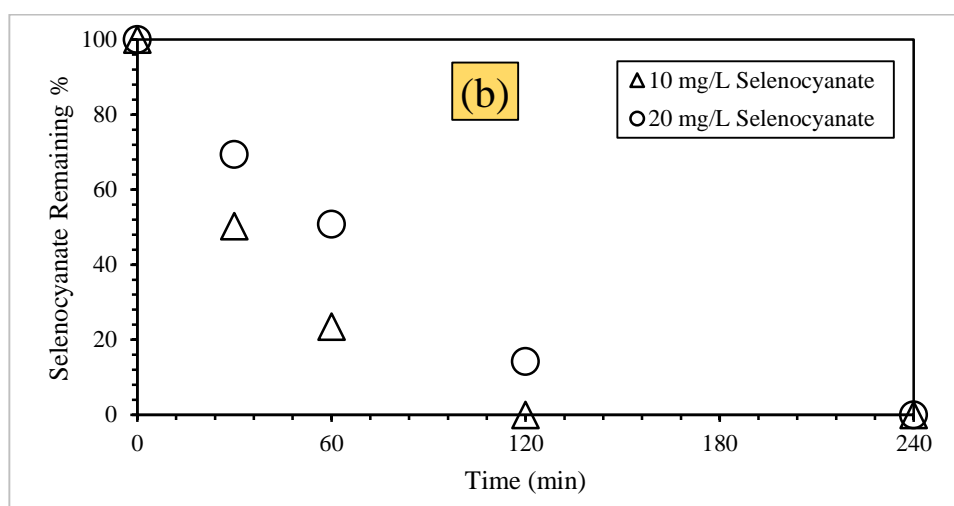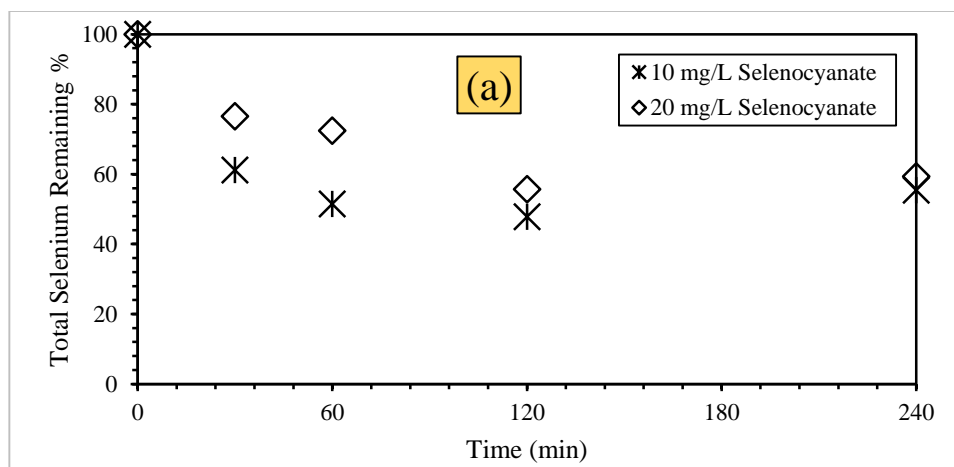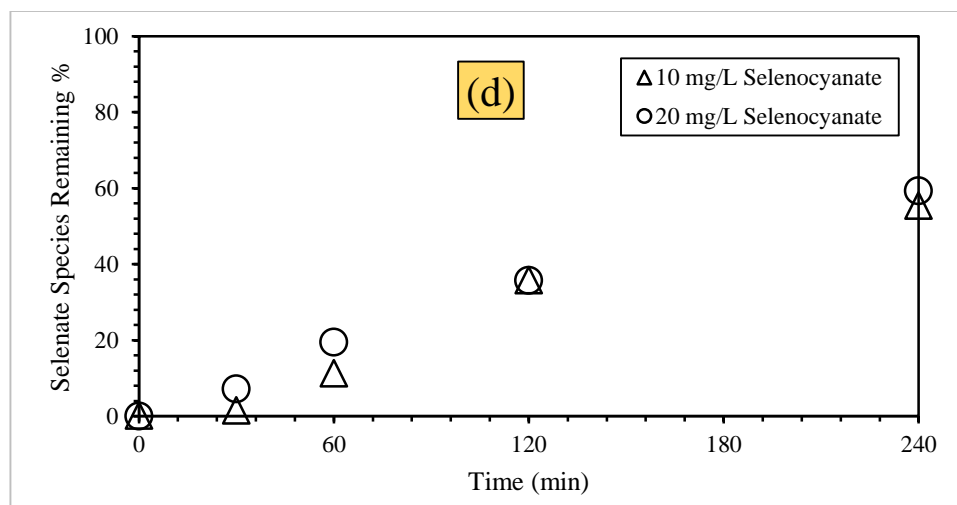
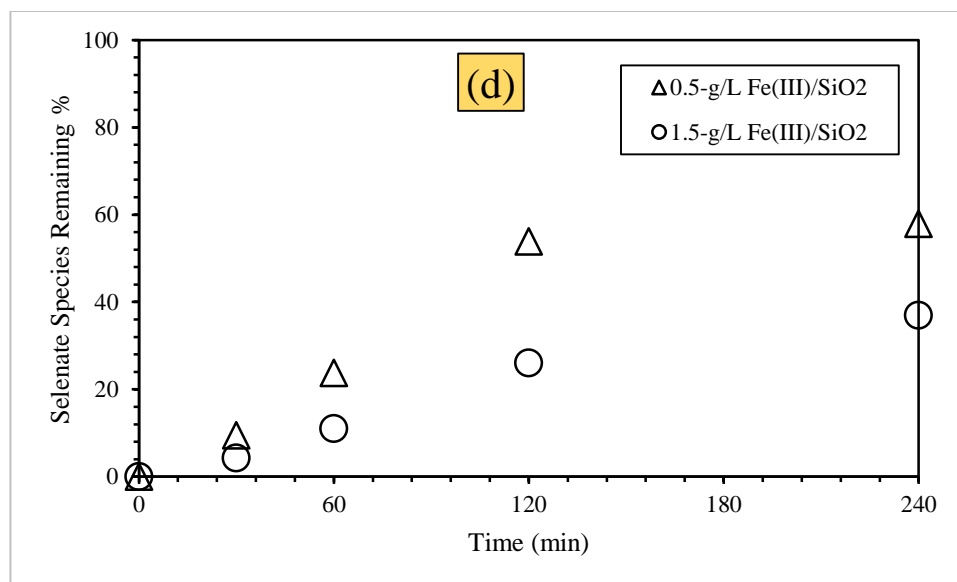Figure 58 The effect of initial selenocyanate concentration onto the removal of selenium species: (a) total selenium, (b) selenocyanate, (c) selenite, and (d) selenate, associated during the selenocyanate complex destruction using photocatalysis with Fe(III)/SiO$_2$ system (1 g/L Fe(III)/SiO$_2$, 1 g/L TiO$_2$, 15 W UV lamp, pH 9).

CHAPTER 6

CONCLUSIONS AND RECOMMENDATIONS

6.1 Conclusions

The removal of selenocyanate ($SeCN^-$) species was investigated in the present work using different iron-based technologies including, classical Fenton process, photo-Fenton (PF) process, two-line ferrihydrite (2LFh), and $Fe(III)/SiO_2$ binary oxide systems, and a combination of TiO_2-based photocatalysis with adsorbent 2LFh and $Fe(III)/SiO_2$ binary oxide. Initial results from using only Fe(II) species revealed its poor role for selenocyanate removal even in the presence of UV light. However, use of simple Fenton reaction at acidic pH showed higher selenocyanate removal. Furthermore, the adsorption of selenocyanate species onto 2LFh was also assessed. 2LFh species showed lower affinity for selenocyanate adsorption at acidic conditions. Langmuir isotherm model was suitable to describe selenocyanate adsorption onto 2LFh, and the adsorption kinetics data better fitted to second order kinetics model. Moreover, use of 2LFh along with TiO_2-PCD offered a viable process for the treatment of selenocyanate contaminated waters. Simply, TiO_2-based photocatalysis destroyed selenocyanate complex, and the produced selenium oxyanions (selenite, selenate) were adsorbed onto 2LFh. This process was affected significantly by pH conditions. Total selenium removal decreases significantly as pH increases. Furthermore, the response surface methodology (RSM)-based models also showed that the RSM approach can be used to predict aqueous phase selenocyanate removal under a varying set of operational conditions. The adsorption of selenocyanate using ($Fe(III)/SiO_2$) binary oxide system showed comparatively lower selenocyanate removal. The adsorption data

better fitted to Freundlich isotherm model. The combination of TiO_2 photocatalysis with Fe(III)/SiO_2 based adsorption was also used for the degradation of selenocyanate followed by the removal of released selenium species via adsorption onto Fe(III)/SiO_2. Near complete selenium removal was noted at acidic pH. However, selenium removal deceased with an increase in pH. In general, the present work shows successful removal of selenocyanate species from aqueous phase under varying set of process conditions using several Fe-based systems.

6.2   Recommendations

Based on the outcomes of this research, it is recommended that further research be conducted as mentioned below:

1. The adsorption of selenite species onto 2LFh should be investigated.

2. The competitive adsorption of multicomponent selenite, selenate, and selenocyanate onto 2LFh and Fe(III)/SiO_2 should be assessed.

3. The efficiency of TiO_2/2LFh and TiO_2/Fe(III)-SiO_2 photocatalysis systems for selenocyanate removal in the presence of specific co-pollutants such as phenol should also be investigated.

REFERENCES

[1]   T.T.Y. Tan, D. Beydoun, R. Amal, Photocatalytic Reduction of Se (VI) in Aqueous Solutions in UV / TiO 2 System : Kinetic Modeling and Reaction Mechanism, J. Phys. Chem. B. 107 (2003) 4296–4303. doi:10.1021/jp026149+.

[2]   World Health Organization, Selenium in Drinking-water, World Heal. Organ. Geneva. (2011) 1–22. doi:WHO/HSE/WSH/10.01/14.

[3]   D.M. Janz, D.D. K., M.L. Brooks, P.M. Chapman, G. Gilron, D. Hoff, W.A. Hopkins, O. McIntyre, Dennis, C.A. Mebane, V.P. Palace, J.P. Skorupa, M. Wayland, Ecological Assessment of Selenium in the Aquatic Environment, in: Ecol. Assess.   Selenium   Aquat.   Environ.,   2010:   pp.   141–231. doi:10.1201/EBK1439826775.

[4]   U. Tinggi, Essentiality and toxicity of selenium and its status in Australia: A review, Toxicol. Lett. 137 (2003) 103–110. doi:10.1016/S0378-4274(02)00384-3.

[5]   K.H. Goh, T.T. Lim, Geochemistry of inorganic arsenic and selenium in a tropical soil: Effect of reaction time, pH, and competitive anions on arsenic and selenium adsorption,   Chemosphere.   55   (2004)   849–859. doi:10.1016/j.chemosphere.2003.11.041.

[6]   L.G. Twidwell, J. McCloskey, P. Miranda, M. Gale, Technologies and Potential Technologies for Removing Selenium from Process and Mine Wastewater, Glob. Symp.   Recycl.   Waste   Treat.   Clean   Technol.   (1999)   1645–1656. http://webcache.googleusercontent.com/search?q=cache:y3_cER4cpHQJ:www.res earchgate.net/profile/Larry_Twidwell/publication/264856347_TECHNOLOGIES_ AND_POTENTIAL_TECHNOLOGIES_FOR_REMOVING_SELENIUM_FRO M_PROCESS_AND_MINE_WASTEWATER/links/53ff7daf0cf2194bc29a85.

[7]   MSE Technology Applications Inc., Selenium Treatment/Removal Alternatives Demonstration Project: Mine Waste Technology Program Activity III , Project 20, (2001) 1–133. doi:10.1007/s10811-012-9939-5.

[8]   L.R. Moore, K. Oil, a Mahmoudkhani, L. Sanders, J.R. Durand, Methods for Removing Arsenic From Aqueous Systems, (2012) 1–5.

[9]   N. Bleiman, Y.G. Mishael, Selenium removal from drinking water by adsorption to chitosan–clay composites and oxides: Batch and columns tests, J. Hazard. Mater. 183 (2010) 590–595. doi:10.1016/j.jhazmat.2010.07.065.

[10]   J. Das, D. Das, G.P. Dash, K.M. Parida, Studies on Mg/Fe Hydrotalcite-Like- Compound   (HTlc),   J.   Colloid   Interface   Sci.   251   (2002)   26–32. doi:10.1006/jcis.2002.8319.

[11]   K. Hashimoto, H. Irie, A. Fujishima, TiO 2 Photocatalysis: A Historical Overview and   Future   Prospects,   Jpn.   J.   Appl.   Phys.   44   (2005)   8269–8285.

doi:10.1143/JJAP.44.8269.

[12]   A. Machulek, F.H. Quina, F. Gozzi, Fundamental Mechanistic Studies of the Photo-Fenton Reaction for the Degradation of Organic Pollutants, Org. Pollut. Intech Publ. Inc., Rijeka. (2012) 271–292. doi:10.5772/30995.

[13]   V.J.P. Vilar, E.M.R. Rocha, F.S. Mota, A. Fonseca, I. Saraiva, R. a R. Boaventura, Treatment of a sanitary landfill leachate using combined solar photo-Fenton and biological immobilized biomass reactor at a pilot scale, Water Res. 45 (2011) 2647–2658. doi:10.1016/j.watres.2011.02.019.

[14]   C. Sirtori, A. Zapata, W. Gernjak, S. Malato, A. Lopez, A. Agüera, Solar photo-Fenton degradation of nalidixic acid in waters and wastewaters of different composition. Analytical assessment by LC-TOF-MS., Water Res. 45 (2011) 1736–44. doi:10.1016/j.watres.2010.11.023.

[15]   ∗ M. Agulló-Barcelób, M.I. Polo-Lópeza, F. Lucenab, J. Jofreb, P. Fernández-Ibá˜neza, Solar Advanced Oxidation Processes as disinfection tertiary treatments for real wastewater: Implications for water reclamation, Appl. Catal. B Environ. 136–137 (2013) 341–350.

[16]   H. Shemer, Y.K. Kunukcu, K.G. Linden, Degradation of the pharmaceutical Metronidazole via UV, Fenton and photo-Fenton processes, Chemosphere. 63 (2006) 269–276. doi:10.1016/j.chemosphere.2005.07.029.

[17]   Z. Eren, F.N. Acar, N.H. Ince, Fenton and Fenton-like oxidation of CI Basic Yellow 51: A comparative study, Color. Technol. 126 (2010) 337–341. doi:10.1111/j.1478-4408.2010.00266.x.

[18]   A.K. Abdessalem, N. Bellakhal, N. Oturan, M. Dachraoui, M.A. Oturan, Treatment of a mixture of three pesticides by photo- and electro-Fenton processes, Desalination. 250 (2010) 450–455. doi:10.1016/j.desal.2009.09.072.

[19]   Donald L. Sparks, Environmental Soil Chemistry, 2002. doi:10.1097/00010694-199703000-00009.

[20]   Y.T. Chan, W.H. Kuan, T.Y. Chen, M.K. Wang, Adsorption mechanism of selenate and selenite on the binary oxide systems, Water Res. 43 (2009) 4412–4420. doi:10.1016/j.watres.2009.06.056.

[21]   S. Das, M. Jim Hendry, J. Essilfie-Dughan, Adsorption of selenate onto ferrihydrite, goethite, and lepidocrocite under neutral pH conditions, Appl. Geochemistry. 28 (2013) 185–193. doi:10.1016/j.apgeochem.2012.10.026.

[22]   Fiona M. Fordyce, Selenium Deficiency and Toxicity in the Environment, in: Essentials Med. Geol., 2013: pp. 375–416. doi:10.1007/978-94-007-4375-5.

[23]   A.D. Lemly, Aquatic selenium pollution is a global environmental safety issue, Ecotoxicol. Environ. Saf. 59 (2004) 44–56. doi:10.1016/S0147-6513(03)00095-2.

[24] J.M. J. Adams, T. P., Biotechnologies for Metal and Toxic Inorganic Removal from Mining Process and Waste Solutions, Randol Gold Forum =96 4. (1996).

[25] B. Soediono, liquid chromatography of natural pigments and synthetic dyes, J. Chem. Inf. Model. 53 (1989) 160. doi:10.1017/CBO9781107415324.004.

[26] D.L. Gallup, Removal of selenocyanate in water by precipitation: characterization of copper - selenium precipitate by X-ray diffraction, infrared, and X-ray absorption spectroscopy, Environ. Sci. Technol. 31 (1997) 968–976. doi:10.1021/es960138a.

[27] X. Meng, S. Bang, G.P. Korfiatis, Removal of selenocyanate from water using elemental iron., Water Res. 36 (2002) 3867–73. doi:10.1016/S0043-1354(02)00086-6.

[28] WSPA., Selenium Removal Technology Study, Concord, CA, 1995.

[29] D. Water, H. Basics, F. Asked, L.D. Water, N. Primary, P.D. Water, S. Water, U. Injection, S.D. Water, N. Drinking, W. Advisory, W. Infrastructure, Ground Water & Drinking Water Consumer Factsheet on : BARIUM, (2007) 1–4.

[30] M.O.M. Sharrad, H. Liu, M. Fan, Evaluation of FeOOH performance on selenium reduction, Sep. Purif. Technol. 84 (2012) 29–34. doi:10.1016/j.seppur.2011.07.011.

[31] A. Fernandez-Martinez, L. Charlet, Selenium environmental cycling and bioavailability: a structural chemist point of view, Rev. Environ. Sci. Biotechnol. 8 (2009) 81–110.

[32] and J.L.G.-T. C. M. Gonzalez, J. Hernandez, J. G. Parsons, Adsorption of Selenite and Selenate By a High- and Low-Pressure Aged Manganese Oxide Nanomaterial, Instrum. Sci. Technol. 39 (2011) 1–19.

[33] A. Benedicto, T. Missana, C. Degueldre, Predictions of TiO2-driven migration of Se(IV) based on an integrated study of TiO2 colloid stability and Se(IV) surface adsorption, Sci. Total Environ. 449 (2013) 214–222. doi:10.1016/j.scitotenv.2013.01.058.

[34] Y. Lei, F. Chen, Y. Luo, L. Zhang, Synthesis of three-dimensional graphene oxide foam for the removal of heavy metal ions, Chem. Phys. Lett. 593 (2014) 122–127. doi:10.1016/j.cplett.2013.12.066.

[35] H.-J. Sun, B. Rathinasabapathi, B. Wu, J. Luo, L.-P. Pu, L.Q. Ma, Arsenic and selenium toxicity and their interactive effects in humans., Environ. Int. 69 (2014) 148–58. doi:10.1016/j.envint.2014.04.019.

[36] R. Lavado, D. Shi, D. Schlenk, Effects of salinity on the toxicity and biotransformation of L-selenomethionine in Japanese medaka (Oryzias latipes) embryos: mechanisms of oxidative stress., Aquat. Toxicol. 108 (2011) 18–22. doi:10.1016/j.aquatox.2011.07.001.

[37] M. Mézes, K. Balogh, Prooxidant mechanisms of selenium toxicity - A review, Acta

Biol. Szeged. 53 (2009) 15–18.

[38] C. Herrero Latorre, J. Barciela García, S. García Martín, R.M. Peña Crecente, Solid phase extraction for the speciation and preconcentration of inorganic selenium in water samples: A review, Anal. Chim. Acta. 804 (2013) 37–49. doi:10.1016/j.aca.2013.09.054.

[39] H. Khakpour, H. Younesi, M. Mohammadhosseini, Two-stage biosorption of selenium from aqueous solution using dried biomass of the baker's yeast Saccharomyces cerevisiae, J. Environ. Chem. Eng. 2 (2014) 532–542. doi:10.1016/j.jece.2013.10.010.

[40] S.B. Goldhaber, Trace element risk assessment: essentiality vs. toxicity, Regul. Toxicol. Pharmacol. 38 (2003) 232–242. doi:10.1016/S0273-2300(02)00020-X.

[41] Scientific Committee on Food, Opinion of the Scientific Committee on Food on the Tolerable Upper Intake Level of Vitamin E. SCF/CS/NUT/UPPLEV/31 Final., (2003) 1–18.

[42] H.G. Gorchev, G. Ozolins, WHO guidelines for drinking-water quality., 4th ed., 2011. doi:10.1016/S1462-0758(00)00006-6.

[43] J. Risher, R.A. McDonald, M.J. Citra, S. Bosch, R.J. Amata, Toxicological Profile for Selenium, 2003.

[44] W.Z. Tang, H. An, Photocatalytic degradation kinetics and mechanism of acid blue 40 by TiO2/UV in aqueous solution, Chemosphere. 31 (1995) 4171–4183. doi:10.1016/0045-6535(95)80016-E.

[45] R. Andreozzi, Advanced oxidation processes (AOP) for water purification and recovery, Catal. Today. 53 (1999) 51–59. doi:10.1016/S0920-5861(99)00102-9.

[46] P. Maletzky, R. Bauer, the Photo-Fenton Nitrogen Degradation of Containing Organic Compounds, Chemosphere. 37 (1998) 899–909.

[47] T. Krutzler, R. Bauer, Optimization of a photo-fenton prototype reactor, Chemosphere. 38 (1999) 2517–2532. doi:10.1016/S0045-6535(98)00460-3.

[48] C.M. Lewandowski, Pillared Clays and Related Catalysts, Eff. Br. Mindfulness Interv. Acute Pain Exp. An Exam. Individ. Differ. 1 (2010). doi:10.1017/CBO9781107415324.004.

[49] Julián Blanco-Galvez, Pilar Fernández-Ibáñez, Sixto Malato-Rodríguez, Solar photocatalytic detoxification and disinfection of water: Recent Overview, J. Sol. Energy Eng. 129 (2007) 4–15.

[50] M.S. Vohra, SELENOCYANATE (SeCN -) CONTAMINATED WASTE-WATER TREATMENT USING TiO 2 PHOTOCATALYSIS : SeCN - COMPLEX DESTRUCTION , INTERMEDIATES FORMATION , AND REMOVAL OF SELENIUM SPECIES, 24 (2015) 8–11.

[51] T. Tan, D. Beydoun, R. Amal, Effects of organic hole scavengers on the photocatalytic reduction of selenium anions, J. Photochem. Photobiol. A Chem. 159 (2003) 273–280. doi:10.1016/S1010-6030(03)00171-0.

[52] T.T.. Tan, C.. Yip, D. Beydoun, R. Amal, Effects of nano-Ag particles loading on TiO2 photocatalytic reduction of selenate ions, Chem. Eng. J. 95 (2003) 179–186. doi:10.1016/S1385-8947(03)00103-7.

[53] and B.H. Qiuquan Wang, Jing Liang, a Jianhua Qiua, Online pre-reduction of selenium((VI)) with a newly designed UV/TiO2 photocatalysis reduction device, J. Anal. At. Spectrom. 19 (2004) 715–716.

[54] T. Nakajima, K. Yamada, H. Idehara, H. Takanashi, A. Ohki, Removal of Selenium (VI) from Simulated Wet Flue Gas Desulfurization Wastewater Using Photocatalytic Reduction, J. Water Environ. Technol. 9 (2011) 13–19. doi:10.2965/jwet.2011.13.

[55] B. a. Labaran, M.S. Vohra, Photocatalytic removal of selenite and selenate species: effect of EDTA and other process variables, Environ. Technol. 35 (2014) 1091–1100. doi:10.1080/09593330.2013.861857.

[56] K.L. Wasewar, B. Prasad, S. Gulipalli, Adsorption of selenium using bagasse fly ash, Clean - Soil, Air, Water. 37 (2009) 534–543. doi:10.1002/clen.200800183.

[57] Y. Zhang, C. Amrhein, W.T. Frankenberger, Effect of arsenate and molybdate on removal of selenate from an aqueous solution by zero-valent iron, Sci. Total Environ. 350 (2005) 1–11. doi:10.1016/j.scitotenv.2005.02.032.

[58] J.T. Olegario, N. Yee, M. Miller, J. Sczepaniak, B. Manning, Reduction of Se(VI) to Se(-II) by zerovalent iron nanoparticle suspensions, J. Nanoparticle Res. 12 (2010) 2057–2068. doi:10.1007/s11051-009-9764-1.

[59] L. Liang, W. Yang, X. Guan, J. Li, Z. Xu, J. Wu, Y. Huang, X. Zhang, Kinetics and mechanisms of pH-dependent selenite removal by zero valent iron, Water Res. 47 (2013) 5846–5855. doi:10.1016/j.watres.2013.07.011.

[60] L. Liang, W. Sun, X. Guan, Y. Huang, W. Choi, H. Bao, L. Li, Z. Jiang, Weak magnetic field significantly enhances selenite removal kinetics by zero valent iron, Water Res. 49 (2014) 371–380. doi:10.1016/j.watres.2013.10.026.

[61] C. Tang, Y.H. Huang, H. Zeng, Z. Zhang, Reductive removal of selenate by zero-valent iron: The roles of aqueous Fe2+ and corrosion products, and selenate removal mechanisms, Water Res. 67 (2014) 166–174. doi:10.1016/j.watres.2014.09.016.

[62] C. Tang, Y.H. Huang, H. Zeng, Z. Zhang, Promotion effect of Mn2+ and Co2+ on selenate reduction by zero-valent iron, Chem. Eng. J. 244 (2014) 97–104. doi:10.1016/j.cej.2014.01.059.

[63] C. Tang, Y. Huang, Z. Zhang, J. Chen, H. Zeng, Y.H. Huang, Rapid removal of selenate in a zero-valent iron/Fe3O4/Fe2+ synergetic system, Appl. Catal. B

Environ. 184 (2016) 320–327. doi:10.1016/j.apcatb.2015.11.045.

[64]   F. Fu, J. Lu, Z. Cheng, B. Tang, Removal of selenite by zero-valent iron combined with ultrasound: Se(IV) concentration changes, Se(VI) generation, and reaction mechanism, Ultrason. Sonochem. 29 (2016) 328–336. doi:10.1016/j.ultsonch.2015.10.007.

[65]   I.H. Yoon, S. Bang, K.W. Kim, M.G. Kim, S.Y. Park, W.K. Choi, Selenate removal by zero-valent iron in oxic condition: the role of Fe(II) and selenate removal mechanism, Environ. Sci. Pollut. Res. 23 (2016) 1081–1090. doi:10.1007/s11356-015-4578-4.

[66]   L. Ling, B. Pan, W. xian Zhang, Removal of selenium from water with nanoscale zero-valent iron: Mechanisms of intraparticle reduction of Se(IV), Water Res. 71 (2015) 274–281. doi:10.1016/j.watres.2015.01.002.

[67]   S. Jevti??, I. Ar??on, A. Re??nik, B. Babi??, M. Mazaj, J. Pavlovi??, D. Matija??evic, M. Nik??i??, N. Raji??, The iron(III)-modified natural zeolitic tuff as an adsorbent and carrier for selenium oxyanions, Microporous Mesoporous Mater. 197 (2014) 92–100. doi:10.1016/j.micromeso.2014.06.008.

[68]   X. Wei, S. Bhojappa, L.-S. Lin, R.C. Viadero, Performance of nano-magnetite for removal of selenium from aqueous solutions, Environ. Eng. Sci. 29 (2012) 526–532. doi:10.1089/ees.2011.0383.

[69]   S. a. Davis, M. Misra, Transport Model for the Adsorption of Oxyanions of Selenium (IV) and Arsenic (V) from Water onto Lanthanum- and Aluminum-Based Oxides, J. Colloid Interface Sci. 188 (1997) 340–350. doi:10.1006/jcis.1997.4775.

[70]   Y. You, G.F. Vance, H. Zhao, Selenium adsorption on Mg-Al and Zn-Al layered double hydroxides, Appl. Clay Sci. 20 (2001) 13–25. doi:10.1016/S0169-1317(00)00043-0.

[71]   J.S. Yamani, A.W. Lounsbury, J.B. Zimmerman, Adsorption of selenite and selenate by nanocrystalline aluminum oxide, neat and impregnated in chitosan beads, Water Res. 50 (2013) 373–381. doi:10.1016/j.watres.2013.10.054.

[72]   U. Schwertmann R. M. Cornell, Iron Oxides in the Laboratory, second ed., 2000. doi:10.1180/minmag.1992.056.383.20.

[73]   M. Villacís-García, M. Ugalde-Arzate, K. Vaca-Escobar, M. Villalobos, R. Zanella, N. Martínez-Villegas, Laboratory synthesis of goethite and ferrihydrite of controlled particle sizes, Bol. La Soc. Geol. Mex. 67 (2015) 433–446.

[74]   D. Baş, İ.H. Boyacı, D. Bas, I.H. Boyaci, D. Baş, İ.H. Boyacı, D. Bas, I.H. Boyaci, Modeling and optimization I: Usability of response surface methodology, J. Food Eng. 78 (2007) 836–845. doi:10.1016/j.jfoodeng.2005.11.024.

[75]   K. Rout, M. Mohapatra, S. Anand, 2-line ferrihydrite: synthesis, characterization and its adsorption behaviour for removal of Pb(II), Cd(II), Cu(II) and Zn(II) from

aqueous solutions., Dalt. Trans. 41 (2012) 3302–12. doi:10.1039/c2dt11651k.

[76] D.B. Hausner, N. Bhandari, A.M. Pierre-Louis, J.D. Kubicki, D.R. Strongin, Ferrihydrite reactivity toward carbon dioxide, J. Colloid Interface Sci. 337 (2009) 492–500. doi:10.1016/j.jcis.2009.05.069.

[77] N. Abdus-salam, F.A. M'Civer, Synthesis, Characterisation and Application of 2-Line and 6-Line Ferrihydrite to Pb(II) Removal from Aqueous Solution, J. Appl. Sci. Environ. Manag. 16 (2012) 327–336.

[78] F.E. Rhoton, J.M. Bigham, Phosphate adsorption by ferrihydrite-amended soils., J. Environ. Qual. 34 (2005) 890–896. doi:10.2134/jeq2004.0176.

[79] L. Brinza, L.G. Benning, P.J. Statham, Adsorption studies of Mo and V onto ferrihydrite, Mineral. Mag. 72 (2008) 385–388. doi:10.1180/minmag.2008.072.1.385.

[80] K. Rout, M. Mohapatra, S. Anand, 2-line ferrihydrite: synthesis, characterization and its adsorption behaviour for removal of Pb(II), Cd(II), Cu(II) and Zn(II) from aqueous solutions., Dalt. Trans. 41 (2012) 3302–12. doi:10.1039/c2dt11651k.

[81] G.P. Clair Sawyer, Perry McCarty, Chemistry for Environmental Engineering and Science, 5th Editio, Mc Graw Hill, 2003.

[82] H.D.S. Metcalf & Eddy Inc. , George Tchobanoglous , Franklin L Burton, Wastewater engineering: treatment and reuse, 4 th eddit, 2003.

[83] A.K. Bhattacharya, T.K. Naiya, S.N. Mandal, S.K. Das, Adsorption, kinetics and equilibrium studies on removal of Cr(VI) from aqueous solutions using different low-cost adsorbents, Chem. Eng. J. 137 (2008) 529–541. doi:10.1016/j.cej.2007.05.021.

[84] H. Qiu, L. Lv, B. Pan, Q.Q. Zhang, W. Zhang, Q.Q. Zhang, Critical review in adsorption kinetic models, J. Zhejiang Univ. Sci. A. 10 (2009) 716–724. doi:10.1631/jzus.A0820524.

[85] W. and B. Hoffmann, M.R., Martin, S.T. Choi, D.W, Environmental applications of semi-conductor photocatalysis, Chem. Rev. 95 (1995) 69–96.

[86] D. Peak, D.L. Sparks, Mechanisms of selenate adsorption on iron oxides and hydroxides, Environ. Sci. Technol. 36 (2002) 1460–1466. doi:10.1021/es0156643.

[87] M.M.S. Wooyong Um, Adsorption Mechanisms and Transport Behavior between Selenate and Selenite on Different Sorbents, Int. J. Waste Resour. 4 (2014). doi:10.4172/2252-5211.1000144.

[88] M. Brigante, M.E. Parolo, P.C. Schulz, M. Avena, Synthesis, characterization of mesoporous silica powders and application to antibiotic remotion from aqueous solution. Effect of supported Fe-oxide on the SiO2 adsorption properties, Powder Technol. 253 (2014) 178–186. doi:10.1016/j.powtec.2013.11.008.

[89] A. Gervasini, C. Messi, P. Carniti, A. Ponti, N. Ravasio, F. Zaccheria, Insight into the properties of Fe oxide present in high concentrations on mesoporous silica, J. Catal. 262 (2009) 224–234. doi:10.1016/j.jcat.2008.12.016.

[90] G. Ennas, A. Musinu, G. Piccaluga, D. Zedda, D. Gatteschi, C. Sangregorio, J.L. Stanger, G. Concas, G. Spano, Characterization of Iron Oxide Nanoparticles in an Fe2O3−SiO2 Composite Prepared by a Sol−Gel Method, Chem. Mater. 10 (1998) 495–502. doi:10.1021/cm970400u.

[91] K.M.S. Khalil, H.A. Mahmoud, T.T. Ali, Direct formation of thermally stabilized amorphous mesoporous Fe 2O3/SiO2 nanocomposites by hydrolysis of aqueous iron (III) nitrate in sols of spherical silica particles, Langmuir. 24 (2008) 1037–1043. doi:10.1021/la702904h.

[92] Y. Wang, J. Ren, X. Liu, Y. Wang, Y. Guo, Y. Guo, G. Lu, Facile synthesis of ordered magnetic mesoporous γ -Fe2O3/SiO2 nanocomposites with diverse mesostructures, J. Colloid Interface Sci. 326 (2008) 158–165. doi:10.1016/j.jcis.2008.07.012.

[93] K. Gude, V.M. Gun'ko, J.P. Blitz, Adsorption and photocatalytic decomposition of methylene blue on surface modified silica and silica-titania, Colloids Surfaces A Physicochem. Eng. Asp. 325 (2008) 17–20. doi:10.1016/j.colsurfa.2008.04.035.

VITAE

Name   : Sameh Abdelfattah Araby Ahmed

Nationality   : Egyptian

Date of Birth   : Sept. 09, 1989

Email   : Sameh.araby@aswu.edu.eg

Address   : Civil Engineering Dept., Aswan University, Aswan, Egypt

Academic Background   : Civil Engineering